AD-A066 566 SYRACUSE UNIV NY DEPT OF ELECTRICAL AND COMPUTER EN--ETC F/G 9/5
A STUDY OF A REACTIVELY LOADED FINITE PLANAR RECTANGULAR WAVEGU--ETC(U)
FEB 79 J LUZWICK, R F HARRINGTON N00014-76-C-0225

UNCLASSIFIED TR-79-2 NL

1 OF 2
AD A066566

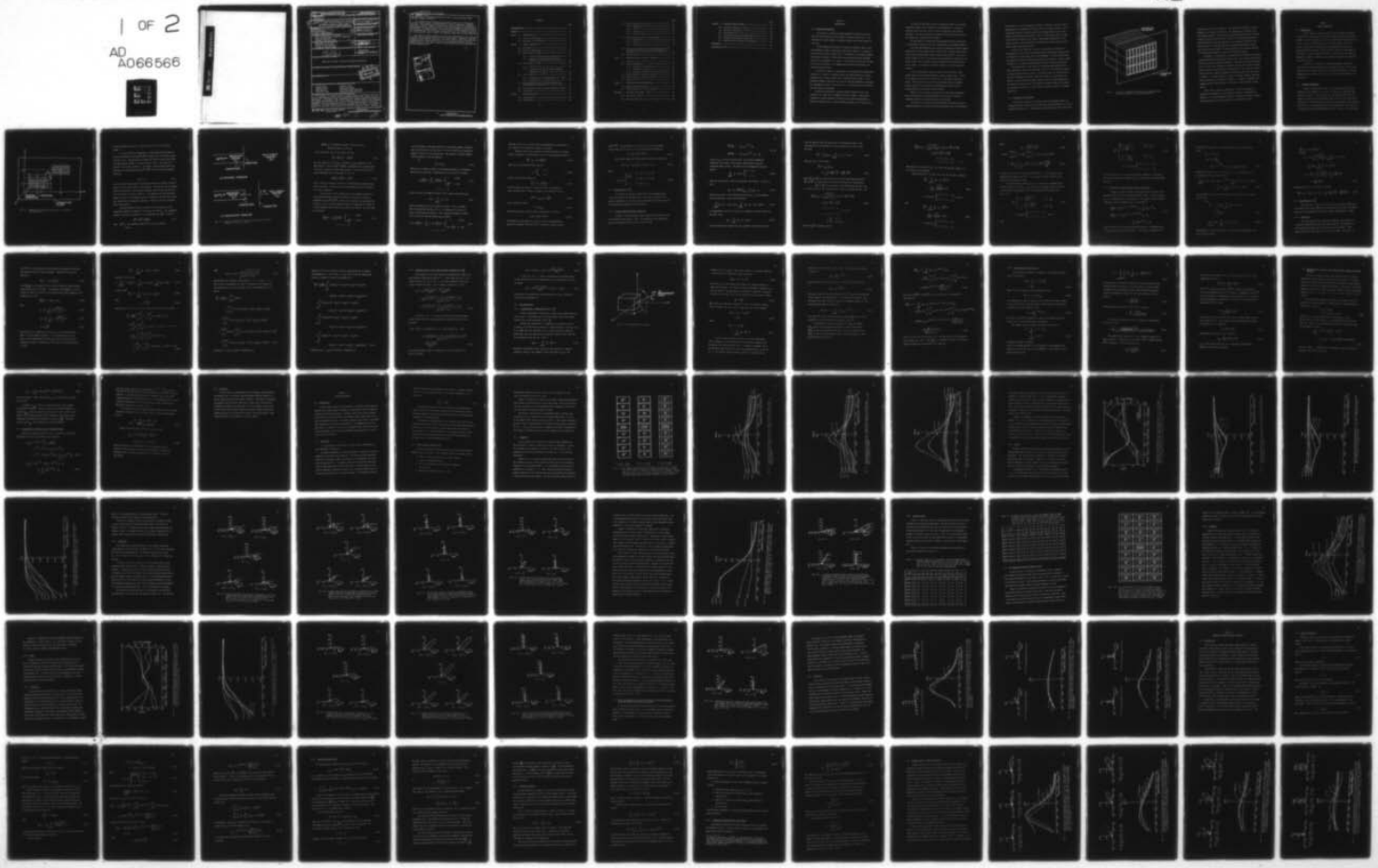

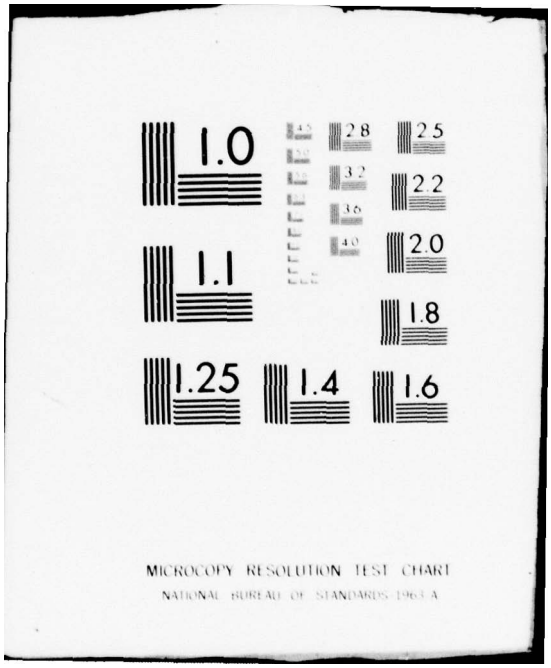
1.0
1.1
1.25
1.4
1.6
2.8
3.2
3.6
4.0
2.5
2.2
2.0
1.8
MICROCOPY RESOLUTION TEST CHART
NATIONAL BUREAU OF STANDARDS 1963-A

SECURITY CLASSIFICATION OF THIS PAGE (When Data Entered)

(14) **REPORT DOCUMENTATION PAGE**

READ INSTRUCTIONS BEFORE COMPLETING FORM

1. REPORT NUMBER: TR-79-2	2. GOVT ACCESSION NO.
3. RECIPIENT'S CATALOG NUMBER	
4. TITLE (and Subtitle): (6) A STUDY OF A REACTIVELY LOADED FINITE PLANAR RECTANGULAR WAVEGUIDE ANTENNA ARRAY	5. TYPE OF REPORT & PERIOD COVERED: (9) Technical Report, No. 9
	6. PERFORMING ORG. REPORT NUMBER
7. AUTHOR(s): (10) John Luzwick, Roger F. Harrington	8. CONTRACT OR GRANT NUMBER(s): (15) N00014-76-C-0225
9. PERFORMING ORGANIZATION NAME AND ADDRESS: Dept. of Electrical & Computer Engineering, Syracuse University, Syracuse, New York 13210	10. PROGRAM ELEMENT, PROJECT, TASK AREA & WORK UNIT NUMBERS
11. CONTROLLING OFFICE NAME AND ADDRESS: Department of the Navy, Office of Naval Research, Arlington, Virginia 22217	(11) 12. REPORT DATE: February 1979
	13. NUMBER OF PAGES: 125
14. MONITORING AGENCY NAME & ADDRESS (if different from Controlling Office): (12) 125 p.	15. SECURITY CLASS. (of this report): UNCLASSIFIED
	15a. DECLASSIFICATION/DOWNGRADING SCHEDULE

16. DISTRIBUTION STATEMENT (of this Report)

Approved for public release; distribution unlimited

17. DISTRIBUTION STATEMENT (of the abstract entered in Block 20, if different from Report)

18. SUPPLEMENTARY NOTES

19. KEY WORDS (Continue on reverse side if necessary and identify by block number)

Antenna array	Parasitic feed
Aperture array	Pattern synthesis
Beam steering	Reactively loaded apertures
Directive array	Waveguide-backed apertures

20. ABSTRACT (Continue on reverse side if necessary and identify by block number)

An analysis of a general class of antenna arrays, specifically the reactively loaded parasitically excited waveguide-backed aperture antenna array, is presented. The antenna arrays considered have a single waveguide-fed aperture, no complex feed network to all of the apertures, and one reactive load (shorted waveguide) for each remaining aperture. By varying the position of the short circuits, a directive beam can be steered through 180° in space. Only partial control of the array characteristics is possible using this scheme. However,

DD FORM 1 JAN 73 1473 EDITION OF 1 NOV 65 IS OBSOLETE S/N 0102-014-6601

SECURITY CLASSIFICATION OF THIS PAGE (When Data Entered) UNCLASSIFIED

406 737 (Jcp) 4/B

20. ABSTRACT (cont.)
the simplicity of antenna feed design and ease of pattern control makes reactive loading attractive.

The antenna arrays investigated have both linear and two dimensional lattices. Each antenna is characterized in terms of power gain, bandwidth, and match. Several examples of magnitude pattern synthesis are presented to show antenna pattern limitations for a given antenna geometry and excitation. In addition, an example using a double-frequency synthesis procedure is given for reshaping gain versus frequency characteristics in the endfire direction. In this direction, gain is higher and bandwidth lower than in other directions.

The reactive loading equations for gain and synthesis error are nonlinear equations which normally cannot be solved analytically. Therefore, numerical techniques (optimization algorithms) are used to find reactive loads for both maximum gain in a specified direction and a synthesized pattern. A brief summary is given of the major computer program subroutines used in generating the calculated results.

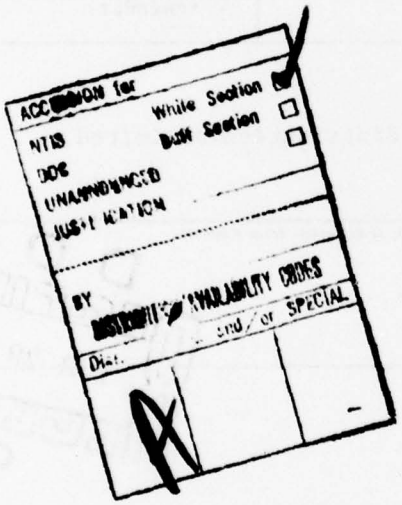

CONTENTS

Chapter 1

INTRODUCTION

1-1. Historical Background

The concept of reactively loaded antennas with parasitic excitation has been studied by several authors in recent years [1-11]. The following is a brief summary of important papers and reports written in this area.

In 1961 Simpson and Tillman [1] found that sidelobe control could be obtained by tuning a reactively loaded center element of a parasitically excited circular antenna array. In addition to the center element, the antenna consisted of N identical parallel dipoles spaced uniformly around the circumference of a circle. The antenna was excited by driving one of the ring dipoles. By commutating the excited ring dipole, the antenna beam was steered.

In 1963 Berry, Malech, and Kennedy [2] investigated an antenna which consisted of a surface or aperture which was characterized by a surface impedance and a primary radiator that illuminated this surface. An experimental example consisted of an array of shorted waveguides illuminated by a waveguide in front of the array face. By moving the short positions, the beam pattern was steered.

In 1964 Coe and Held [3] obtained endfire radiation from a slot equivalent of a Yagi array of magnetic current elements. The antenna consisted of tunable parasitic directive slots (shorted waveguides), a parasitic reflector slot to reduce backlobe radiation, and a driven slot.

In 1973 Seth and Chow [4] found a significant shift of the center operating frequency and a widening of the bandwidth for a center reactively loaded parasitic array of dipoles radiating in the endfire direction. The array consisted of unloaded reflector and feed dipoles and capacitively loaded director dipoles.

In 1974 Mathur [5] found that beam scanning could be achieved for a cavity-backed narrow slot array by varying the cavity backing widths.

From 1974-1978 Harrington and others investigated reactively loaded parasitically excited linear dipole arrays [6-7], circular dipole arrays [8-9], and waveguide-backed linear aperture arrays [10-11]. The excitation scheme for all of the various antenna geometries consisted of one driven element with the other elements parasitically excited and reactively loaded. By varying the reactive loading, a directive beam was steered.

In this dissertation a study is made of the reactively loaded parasitically excited waveguide-backed aperture antenna array. A part of the analysis involves the calculation of a half-space admittance matrix. The calculation of half-space admittance (mutual coupling) between apertures in a perfectly conducting ground plane has been studied previously by several authors [12-18].

Borgiotti [12] obtained an expression for the mutual admittance between two identical radiating apertures in the form of a Fourier transform related to the power pattern of the element.

In the first of two papers [13-14] Mailloux found the near field coupling between two collinear open-ended waveguide slots by formulating

the problem as a set of simultaneous integral equations which he solved approximately by expanding the aperture field in a Fourier series. In the second paper Mailloux found the near field coupling between two closely spaced open-ended square waveguide slots by a first-order analysis, based on the method of moments [15], using a single-mode approximation to the aperture field. He also presented an improved first-order analysis which used a higher order mode solution.

A paper by Cha and Hsiao [16] and a dissertation by Hidayet [17] investigated a finite array of waveguide-backed rectangular apertures where the apertures were the same size as the waveguides. In both publications the quadruple half-space admittance integral was reduced to a sum of double integrals by a coordinate transformation and then evaluated numerically.

The method used in this report for evaluating the quadruple half-space admittance integral was published in [18-19]. The procedure assumes a cosine aperture electric field. For apertures that are close together, the normal quadruple half-space admittance integral is analytically reduced to a sum of single integrals, which are then evaluated numerically. For apertures farther apart, the quadruple half-space admittance integral is analytically reduced to a sum of double integrals, which are evaluated numerically.

1-2. Statement of the Problem

This report considers an N element array of waveguide-backed rectangular apertures radiating into a half-space region bounded by an electric conductor (see Fig. 1.1). The perfectly conducting plate covers the entire

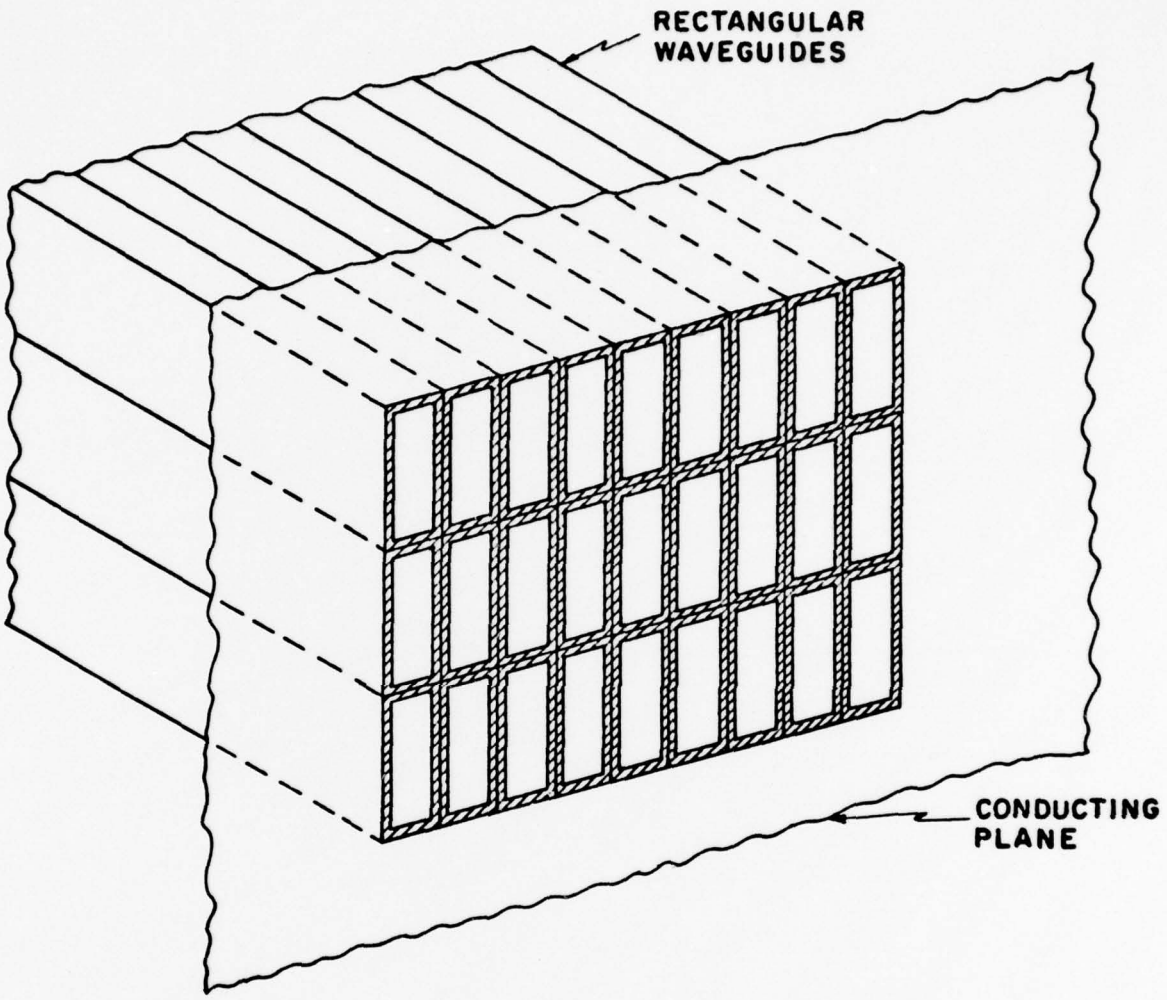

Fig. 1.1. An array of waveguide-backed apertures radiating into half-space bounded by an electric conductor.

z=0 plane except for the apertures. One aperture is fed while the other apertures are parasitically excited. The aperture can be smaller than the feeding waveguide. The parasitically excited apertures are reactively loaded by placing electrical short circuits in the backing waveguides at variable distances from the apertures. By varying the position of the short circuits, a directive beam can be steered through 180° in space. The solution uses the method of moments applied to the integral equation for the equivalent magnetic current in the aperture region.

In Chapter 2, a formulation is presented for analyzing the reactively loaded waveguide-backed aperture antenna array. The formulas derived have been used to obtain computer programs for expressing the antenna characteristics of power gain, bandwidth, and match for both linear and two dimensional reactively loaded aperture antenna arrays. Some calculated results obtained from the computer programs for several antenna cases are given in Chapter 3. Several examples of single and double frequency magnitude pattern synthesis are presented in Chapter 4. Chapter 5 summarizes and suggests further research areas for reactively loaded aperture antenna arrays.

This report contains two appendices. The first appendix is a mathematical supplement to the half-space admittance formulation in Chapter 2. The second appendix contains a summary of the major computer program subroutines used in generating the calculated results.

Chapter 2

GENERAL FORMULATION

2-1. Introduction

In this chapter a formulation which uses the method of moments is presented for analyzing the reactively loaded aperture antenna array problem. The basic approach is to use the equivalence principle [20, Sec. 3-5] to divide the problem into two separate regions. Once this is done, the aperture characteristics are expressed in terms of two aperture admittance matrices, $[Y^{wg}]$ and $[Y^{hs}]$, which are independent of each other. A single expansion function is used per aperture region to minimize the number of multiplicative operations required for analyzing large finite arrays.

A solution is obtained for the unknown magnetic current for each aperture region by multiplying the impressed sources in the driven waveguide by the inverted sum of the two admittance matrices. Once the unknown magnetic currents are found, the antenna characteristics can be determined.

2-2. Aperture Formulation

Figure 2.1 shows the problem to be considered and defines the coordinates and parameters to be used. The perfectly conducting plate covers the entire $z = 0$ plane except for the apertures which are rectangular in shape with side lengths a' and b' in the x and y directions, respectively. The apertures are centered in the waveguide cross sections. Note that all of the waveguides have the same dimensions (a,b) and all of the apertures have the same dimensions (a',b'). Also z is less than zero

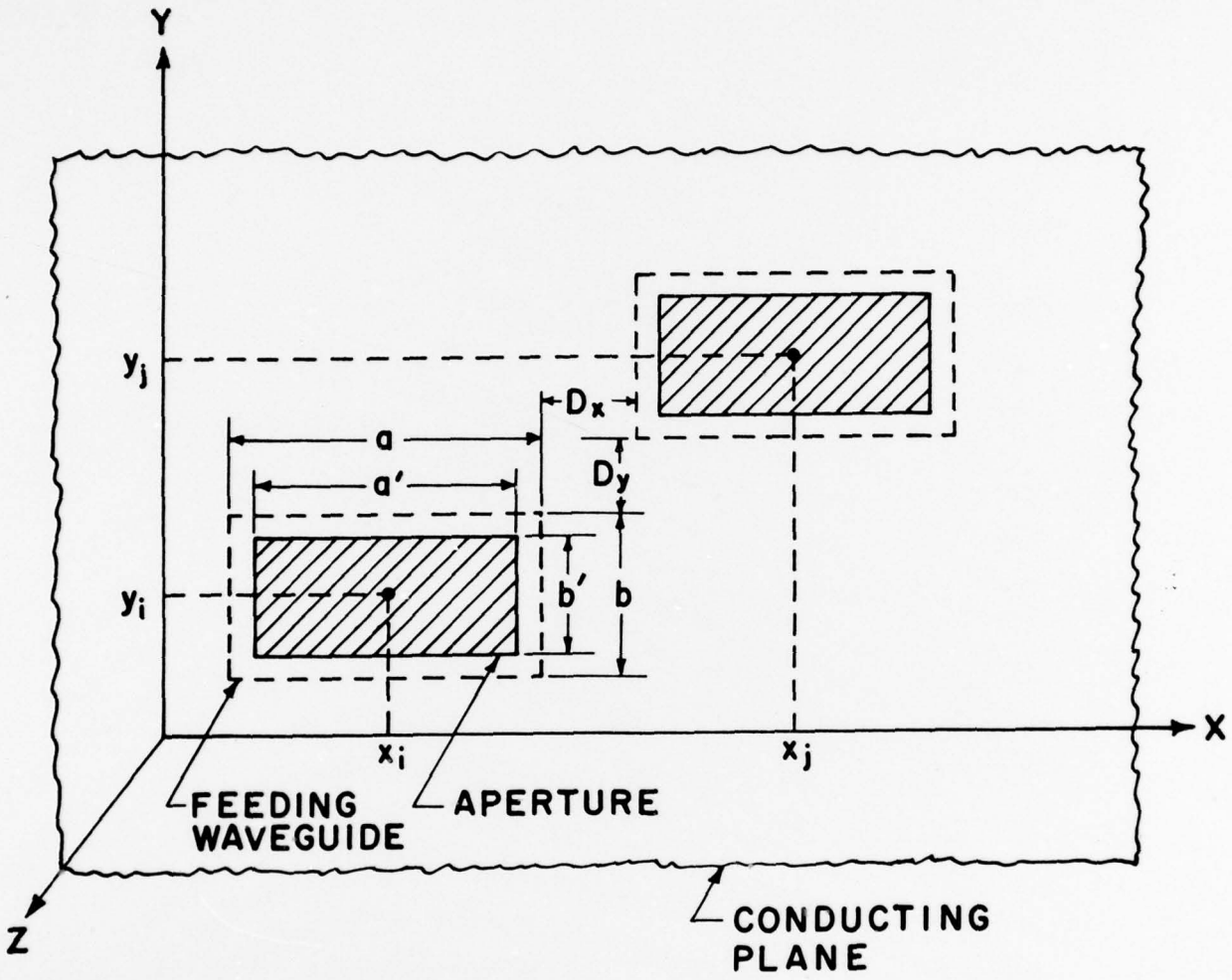

Fig. 2.1. Waveguide-fed rectangular apertures in a perfectly conducting plane.

in the waveguide region and z is greater than zero in the half-space region.

We first consider the problem of a single waveguide-fed aperture excited by impressed sources $\underset{\sim}{J}^{imp}$, $\underset{\sim}{M}^{imp}$ radiating into a half-space region (see Fig. 2.2a). The equivalence principle is used to divide this problem into two separate regions as follows (see Fig. 2.2b). The aperture is covered by an electric conductor. The fields in the waveguide region are produced by the impressed sources $\underset{\sim}{J}^{imp}$, $\underset{\sim}{M}^{imp}$, and the equivalent magnetic current $\underset{\sim}{M}$

$$\underset{\sim}{M} = \underset{\sim}{n} \times \underset{\sim}{E} \tag{2.1}$$

over the aperture region with the aperture covered by an electric conductor and $\underset{\sim}{n}$ is a unit vector normal to the aperture. The fields in the half-space region are produced by the equivalent magnetic current, $-\underset{\sim}{M}$, with the aperture covered by an electric conductor. The condition that the equivalent magnetic current in the waveguide region is $+\underset{\sim}{M}$ and in the half-space region $-\underset{\sim}{M}$, ensures that the tangential component of electric field is continuous across the aperture.

Another necessary boundary condition is the continuity of the tangential component of magnetic field across the aperture. The tangential magnetic field over the aperture on the waveguide side, $\underset{\sim}{H}_t^{wg}$, is equal to

$$\underset{\sim}{H}_t^{wg} = \underset{\sim}{H}_t^{imp} + \underset{\sim}{H}_t^{wg}(\underset{\sim}{M}) \tag{2.2}$$

where $\underset{\sim}{H}_t^{imp}$ is the tangential magnetic field due to impressed sources

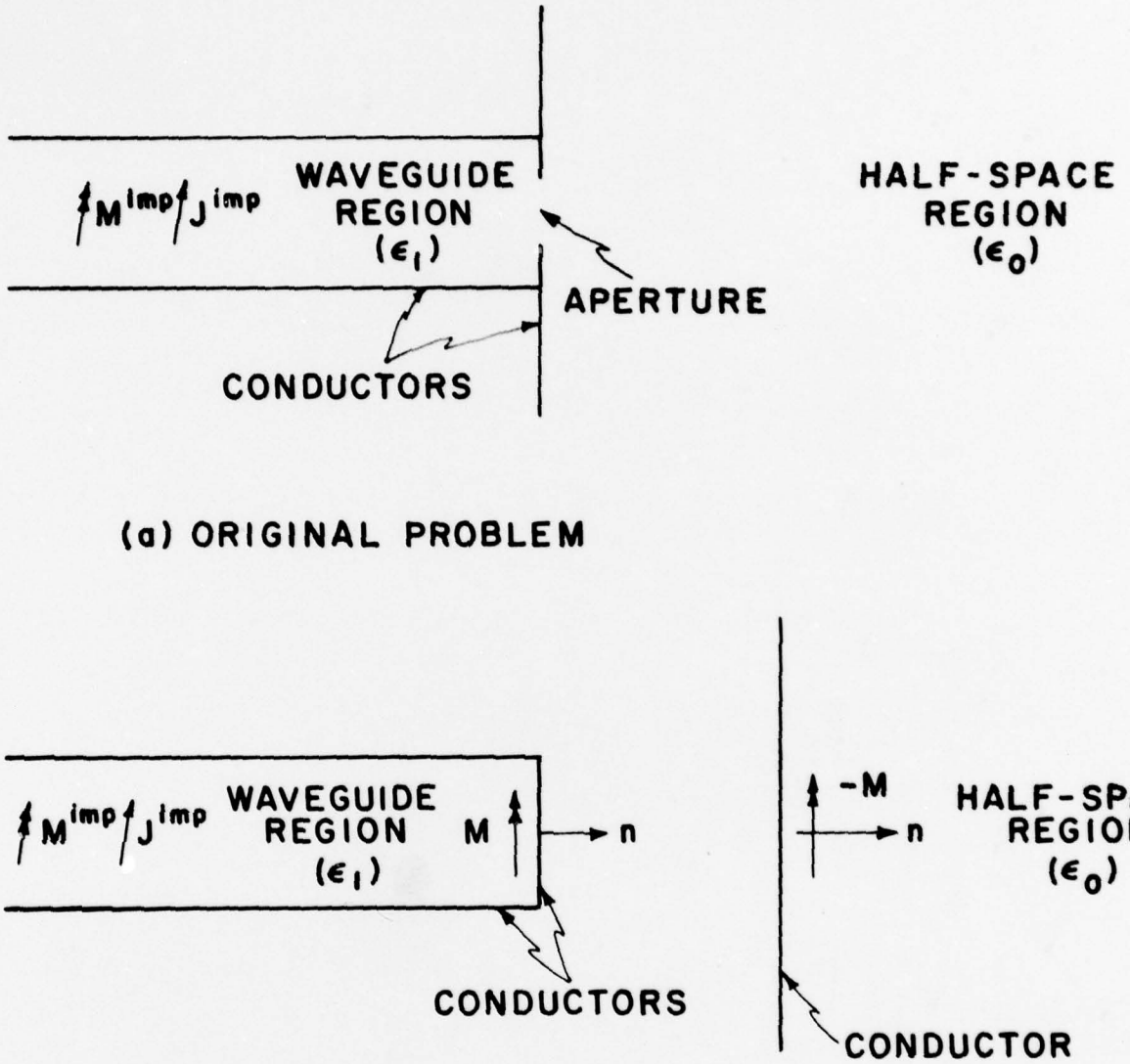

Fig. 2.2. A single waveguide-fed aperture radiating into half-space bounded by an electric conductor.

$\underset{\sim}{H}_t^{wg}(\underset{\sim}{M})$ is the tangential magnetic field due to the equivalent magnetic source $\underset{\sim}{M}$.

On the half-space side of the aperture we have

$$\underset{\sim}{H}_t^{hs} = \underset{\sim}{H}_t^{hs}(-\underset{\sim}{M}) = - \underset{\sim}{H}_t^{hs}(\underset{\sim}{M}) \ . \tag{2.3}$$

The last equality in (2.3) is a consequence of the linearity of the $\underset{\sim}{H}_t^{hs}$ operator. Note that $\underset{\sim}{H}_t^{imp}$, $\underset{\sim}{H}_t^{wg}(\underset{\sim}{M})$, and $\underset{\sim}{H}_t^{hs}(\underset{\sim}{M})$ are all computed with an electric conductor covering the aperture. The true solution is obtained when $\underset{\sim}{H}_t^{wg}$ of (2.2) equals $\underset{\sim}{H}_t^{hs}$ of (2.3) or

$$\underset{\sim}{H}_t^{wg}(\underset{\sim}{M}) + \underset{\sim}{H}_t^{hs}(\underset{\sim}{M}) = - \underset{\sim}{H}_t^{imp} \ . \tag{2.4}$$

This is the basic operator equation for determining the equivalent magnetic current $\underset{\sim}{M}$. In reality, only an approximate solution of equation (2.4) can be obtained.

At this point in the formulation we will extend our results to consider the multiple aperture case where one aperture is driven by impressed sources $\underset{\sim}{J}^{imp}$, $\underset{\sim}{M}^{imp}$, and the other apertures are parasitically excited. In this case the waveguide region is considered to include all of the waveguides and the half-space region is as before. For this case, (2.4) becomes

$$\underset{\sim}{H}_{t_i}^{wg}(\underset{\sim}{M}^i) + \sum_{j=1}^{N} \underset{\sim}{H}_{t_i}^{hs}(\underset{\sim}{M}^j) = \begin{cases} 0 & i \neq NFP \\ -\underset{\sim}{H}_{t_i}^{imp} & i = NFP \end{cases} \tag{2.5}$$

$$i = 1, 2, \ldots, N \ .$$

(N is the number of apertures and NFP is the aperture number corresponding to the driven port of the array.) In Eq. (2.5), $\underset{\sim}{M}^j$ is the equivalent magnetic current for the jth aperture. The subscript i denotes magnetic field evaluation in the ith aperture.

Let

$$\underset{\sim}{M}^j = V_j \, \underset{\sim}{M}_j \tag{2.6}$$

where V_j is a complex constant to be determined and $\underset{\sim}{M}_j$ is an expansion function to be specified. Substituting (2.6) into (2.5), we obtain

$$V_i \, \underset{\sim}{H}^{wg}_{t_i}(\underset{\sim}{M}_i) + \sum_{j=1}^{N} V_j \, \underset{\sim}{H}^{hs}_{t_i}(\underset{\sim}{M}_j) = \begin{cases} 0 & i \neq NFP \\ -\underset{\sim}{H}^{imp}_{t_i} & i = NFP \end{cases} \tag{2.7}$$

$$i = 1, 2, \ldots, N.$$

Next, we define the symmetric product $\langle A,B \rangle$ of two vectors $\underset{\sim}{A}$ and $\underset{\sim}{B}$ by

$$\langle A,B \rangle = \iint_{\text{apert.}} \underset{\sim}{A} \cdot \underset{\sim}{B} \, ds \tag{2.8}$$

where the integral is over all aperture regions. Also, we define a set of testing functions $\{\underset{\sim}{W}_i, \; i=1,2,\ldots,N\}$ which may or may not be equal to the expansion functions. Then, taking the symmetric product of (2.7) with the testing function $\underset{\sim}{W}_i$, we obtain

$$V_i \langle W_i, H^{wg}_{t_i}(M_i) \rangle + \sum_{j=1}^{N} V_j \langle W_i, H^{hs}_{t_i}(M_j) \rangle = \begin{cases} 0 & i \neq NFP \\ -\langle W_i, H^{imp}_{t_i} \rangle & i = NFP \end{cases} \tag{2.9}$$

$$i = 1,2,\ldots, N.$$

Solution of this set of linear equations determines the coefficient V_j and, therefore, the equivalent magnetic current $\underset{\sim}{M}^j$.

Equation (2.9) can be rewritten in matrix notation as follows: Define an element of the admittance matrix for the waveguide regions as

$$Y_{ij}^{wg} = \delta_{ij} \langle -W_i, H_{t_i}^{wg}(M_i) \rangle \tag{2.10}$$

where δ_{ij} is the Kronecker delta function

$$\delta_{ij} = \begin{cases} 1 & i = j \\ 0 & i \neq j \end{cases} \tag{2.11}$$

and for the half-space region as

$$Y_{ij}^{hs} = \langle -W_i, H_{t_i}^{hs}(M_j) \rangle \ . \tag{2.12}$$

The minus signs are placed in (2.10) and (2.12) on the basis of power considerations. Define an element of the source vector as

$$I_i^{imp} = \delta_{i\ NFP} \langle W_i, H_{t_i}^{imp} \rangle \tag{2.13}$$

and a coefficient vector

$$\vec{V} = [V_i]_{N\times 1} \ . \tag{2.14}$$

The resulting matrix equation which is equivalent to (2.9) is

$$[Y^{wg} + Y^{hs}]\vec{V} = \vec{I}^{imp} \ . \tag{2.15}$$

The physical interpretation of (2.15) is that of two generalized admittance networks, $[Y^{wg}]$ and $[Y^{hs}]$, in parallel with the current

source $\vec{I}^{imp}$. By inverting (2.15), we obtain the resulting voltage vector $\vec{V}$ which is the vector of coefficients which determines $\underset{\sim}{M}$

$$\vec{V} = [Y^{wg} + Y^{hs}]^{-1} \vec{I}^{imp} \quad . \tag{2.16}$$

The expansion ($\underset{\sim}{M}_i$) and testing ($\underset{\sim}{W}_i$) functions are defined as

$$\underset{\sim}{M}_i = \underset{\sim}{W}_i = - \underset{\sim}{u}_x \, P_i(x,y) \cos \frac{\pi}{a'} (x - x_i) \tag{2.17}$$

where

$$P_i(x,y) = \begin{cases} \sqrt{\frac{2}{a'b'}} & x_i - \frac{a'}{2} \leq x \leq x_i + \frac{a'}{2} \\ & y_i - \frac{b'}{2} \leq y \leq y_i + \frac{b'}{2} \\ 0 & \text{all other } x, y \, . \end{cases} \tag{2.18}$$

2-3. Determination of Y^{wg}_{ij}

To evaluate the aperture admittance in the waveguide region (2.10), we consider two separate cases. The first case will be the aperture admittance for the driven waveguide while the second case will be for the shorted waveguide (reactive load).

2-3.1. Driven Waveguide Aperture Admittance

Consider a single expansion function $\underset{\sim}{M}_i$ on the z=0 plane in the ith waveguide region where i = NFP. The tangential field produced by $\underset{\sim}{M}_i$ can be expressed in modal form as [20, Sec. 8-1]

$$\underset{\sim}{E}_t^{wg}(\underset{\sim}{M}_i) = \sum_k A_{ik}\, e^{\gamma_k z}\, \underset{\sim}{e}_k$$

$$\underset{\sim}{H}_t^{wg}(\underset{\sim}{M}_i) = -\sum_k A_{ik} Y_k\, e^{\gamma_k z}\, \underset{\sim}{u}_z \times \underset{\sim}{e}_k \tag{2.19}$$

where A_{ik} are modal amplitudes, γ_k are modal propagation constants, Y_k are modal characteristic admittances, and $\underset{\sim}{e}_k$ are normalized modal vectors. The modal vector orthogonality relationship is

$$\iint_{guide} \underset{\sim}{e}_i \cdot \underset{\sim}{e}_j ds = \begin{cases} 0 & i \neq j \\ 1 & i = j \end{cases} \tag{2.20}$$

where the integration is over the waveguide cross section. At z=0, we have

$$\underset{\sim}{M}_i = \underset{\sim}{u}_z \times \underset{\sim}{E}_t^{wg}(\underset{\sim}{M}_i)\Big|_{z=0} = \sum_k A_{ik} \underset{\sim}{u}_z \times \underset{\sim}{e}_k \,. \tag{2.21}$$

Multiply each side of this equation scalarly by $\underset{\sim}{u}_z \times \underset{\sim}{e}_j$ and integrate over the waveguide cross section obtaining

$$\iint_{guide} \underset{\sim}{M}_i \cdot \underset{\sim}{u}_z \times \underset{\sim}{e}_j ds = \sum_k A_{ik} \iint_{guide} (\underset{\sim}{u}_z \times \underset{\sim}{e}_k) \cdot (\underset{\sim}{u}_z \times \underset{\sim}{e}_j) ds \,. \tag{2.22}$$

By orthogonality (2.20), all terms of the summation are zero except the k=j term. Hence

$$A_{ik} = \iint_{apert.} \underset{\sim}{M}_i \cdot \underset{\sim}{u}_z \times \underset{\sim}{e}_k \, ds \,. \tag{2.23}$$

We have replaced the integral over the waveguide cross section by one

over the aperture since $\underset{\sim}{M}_i$ exists only in the aperture region. Substituting the second equation of (2.19) evaluated at z=0 into (2.10), we obtain

$$Y_{ij}^{wg} = \delta_{ij} \sum_k A_{ik} Y_k \iint_{apert.} \underset{\sim}{W}_i \cdot \underset{\sim}{u}_z \times \underset{\sim}{e}_k \, ds \quad . \tag{2.24}$$

Since $\underset{\sim}{M}_i = \underset{\sim}{W}_i$, (2.24) becomes

$$\begin{aligned} Y_{ij}^{wg} &= \delta_{ij} \sum_k A_{ik}^2 Y_k \\ &= \delta_{ij} \{\sum_k [(A_{ik}^{TE})^2 Y_k^{TE} + (A_{ik}^{TM})^2 Y_k^{TM}]\} \end{aligned} \tag{2.25}$$

where A_{ik}^{TE} and A_{ik}^{TM} are respectively the TE and TM modal amplitudes while Y_k^{TE} and Y_k^{TM} are respectively the TE and TM characteristic admittances.

A_{ik}^{TE} and A_{ik}^{TM} are obtained by first splitting the $\underset{\sim}{e}_k$ into a set of TE modes given by [20, Equations (8-34, 3-86), and (3-89) and Sec. 4-3]

$$\begin{aligned} \underset{\sim}{e}_{m+n(L_m+1)}^{TE} = \sqrt{\frac{ab\,\varepsilon_m\,\varepsilon_n}{(mb)^2 + (na)^2}} \Big[\underset{\sim}{u}_x \frac{n}{b} \cos\frac{m\pi x}{a} \sin\frac{n\pi y}{b} \\ - \underset{\sim}{u}_y \frac{m}{a} \sin\frac{m\pi x}{a} \cos\frac{n\pi y}{b} \Big] \end{aligned} \tag{2.26}$$

$$m = 0, 1, 2, \ldots, L_m$$

$$m + n \neq 0$$

$$n = 0, 1, 2, \ldots, L_n$$

$$\varepsilon_m = \begin{cases} 1 & m = 0 \\ 2 & m = 1,2,\ldots \end{cases}$$

and a set $\underset{\sim}{e}_k^{TM}$ of TM modes given by

$$\underset{\sim}{e}^{TM}_{m+(n-1)L_m} = 2\sqrt{\frac{ab}{(mb)^2 + (na)^2}}\ \left[\underset{\sim}{u}_x \frac{m}{a} \cos\frac{m\pi x}{a} \sin\frac{n\pi y}{b}\right.$$

$$\left. + \underset{\sim}{u}_y \frac{n}{b} \sin\frac{m\pi x}{a} \cos\frac{n\pi y}{b}\right] \qquad (2.27)$$

$$m = 1, 2, 3, \ldots, L_m$$

$$n = 1, 2, 3, \ldots, L_n \ .$$

Note that Eqs. (2.26) and (2.27) are valid only when the origin is at the corner of the waveguide.

Substituting (2.17), (2.26), and (2.27) into (2.23), we obtain

$$A^{TE}_{ik} = \iint_{apert.} \underset{\sim}{M}_i \cdot \underset{\sim}{u}_z \times \underset{\sim}{e}^{TE}_k \, ds$$

$$= -\frac{m\pi}{k_{mn} a}\sqrt{\frac{2\varepsilon_m \varepsilon_n}{aa'bb'}}\ I(m,n) \qquad (2.28)$$

$$k = m+n(L_m+1) \begin{cases} m = 0, 1, 2, \ldots, L_m \\ n = 0, 1, 2, \ldots, L_n \end{cases} \qquad m+n \neq 0$$

and

$$A^{TM}_{ik} = \iint_{apert.} \underset{\sim}{M}_i \cdot \underset{\sim}{u}_z \times \underset{\sim}{e}^{TM}_k \, ds$$

$$= \frac{2n\pi}{k_{mn} b}\sqrt{\frac{2}{aa'bb'}}\ I(m,n) \qquad (2.29)$$

$$k = m+(n-1)L_m \begin{cases} m = 1, 2, 3, \ldots, L_m \\ n = 1, 2, 3, \ldots, L_n \end{cases}$$

where

$$k_{mn} = \sqrt{\left(\frac{m\pi}{a}\right)^2 + \left(\frac{n\pi}{b}\right)^2} \tag{2.30}$$

$$I(m,n) = \int_{(b-b')/2}^{(b+b')/2} dy \cos\frac{n\pi y}{b} \int_{(a-a')/2}^{(a+a')/2} dx \cos\frac{\pi}{a'}\left(x - \frac{a}{2}\right) \sin\frac{m\pi x}{a}$$

$$= -\frac{2b'}{\pi a'} \frac{1}{\left(\frac{m^2}{a^2} - \frac{1}{a'^2}\right)} \sin\frac{m\pi}{2} \cos\frac{n\pi}{2} \cos\frac{m\pi a'}{2a} \frac{\sin\frac{n\pi b'}{2b}}{\frac{n\pi b'}{2b}} \quad . \tag{2.31}$$

If $(a/a' = m)$ in (2.31), the $\cos(m\pi a'/2a)/(m^2/a^2 - 1/a'^2)$ term is to be replaced by its limit $(-\pi a'^2/4)$. If n is zero in (2.31), the sin ( )/( ) term is to be replaced by unity.

The characteristic admittances Y_i of a rectangular waveguide with relative dielectric constant ε_r and relative permeability unity are classified as either TE admittances Y_i^{TE} or TM admittances Y_i^{TM} given by [20, Sec. 4-3],

$$Y_i^{TE} = \begin{cases} -\frac{j}{\eta} \sqrt{\left(\frac{k_{mn}}{k}\right)^2 - \varepsilon_r} & k\sqrt{\varepsilon_r} < k_{mn} \\ \frac{1}{\eta} \sqrt{\varepsilon_r - \left(\frac{k_{mn}}{k}\right)^2} & k\sqrt{\varepsilon_r} > k_{mn} \end{cases} \tag{2.32}$$

$$i = m+n(L_m+1) \quad \begin{cases} m = 0, 1, 2, \ldots, L_m \\ n = 0, 1, 2, \ldots, L_n \end{cases} \qquad m+n \neq 0$$

and

$$Y_i^{TM} = \begin{cases} \dfrac{j}{\eta} \dfrac{\varepsilon_r}{\sqrt{(\frac{k_{mn}}{k})^2 - \varepsilon_r}} & k\sqrt{\varepsilon_r} < k_{mn} \\ \dfrac{1}{\eta} \dfrac{\varepsilon_r}{\sqrt{\varepsilon_r - (\frac{k_{mn}}{k})^2}} & k\sqrt{\varepsilon_r} > k_{mn} \end{cases} \tag{2.33}$$

$$i = m + (n-1)L_m \begin{cases} m = 1, 2, 3, \ldots, L_m \\ n = 1, 2, 3, \ldots, L_n \end{cases} .$$

In (2.32) and (2.33), η is the characteristic impedance of free space, k is the free space wave number, and k_{mn} is the cutoff wave number given by (2.30).

2-3.2. *Reactively Loaded Waveguide Aperture Admittance*

Consider a single expansion function $\underset{\sim}{M}_i$ on the z=0 plane in the waveguide region for the ith waveguide where i ≠ NFP. A short is placed at $z = -d_i$ with respect to the aperture. The tangential field produced by $\underset{\sim}{M}_i$ where only the dominant mode is propagating is

$$\underset{\sim}{E}_{t_i}^{wg}(\underset{\sim}{M}_i) = A'_{io}(e^{\gamma_o z} - e^{-\gamma_o(2d_i+z)})\,\underset{\sim}{e}_o + \sum_{k=1}^{\infty} A'_{ik}\, e^{\gamma_k z}\,\underset{\sim}{e}_k$$

$$\underset{\sim}{H}_{t_i}^{wg}(\underset{\sim}{M}_i) = -A'_{io}Y_o(e^{\gamma_o z} + e^{-\gamma_o(2d_i+z)})\,\underset{\sim}{u}_z \times \underset{\sim}{e}_o \tag{2.34}$$

$$- \sum_{k=1}^{\infty} A'_{ik}Y_k\, e^{\gamma_k z}\,\underset{\sim}{u}_z \times \underset{\sim}{e}_k$$

where the subscript o denotes the dominant mode and ' distinguishes A'_{ik} from A_{ik} used in the previous section. In (2.34), d_i is assumed to be

sufficiently large so that no evanescent modes are reflected by the short.

At $z = 0$, we have

$$\underset{\sim}{M}_i = \underset{\sim}{u}_z \times \underset{\sim}{E}_{t_i}^{wg}\Big|_{z=0}$$

$$= A'_{io}(1 - e^{-2\gamma_o d_i})\, \underset{\sim}{u}_z \times \underset{\sim}{e}_o + \sum_{k=1}^{\infty} A'_{ik}\, \underset{\sim}{u}_z \times \underset{\sim}{e}_k \ . \qquad (2.35)$$

Multiply each side of (2.35) scalarly by $\underset{\sim}{u}_z \times \underset{\sim}{e}_j$ and integrate over the waveguide cross section obtaining

$$\iint_{guide} \underset{\sim}{M}_i \cdot \underset{\sim}{u}_z \times \underset{\sim}{e}_j ds = A'_{io}(1 - e^{-2\gamma_o d_i}) \iint_{guide} (\underset{\sim}{u}_z \times \underset{\sim}{e}_o) \cdot (\underset{\sim}{u}_z \times \underset{\sim}{e}_j) ds$$

$$+ \sum_{k=1}^{\infty} A'_{ik} \iint_{guide} (\underset{\sim}{u}_z \times \underset{\sim}{e}_k) \cdot (\underset{\sim}{u}_z \times \underset{\sim}{e}_j) ds \ . \qquad (2.36)$$

By orthogonality, all terms of the summation in (2.36) are zero except the k=j term.

Hence,

$$A'_{io} = \frac{1}{1 - e^{-2\gamma_o d_i}} \iint_{apert.} \underset{\sim}{M}_i \cdot \underset{\sim}{u}_z \times \underset{\sim}{e}_o \, ds$$

$$= \frac{A_{io}}{1 - e^{-2\gamma_o d_i}} \qquad (2.37)$$

$$A'_{ik} = A_{ik} = \iint_{apert.} \underset{\sim}{M}_i \cdot \underset{\sim}{u}_z \times \underset{\sim}{e}_k \, ds \ . \qquad (2.38)$$
$$(k \neq 0)$$

Substituting (2.37) and (2.38) into (2.34) and then substituting (2.34) into (2.10), we obtain

$$Y_{ij}^{wg} = \delta_{ij} \langle -W_i, H_{t_i}^{wg}(M_i) \rangle$$

$(i \neq NFP)$

$$= \delta_{ij} \left\{ A_{io} \frac{(1 + e^{-2\gamma_o d_i})}{(1 - e^{-2\gamma_o d_i})} Y_o \iint_{apert.} \underset{\sim}{M}_i \cdot \underset{\sim}{u}_z \times \underset{\sim}{e}_o \, ds \right.$$

$$\left. + \sum_{k=1}^{\infty} A_{ik} Y_k \iint_{apert.} \underset{\sim}{M}_i \cdot \underset{\sim}{u}_z \times \underset{\sim}{e}_k \, ds \right\}$$

$$= \delta_{ij} \left\{ A_{io}^2 Y_o \frac{(1 + e^{-2\gamma_o d_i})}{(1 - e^{-2\gamma_o d_i})} + \sum_{k=1}^{\infty} \left[(A_{ik}^{TE})^2 Y_k^{TE} \right. \right.$$

$$\left. \left. + (A_{ik}^{TM})^2 Y_k^{TM} \right] \right\} . \qquad (2.39)$$

Substituting $j\beta_o$ for γ_o in (2.39), we obtain

$$Y_{ij}^{wg} = \delta_{ij} \left\{ - jA_{io}^2 Y_o \cot \beta_o d_i + \sum_{k=1}^{\infty} \left[(A_{ik}^{TE})^2 Y_k^{TE} + (A_{ik}^{TM})^2 Y_k^{TM} \right] \right\} . \qquad (2.40)$$

2-4. Determination of Y_{ij}^{hs}

The first part of this section will derive the aperture admittance in the half space region (Y_{ij}^{hs}) while the second part will treat the singular points of the integrands for the single integral representation of Y_{ij}^{hs}.

2-4.1. Derivation

Since the apertures are covered by conductors, the z=0 plane is a complete conducting plane and image theory applies. The magnetic current expansion functions are on the surface of the z=0 plane. Their images are equal to them and are also on the z=0 plane. The result is

that $[Y^{hs}]$ is the admittance matrix obtained using expansion functions $2\underset{\sim}{M}_j$ radiating into free space everywhere. Therefore, (2.12) can be written as

$$Y_{ij}^{hs} = - 2 \langle W_i, H_{t_i}^{fs}(M_j) \rangle \tag{2.41}$$

where $\underset{\sim}{H}_{t_i}^{fs}(\underset{\sim}{M}_j)$ is the magnetic field in the ith aperture region produced by $\underset{\sim}{M}_j$ radiating into free space. The magnetic field $\underset{\sim}{H}_{t_i}^{fs}(\underset{\sim}{M}_j)$ can be expressed in terms of an electric vector potential $\underset{\sim}{F}_{ij}$ and a magnetic scalar potential ϕ_{ij} as [21]

$$\underset{\sim}{H}_{t_i}^{fs}(\underset{\sim}{M}_j) = - j\omega \underset{\sim}{F}_{ij} - \nabla\phi_{ij} \tag{2.42}$$

where

$$\underset{\sim}{F}_{ij} = \frac{\varepsilon}{4\pi} \iint_{apert.} \underset{\sim}{M}_j \frac{e^{-jk|\underset{\sim}{r}-\underset{\sim}{r}'|}}{|\underset{\sim}{r} - \underset{\sim}{r}'|} ds \tag{2.43}$$

$$\phi_{ij} = \frac{1}{4\pi\mu} \iint_{apert.} \rho_j \frac{e^{-jk|\underset{\sim}{r}-\underset{\sim}{r}'|}}{|\underset{\sim}{r} - \underset{\sim}{r}'|} ds \tag{2.44}$$

$$\rho_j = \frac{\nabla \cdot \underset{\sim}{M}_j}{- j\omega} \tag{2.45}$$

where $\underset{\sim}{r}$ and $\underset{\sim}{r}'$ are respectively the vectors to the field and source points, ω is the angular frequency, ε is the permittivity of free space, μ is the permeability of free space, and k is the free space propagation constant. Substituting (2.42) into (2.41) and using (2.8), we obtain

$$Y_{ij}^{hs} = 2 \iint_{apert.} \underset{\sim}{W}_i \cdot (j\omega \underset{\sim}{F}_{ij} + \underset{\sim}{\nabla}\phi_{ij})ds \quad . \tag{2.46}$$

Because of the identity

$$0 = \iint_{apert.} \underset{\sim}{\nabla} \cdot (\phi_{ij}\underset{\sim}{W}_i)ds = \iint_{apert.} \underset{\sim}{W}_i \cdot \underset{\sim}{\nabla}\phi_{ij} ds + \iint_{apert.} \phi_{ij}\underset{\sim}{\nabla} \cdot \underset{\sim}{W}_i ds \ , \tag{2.47}$$

(2.46) becomes

$$Y_{ij}^{hs} = 2j\omega \iint_{apert.} (\underset{\sim}{F}_{ij} \cdot \underset{\sim}{W}_i + \phi_{ij}\rho_i)ds \tag{2.48}$$

where

$$\rho_i = \frac{\underset{\sim}{\nabla} \cdot \underset{\sim}{W}_i}{-j\omega} \quad . \tag{2.49}$$

Substituting (2.17), (2.43), (2.44), and (2.49) into (2.48), we obtain

$$\begin{aligned} Y_{ij}^{hs} = {} & \frac{j\omega\varepsilon}{\pi a' b'} \int_{y_i - \frac{b'}{2}}^{y_i + \frac{b'}{2}} dy \int_{x_i - \frac{a'}{2}}^{x_i + \frac{a'}{2}} dx \cos\frac{\pi}{a'}(x - x_i) \\ & \cdot \int_{y_j - \frac{b'}{2}}^{y_j + \frac{b'}{2}} dy' \int_{x_j - \frac{a'}{2}}^{x_j + \frac{a'}{2}} dx' \cos\frac{\pi}{a'}(x' - x_j)\, G(x' - x, y' - y) \\ & - \frac{j\pi}{\omega\mu a'^3 b'} \int_{y_i - \frac{b'}{2}}^{y_i + \frac{b'}{2}} dy \int_{x_i - \frac{a'}{2}}^{x_i + \frac{a'}{2}} dx \sin\frac{\pi}{a'}(x - x_i) \\ & \cdot \int_{y_j - \frac{b'}{2}}^{y_j + \frac{b'}{2}} dy' \int_{x_j - \frac{a'}{2}}^{x_j + \frac{a'}{2}} dx' \sin\frac{\pi}{a'}(x' - x_j)\, G(x'-x, y'-y) \end{aligned} \tag{2.50}$$

where

$$G(x'-x,\ y'-y) = \frac{e^{-jk\sqrt{(x'-x)^2 + (y'-y)^2}}}{\sqrt{(x'-x)^2 + (y'-y)^2}} . \qquad (2.51)$$

Substituting the coordinate transformation $x' = u + x$ and $y' = v + y$ into (2.50), interchanging the order of integration and carrying out the integrations in the two variables x and y (see Appendix A.1), we obtain

$$Y_{ij}^{hs} = \frac{jk}{2\pi\eta a'b'} \left\{ \int_{y_j-y_i-b'}^{y_j-y_i} dv(K_1+v) \right.$$

$$\cdot \left[\int_{x_j-x_i-a'}^{x_j-x_i} du\ G(u,v)\left[(K_2+K_3u)\cos\frac{\pi u}{a'} + (K_4+K_5u)\sin\frac{\pi u}{a'}\right]\right.$$

$$\left. + \int_{x_j-x_i}^{x_j-x_i+a'} du\ G(u,v)\left[(K_7-K_3u)\cos\frac{\pi u}{a'} + (K_8-K_5u)\sin\frac{\pi u}{a'}\right]\right]$$

$$+ \int_{y_j-y_i}^{y_j-y_i+b'} dv(K_6-v)\left[\int_{x_j-x_i-a'}^{x_j-x_i} du\ G(u,v)\left[(K_2+K_3u)\cos\frac{\pi u}{a'} + (K_4+K_5u)\sin\frac{\pi u}{a'}\right]\right.$$

$$\left. \left. + \int_{x_j-x_i}^{x_j-x_i+a'} du\ G(u,v)\ \left[(K_7-K_3u)\cos\frac{\pi u}{a'} + (K_8-K_5u)\sin\frac{\pi u}{a'}\right]\right]\right\} \qquad (2.52)$$

(constants K_1 - K_8 are defined in Appendix A.1).

Equation (2.52) can be further reduced by substituting the coordinate transformation $u = \rho \cos\theta$ and $v = \rho \sin\theta$ into (2.52) and integrating out the ρ variable to obtain (see Appendix A.1)

$$Y_{ij}^{hs} = \frac{jk}{2\pi\eta a'b'} \{ \underbrace{\int_{\theta_1}^{\theta_2} [K_1[K_2L_1(\theta) + K_3L_3(\theta) + K_4L_2(\theta) + K_5L_4(\theta)]}_{\text{(I)}}$$

$$+ [K_2L_5(\theta) + K_3L_7(\theta) + K_4L_6(\theta) + K_5L_8(\theta)]] \, d\theta$$

$$+ \underbrace{\int_{\theta_3}^{\theta_4} [K_1[K_7L_1(\theta) - K_3L_3(\theta) + K_8L_2(\theta) - K_5L_4(\theta)]}_{\text{(II)}}$$

$$+ [K_7L_5(\theta) - K_3L_7(\theta) + K_8L_6(\theta) - K_5L_8(\theta)]] \, d\theta$$

$$+ \underbrace{\int_{\theta_4}^{\theta_5} [K_6[K_2L_1(\theta) + K_3L_3(\theta) + K_4L_2(\theta) + K_5L_4(\theta)]}_{\text{(III)}}$$

$$- [K_2L_5(\theta) + K_3L_7(\theta) + K_4L_6(\theta) + K_5L_8(\theta)]] \, d\theta$$

$$+ \underbrace{\int_{\theta_6}^{\theta_7} [K_6[K_7L_1(\theta) - K_3L_3(\theta) + K_8L_2(\theta) - K_5L_4(\theta)]}_{\text{(IV)}}$$

$$- [K_7L_5(\theta) - K_3L_7(\theta) + K_8L_6(\theta) - K_5L_8(\theta)]]\} d\theta \qquad (2.53)$$

(constants $L_1(\theta) - L_8(\theta)$ are defined in Appendix A.1).

2-4.2. Singular Points of the Single Integral Formulation of Y_{ij}^{hs}

The integrand of the single integral representation of Y_{ij}^{hs} (2.53) has removable singularities when $ka' \leq \pi$. When either $|\frac{\pi}{a'} \cos\theta - k| < \varepsilon$ (small value) or $|\frac{\pi}{a'} \cos\theta + k| < \varepsilon$, we replace equations (A.25-A.32) by their respective limits. For an example, consider Eq. (A.25)

$$L_1(\theta) = \frac{-j}{2}\left\{\frac{M_1(\theta) - M_2(\theta)}{M_5(\theta)} - \frac{M_3(\theta) - M_4(\theta)}{M_6(\theta)}\right\}$$

$$= \frac{-j}{2}\left\{\frac{e^{j\rho_2(\theta)(\frac{\pi}{a'}\cos\theta - k)} - e^{j\rho_1(\theta)(\frac{\pi}{a'}\cos\theta - k)}}{(\frac{\pi}{a'}\cos\theta - k)}\right.$$

$$\left. - \frac{e^{-j\rho_2(\theta)(\frac{\pi}{a'}\cos\theta + k)} - e^{-j\rho_1(\theta)(\frac{\pi}{a'}\cos\theta + k)}}{(\frac{\pi}{a'}\cos\theta + k)}\right\} . \qquad (A.25)$$

If $|\frac{\pi}{a'} \cos\theta - k| < \varepsilon$, then by retaining the first three terms of the Taylor series for the exponentials in the first half of (A.25), we obtain

$$L_1(\theta) = \frac{-j}{2}\left\{1 + j\rho_2(\theta)(\frac{\pi}{a'}\cos\theta - k) - \frac{1}{2}[\rho_2(\theta)(\frac{\pi}{a'}\cos\theta - k)]^2\right.$$

$$\frac{-1 - j\rho_1(\theta)(\frac{\pi}{a'}\cos\theta - k) + \frac{1}{2}[\rho_1(\theta)(\frac{\pi}{a'}\cos\theta - k)]^2}{\frac{\pi}{a'}\cos\theta - k}$$

$$\left. - \frac{M_3(\theta) - M_4(\theta)}{M_6(\theta)}\right\} . \qquad (2.54)$$

If we take the limit as $\frac{\pi}{a'}\cos\theta$ approaches k for the first half of (2.54), we obtain

$$L_1(\theta) = \frac{1}{2}\,(\rho_2(\theta) - \rho_1(\theta)) + \frac{j}{2}\,\left(\frac{M_3(\theta) - M_4(\theta)}{M_6(\theta)}\right) \quad . \tag{2.55}$$

If $\left|\frac{\pi}{a'}\cos\theta + k\right| < \varepsilon$, then by retaining the first three terms of the Taylor series for the exponentials in the second half of (A.25), we obtain

$$L_1(\theta) = \frac{-j}{2}\,\left(\frac{M_1(\theta) - M_2(\theta)}{M_5(\theta)}\right) + \frac{1}{2}\,(\rho_2(\theta) - \rho_1(\theta)) \quad . \tag{2.56}$$

The results for applying the preceding procedure to Eqs. (A.26-A.32) can be found in Appendix A.2.

2-5. Gain Formulation

2-5.1. Determination of Measurement Vector - $\vec{P}^m$

A linear measurement is defined as a number which depends linearly on the source. Measurements made in the half-space region will depend linearly only on the equivalent current $-\underset{\sim}{M}^i$.

Consider the measurement of a component H_m of magnetic field at a point $\underset{\sim}{r}_m$ in the half-space region for a single aperture i (see Fig. 2.3). It is known that this component can be obtained by placing a magnetic dipole $K\ell_m$ at $\underset{\sim}{r}_m$, and applying the reciprocity theorem to its field and to the original field [20, Sec. 3-8] or

$$H_m K\ell_m = -\iint_{\text{apert.}} \underset{\sim}{M}^i \cdot \underset{\sim}{H}_t^m \, ds \quad . \tag{2.57}$$

Here $\underset{\sim}{H}_t^m$ is the magnetic field from $K\ell_m$ in the presence of a complete conductor, and H_m is the component in the direction of $K\ell_m$ of the

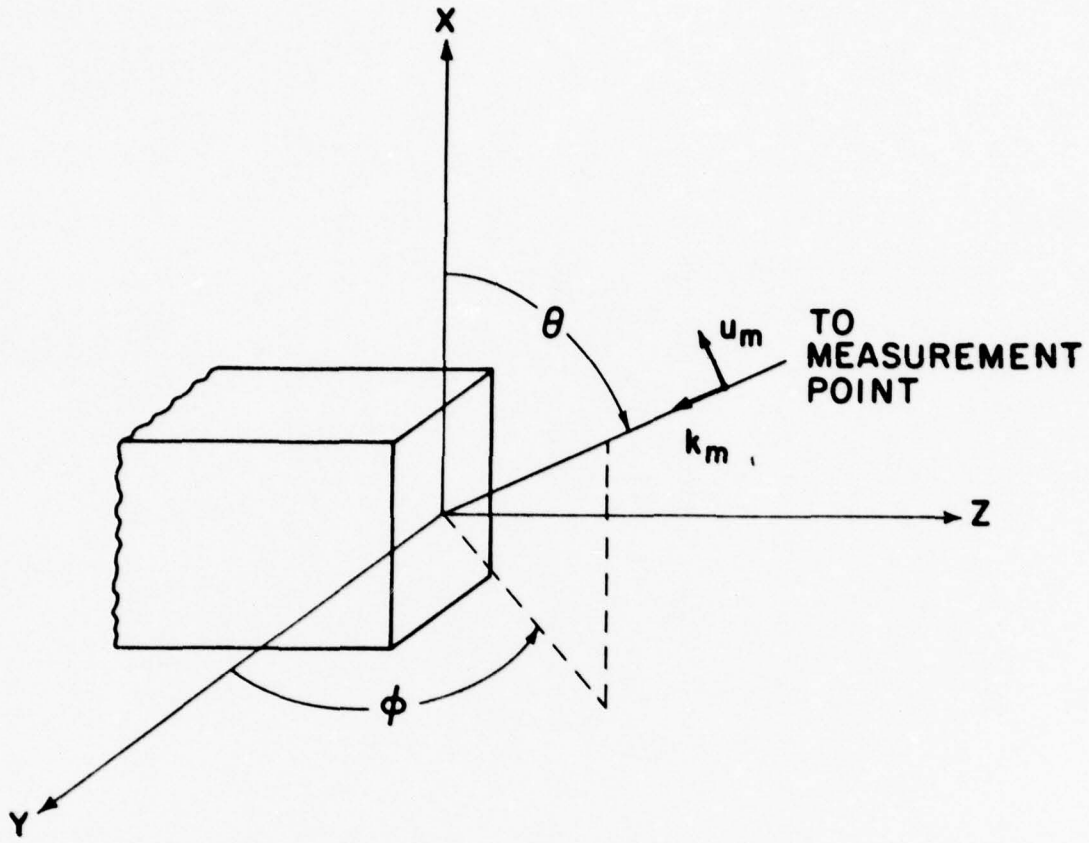

Fig. 2.3. Measurement vector geometry.

magnetic field at $\underset{\sim}{r}_m$ due to $-\underset{\sim}{M}^i$ in the presence of a complete conductor. To evaluate (2.57), substitute for $\underset{\sim}{M}^i$ and obtain

$$H_m K\ell_m = V_i <- M_i, H_t^m> . \tag{2.58}$$

Now since $K\ell_m$ is radiating in the presence of a complete conductor, image theory applies. The result is that the tangential component of $\underset{\sim}{H}$ over the aperture from $K\underset{\sim}{\ell}_m$ when the z=0 plane is covered by a conductor is equal to twice what it is for the same source in free space. Hence,

$$\underset{\sim}{H}_t^m = 2\ \underset{\sim}{H}_t^{mo} . \tag{2.59}$$

$\underset{\sim}{H}_t^{mo}$ denotes the tangential component of H over the aperture from $K\underset{\sim}{\ell}_m$ when it radiates into free space. Using this fact, (2.58) becomes

$$\begin{aligned} H_m K\ell_m &= 2\ V_i <- M_i, H_t^{mo}> \\ &= I_i^m V_i \end{aligned} \tag{2.60}$$

where

$$\begin{aligned} I_i^m &= 2 <- M_i, H_t^{mo}> \\ &= -2 \iint_{\text{apert.}} \underset{\sim}{M}_i \cdot \underset{\sim}{H}_t^{mo}\ ds . \end{aligned} \tag{2.61}$$

A case of special interest is that of far-field measurement. This is obtained by a procedure dual to that used for radiation and scattering from conducting wires [15]. To obtain a component of $\underset{\sim}{H}$ on the radiation sphere, we take a source $K\underset{\sim}{\ell}_m$ perpendicular to $\underset{\sim}{r}_m$ and let $r_m \to \infty$. At the same time we adjust $K\ell_m$ so that it produces a unit

plane wave in the vicinity of the origin. The required dipole moment is given by

$$\frac{1}{K\ell_m} = \frac{-j\omega\varepsilon}{4\pi r_m} e^{-jkr_m} \tag{2.62}$$

and the plane wave field it produces in the vicinity of the origin is

$$\underset{\sim}{H}^{mo} = \underset{\sim}{u}_m e^{-j\underset{\sim}{k}_m \cdot \underset{\sim}{r}} . \tag{2.63}$$

Here $\underset{\sim}{u}_m$ is a unit vector in the direction of $\underset{\sim}{H}^{mo}$, $\underset{\sim}{k}_m$ is the propagation vector, and $\underset{\sim}{r}$ is the radius vector to an arbitrary field point. Substituting (2.63) into (2.61), we obtain the components $P_i^m(\theta,\phi)$ of the far-field measurement vector $\vec{P}^m$ where

$$P_i^m(\theta,\phi) = -2 \iint_{\text{apert.}} \underset{\sim}{M}_i \cdot \underset{\sim}{u}_m e^{-j\underset{\sim}{k}_m \cdot \underset{\sim}{r}} ds \tag{2.64}$$

(the symbol $\vec{P}^m$ is used for this particular measurement vector to distinguish it from a more general measurement vector $\vec{I}^m$).

Two measurement vectors of interest are $(P_i^m)_{xx}$ and $(P_i^m)_{\theta\phi}$. $(P_i^m)_{xx}$ is for a $\underset{\sim}{u}_x$ polarized measurement in the x=0 plane while $(P_i^m)_{\theta\phi}$ is for a $\underset{\sim}{u}_\theta$ polarized measurement in the ϕ = constant plane. $(P_i^m)_{xx}$ is used to obtain E-plane pattern gain while $(P_i^m)_{\theta\phi}$ is used to obtain H-plane pattern gain.

$$(P_i^m)_{xx} = -2 \iint_{\text{apert.}} \underset{\sim}{M}_i \cdot \underset{\sim}{u}_x \, e^{jky \cos\phi} \, dxdy$$

$$= 2\sqrt{\frac{2}{a'b'}} \int_{x_i - \frac{a'}{2}}^{x_i + \frac{a'}{2}} dx \cos\frac{\pi}{a'}(x-x_i) \int_{y_i - \frac{b'}{2}}^{y_i + \frac{b'}{2}} e^{jky\cos\phi} \, dy$$

$$= \frac{4}{\pi}\sqrt{2a'b'}\, e^{jky_i\cos\phi} \, \frac{\sin(\frac{kb'}{2}\cos\phi)}{\frac{kb'}{2}\cos\phi} \quad . \tag{2.65}$$

For $\phi = \frac{\pi}{2}$, $\sin(\frac{kb'}{2}\cos\phi)/(\frac{kb'}{2}\cos\phi)$ in (2.65) is to be replaced by its limit one.

$$(P_i^m)_{\theta\phi} = -2 \iint_{\text{apert.}} \underset{\sim}{M}_i \cdot \underset{\sim}{u}_\theta \, e^{jk(x\cos\theta + y\sin\theta\cos\phi)} \, dxdy$$

$$= -2\sqrt{\frac{2}{a'b'}} \sin\theta \int_{y_i - \frac{b'}{2}}^{y_i + \frac{b'}{2}} dy \, e^{jky\sin\theta\cos\phi} \int_{x_i - \frac{a'}{2}}^{x_i + \frac{a'}{2}} \cos\frac{\pi}{a'}(x-x_i) e^{jkx\cos\theta} dx$$

$$= -4\pi\sqrt{2a'b'}\sin\theta \, e^{jk(x_i\cos\theta + y_i\sin\theta\cos\phi)} \, \frac{\cos(\frac{ka'}{2}\cos\theta)}{\pi^2 - k^2a'^2\cos^2\theta}$$

$$\cdot \frac{\sin(\frac{kb'}{2}\sin\theta\cos\phi)}{\frac{kb'}{2}\sin\theta\cos\phi} \quad . \tag{2.66}$$

For $\theta = 0$ or π or $\phi = \frac{\pi}{2}$, the sin ( )/( ) term in (2.66) is to be replaced by its limit one. For $\theta = \cos^{-1}(\frac{\pm\pi}{ka'})$, the $\cos(\frac{ka'}{2}\cos\theta)/(\pi^2 - k^2a'^2\cos^2\theta)$ term in (2.66) is to be replaced by its limit $\frac{1}{4\pi}$.

2-5.2. Determination of Pattern Gain

If we extend the preceding development to the multiple aperture case, (2.58) becomes

$$H_m K\ell_m = \sum_{i=1}^{N} V_i \, \langle - M_i, H^m_{t_i} \rangle$$

$$= \tilde{I}^m \vec{V} \tag{2.67}$$

where $\tilde{I}^m$ is the transpose of the measurement vector

$$\vec{I}^m = [\langle - M_i, H^m_{t_i} \rangle]_{N\times 1} \quad . \tag{2.68}$$

If we adjust $K\ell_m$ so that it produces a unit plane wave in the vicinity of the origin (2.62), then substituting (2.62) and (2.64) into (2.67), we obtain the far-zone magnetic field

$$H_m = \frac{-j\omega\epsilon}{4\pi r_m} e^{-jkr_m} \tilde{P}^m \vec{V} \quad . \tag{2.69}$$

The usual two radiation components H_θ and H_ϕ are obtained by orienting $K\ell_m$ in the θ and ϕ directions, respectively.

The complex power P_t transmitted through an aperture is

$$P_t = \iint_{\text{apert.}} \underset{\sim}{E} \times \underset{\sim}{H}^* \cdot \underset{\sim}{u}_z \, ds$$

$$= \iint_{\text{apert.}} \underset{\sim}{M} \cdot \underset{\sim}{H}^* \, ds \tag{2.70}$$

(* signifies complex conjugate).

Since this transmitted power is only dependent on the tangential component of H in the half-space region ($\underset{\sim}{H}^{hs}_t(-\underset{\sim}{M})$), (2.70) becomes for the multiple aperture case

$$P_t = -\sum_{i=1}^{N}\sum_{j=1}^{N} V_i V_j^* \iint_{\text{apert.}} \underset{\sim}{M}_i \cdot (\underset{\sim}{H}^{hs}_{t_i}(\underset{\sim}{M}_j))^* ds$$

$$= \tilde{V}[Y^{hs}]^{*\rightarrow *} V^* \quad . \tag{2.71}$$

The gain (ratio of radiation intensity in a given direction to the radiation which would exist if the total power, P_t, were radiated uniformly over the half-space region) associated with the $\underset{\sim}{u}_m$ component of the magnetic field in the half-space region ($z > 0$) is given by

$$G = \frac{2\pi r_m^2 \eta |H_m|^2}{\text{Real } (P_t)} \quad . \tag{2.72}$$

Substituting (2.69) and (2.71) into (2.72), we obtain

$$G = \frac{k^2}{8\pi\eta} \frac{|\tilde{P}^m V|^2}{\text{Real } (\tilde{V}[Y^{hs}]^{*\rightarrow *} V^*)} \quad . \tag{2.73}$$

The reactively loaded array gain is obtained by substituting (2.16) into (2.73)

$$G = \frac{k^2}{8\pi\eta} \frac{|\tilde{P}^m [Y^{wg+Y^{hs}}]^{-1\rightarrow} I^{imp}|^2}{\text{Real } ([Y^{wg+Y^{hs}}]^{-1\rightarrow} I^{imp} [Y^{hs}]^* [Y^{wg+Y^{hs}}]^{-1*\rightarrow} I^{imp*})} \quad . \tag{2.74}$$

The maximum array gain with all of the elements excited can be found as follows. Using the fact that $[Y^{hs}] = [G^{hs}] + j[B^{hs}]$ and that $[Y^{hs}]$ is symmetric, (2.73) can be written as

$$G = \frac{k^2}{8\pi\eta} \frac{\tilde{V} \vec{P}^m \tilde{P}^{m*} \vec{V}^*}{\tilde{V}[G^{hs}]\vec{V}^*} \quad . \tag{2.75}$$

If V is over the complex field, the stationary points of (2.75) are eigenvalues $8\pi\eta\ G/k^2$ of

$$\vec{P}^m\ \tilde{P}^{m*}\ \vec{V}^* = \frac{8\pi\eta\ G}{k^2}\ [G^{hs}]\vec{V}^* \ . \tag{2.76}$$

Since G^{hs} is positive definite and $\vec{P}^m\ \tilde{P}^*$ is positive semidefinite, all of the eigenvalues are zero or positive. Furthermore, since $\vec{P}^m \cdot \tilde{P}^*$ is a one term dyad, all eigenvalues are zero except one. To find this non-zero eigenvalue, we substitute (2.75) into (2.76) and cancel the common term $\tilde{P}^*\ \vec{V}^*$ to obtain

$$\vec{P}^m = \frac{\tilde{V}\ \vec{P}^m}{\tilde{V}[G^{hs}]\vec{V}^*}\ [G^{hs}]\vec{V}^* \ . \tag{2.77}$$

The quotient term on the right side is just a complex number which we shall denote by $1/C^*$. The required voltage distribution is obtained by inversion of (2.77) which is

$$\vec{V} = C[G^{hs}]^{-1}\ \vec{P}^{m*} \ . \tag{2.78}$$

Substituting (2.78) into (2.75), we obtain

$$G_{max} = \frac{k^2}{8\pi\eta}\ \tilde{P}^m[G^{hs}]^{-1}\ \vec{P}^{m*} \ . \tag{2.79}$$

G_{max} is the maximum gain that can be obtained by using complex equivalent sources for excitation.

2-6. Determination of Reactive Loads which Resonate Complex Equivalent Voltages

In the next chapter, reactive loads which resonate the complex equivalent voltages required for maximum gain are used as a starting point in an optimization subroutine which determines the final optimum loads for a given array radiation requirement. The reactive loads which resonate a vector $\vec{V}$ of complex equivalent voltages are those loads which minimize the norm of the vector $\vec{I}$ of source currents required to maintain $\vec{V}$.

The current source $\vec{I}$ required to produce the complex vector $\vec{V}$ of equivalent voltages required for maximum gain in a loaded waveguide-fed aperture antenna is

$$\begin{aligned}\vec{I} &= [Y^{hs} + Y^{wg}]\vec{V} \\ &= [Y^{hs} + \mathrm{Re}[Y^{wg}] + j\, B_L]\vec{V}\end{aligned} \tag{2-80}$$

where $[B_L]$ is a diagonal matrix whose elements B_{L_i} are real. We can find the reactive loads B_{L_i} by minimizing the source current norm $|\vec{I}|$. Since $|\vec{I}|$ is stationary with respect to the reactive loads at its minimum, we write

$$\begin{aligned}\frac{\partial |\vec{I}|^2}{\partial B_{L_i}} &= \frac{\partial |[Y^{hs} + \mathrm{Re}[Y^{wg}] + j\, B_L]\vec{V}|^2}{\partial B_{L_i}} \\ &= 2\, B_{L_i} |V_i|^2 + 2\, \mathrm{Imag}\, \{V_i^*([Y^{hs} + \mathrm{Re}[Y^{wg}]]\vec{V})_i\} \\ &= 0\end{aligned} \tag{2.81}$$

for all i where $(\ )_i$ denotes the ith component of the enclosed vector. Solving (2.81) for B_{L_i}, we obtain

$$B_{L_i} = -\frac{1}{|V_i|^2}\ \text{Imag}\ \{V_i^*([Y^{hs} + \text{Re}[Y^{wg}]]\vec{V})_i\} \quad . \tag{2.82}$$

For all i except i = NFP, these loads B_{L_i} can be realized by adjusting d_i in (2.40).

In general, $B_{L_{NFP}}$ can not be realized because (2.25) contains no adjustable parameter. However, since only the NFPth waveguide is driven, $B_{L_{NFP}}$, being in parallel with the source, has no effect on the shape of the radiation pattern and the strength of the pattern can be controlled by adjusting the strength of the source I^{imp}_{NFP}. Therefore, control over $B_{L_{NFP}}$ is not essential to pattern synthesis.

2-7. Determination of Relative Power Transmitted (RPT)

Consider the fields transverse to the z direction in the driven waveguide j where only the dominant mode propagates

$$\begin{aligned}
\underset{\sim}{E}_{t_j}(z) &= (e^{-\gamma_o z} - e^{\gamma_o z})\underset{\sim}{e}_o + \underset{\sim}{E}^{wg}_t(\underset{\sim}{M}^j) \\
&= (e^{-\gamma_o z} - e^{\gamma_o z})\underset{\sim}{e}_o + V_j \sum_k A_{jk}\, e^{\gamma_k z}\, \underset{\sim}{e}_k \\
&= [e^{-\gamma_o z} + (V_j A_{jo} - 1)e^{\gamma_o z}]\underset{\sim}{e}_o + V_j \sum_{\substack{k \\ k \neq 0}} A_{jk}\, e^{\gamma_k z}\, \underset{\sim}{e}_k
\end{aligned} \tag{2.83}$$

$$\begin{aligned}
\underset{\sim}{H}_{t_j}(z) &= Y_o[e^{-\gamma_o z} - (V_j A_{jo} - 1)e^{\gamma_o z}]\, \underset{\sim}{u}_z \times \underset{\sim}{e}_o \\
&\quad - V_j \sum_{\substack{k \\ k \neq 0}} A_{jk} Y^*_k\, e^{\gamma_k z}\, \underset{\sim}{u}_z \times \underset{\sim}{e}_k
\end{aligned} \tag{2.84}$$

where the index o denotes the dominant mode, $(e^{-\gamma_o z} - e^{\gamma_o z})\underset{\sim}{e}_o$ is the field due to impressed sources when the aperture is closed with a perfect conductor, γ_k are the modal propagation constants, A_{jk} are the modal constants defined by (2.28) and (2.29), V_j is the unknown magnetic current coefficient determined by (2.16), and the Y_k are modal characteristic admittances defined by (2.32) and (2.33).

If we define the relative power transmitted (RPT) as the real power transmitted divided by the real incident power in the driven waveguide, we have

$$RPT = \frac{\text{Re}\left\{\iint_{\text{apert.}} \underset{\sim}{E}_t \times \underset{\sim}{H}_t^* \cdot \underset{\sim}{u}_z \, ds\right\}}{\text{Real Power Incident}} . \tag{2.85}$$

Substituting (2.83) and (2.84) into (2.85), we have

$$RPT_j = \frac{\text{Re}\{Y_o(V_j A_{jo})(2 - V_j^* A_{jo})\}}{Y_o}$$

$$= \text{Re}\{A_{jo}(2V_j - A_{jo}|V_j|^2)\} \tag{2.86}$$

where the subscript j on RPT denotes the jth waveguide (driven). Equation (2.86) represents a parameter which indicates how well the waveguide array is matched (how much power is radiated of the incident power).

2-8. Conclusion

In this chapter an approximation to the boundary value problem of an antenna array of reactively loaded apertures has been reduced to a matrix formulation using the method of moments. Equations for determining waveguide and half-space admittances, power gain, relative power transmitted, maximum array gain with all of the elements excited, and reactive loads which resonate complex equivalent voltages required for maximum gain have been formulated in terms of the derived model. Some numerical results are presented in the next chapter.

Chapter 3

CALCULATED RESULTS

3-1. Introduction

In this chapter results are presented for reactively loaded aperture antenna arrays using computer programs (see Appendix B) based on equations derived in the preceding chapter. Examples chosen for detailed computational effort are three different nine element linear arrays and a 27 element two dimensional array. The results illustrate the effect of different array parameters on the array characteristics of bandwidth, match, and power gain. In addition, the effect of waveguide short position (reactive load) perturbations on the gain and bandwidth characteristics of the antenna array is presented.

3-2. Definitions

It is convenient at this point to define several terms which are used throughout the chapter.

The useful bandwidth of an antenna depends, in general, on both its admittance and pattern characteristics. The relative power transmitted (RPT) over a frequency range is one measure of the bandwidth associated with the antenna array. It depends on both the driving wave admittance and the input admittance of the antenna array. Another measure is the pattern bandwidth, expressed in terms of the 3 dB (half power) points of the power gain pattern over a frequency range. Both bandwidth measures

(RPT and pattern) can be specified as the ratio of f_2 (upper frequency limit) - f_1 (lower frequency limit) to f_0 (center frequency), or in percent as

$$\frac{f_2 - f_1}{f_0} \times 100 \ . \tag{3.1}$$

The matching characteristic of the antenna can be expressed in terms of the ratio of the power radiated into the half-space region to the power incident in the driven waveguide, which is the relative power transmitted (see equation 2.86).

The power gain characteristic of the antenna is the ratio of the radiation intensity in a given direction to the radiation intensity which would exist if the total power P_t were radiated over the half-space (see equation 2.72). For our problem we are assuming that none of the incident power from the impressed sources in the driven waveguide is dissipated in the antenna conducting surfaces.

3-3. Linear Aperture Antenna Array

In this section three different reactively loaded linear aperture antenna arrays are analyzed. The following applies to all three cases:

a) There are nine elements with the center element driven by impressed sources.

b) All of the aperture backing waveguide dimensions are the same.

c) Waveguide separation distance is zero.

The aperture dimensions are the same for all nine elements in each case, but different from case to case.

Figure 3.1 depicts the coupling coefficients (scattering parameters) with respect to the driven port for all three cases. Note that the apertures are oriented for strong coupling and that coupling is greatest for case (c), where the aperture length is 0.500λ.

The antenna characteristics of bandwidth, match, and power gain for these arrays are presented in the following subsections. For all of the figures other than the polar gain plots, a cubic spline function is used as a curve fitting function for the discrete data points (indicated by +'s). A cubic spline function is composed of piecewise polynomials of third degree satisfying certain continuity properties at the junctions.

3-1.1. Bandwidth

In this subsection a comparison of the power gain bandwidth for three different reactively loaded linear arrays is presented. In most of the examples the bandwidth obtained is less than or equal to the bandwidth associated with matching (see Figures 3.6 - 3.8 in the next subsection).

Figures 3.2 - 3.4 show the E-plane power gain of three different nine element reactively loaded aperture antenna arrays as a function of frequency and beam steering angle ϕ. In each example the power gain is optimized at a frequency $f = f_o$. Next, the short positions (reactive loads) obtained from this optimization are kept fixed while the frequency is varied and power gain computed. The most noticeable characteristic of

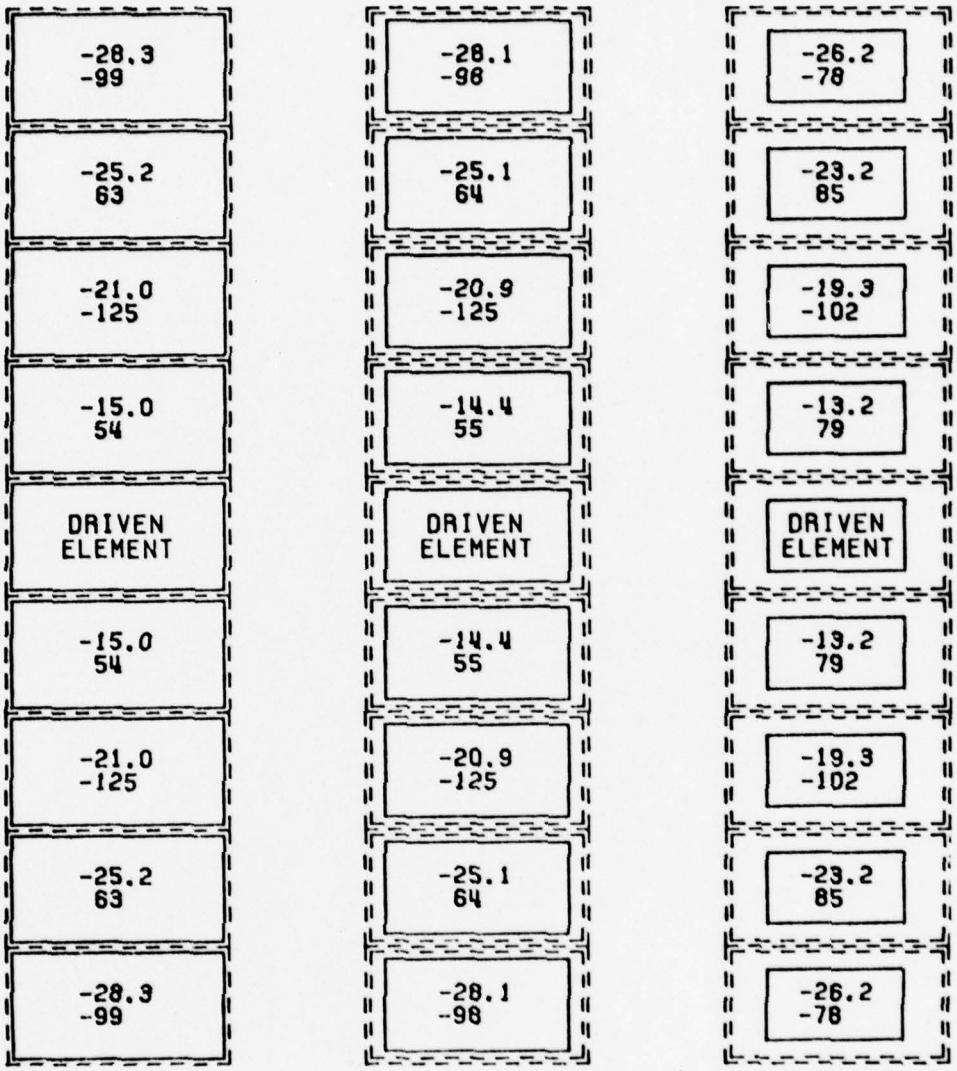

(a) $a'/\lambda = 0.750$, $b'/\lambda = 0.375$ (b) $a'/\lambda = 0.650$, $b'/\lambda = 0.325$ (c) $a'/\lambda = 0.500$, $b'/\lambda = 0.250$

Fig. 3.1. The coupled power 20 log $|S_{i5}|$ and phase of S_{i5} ($i=1,2,\ldots,9-i\neq5$) for a nine element waveguide fed linear aperture antenna array, where $f = f_o$, $a/\lambda = 0.750$, $b/\lambda = 0.375$, $D_y/\lambda = 0$, and $D_t/\lambda = 0.040$. The upper number in each aperture represents coupled power in dB while the lower number represents the phase of S_{i5} in degrees.

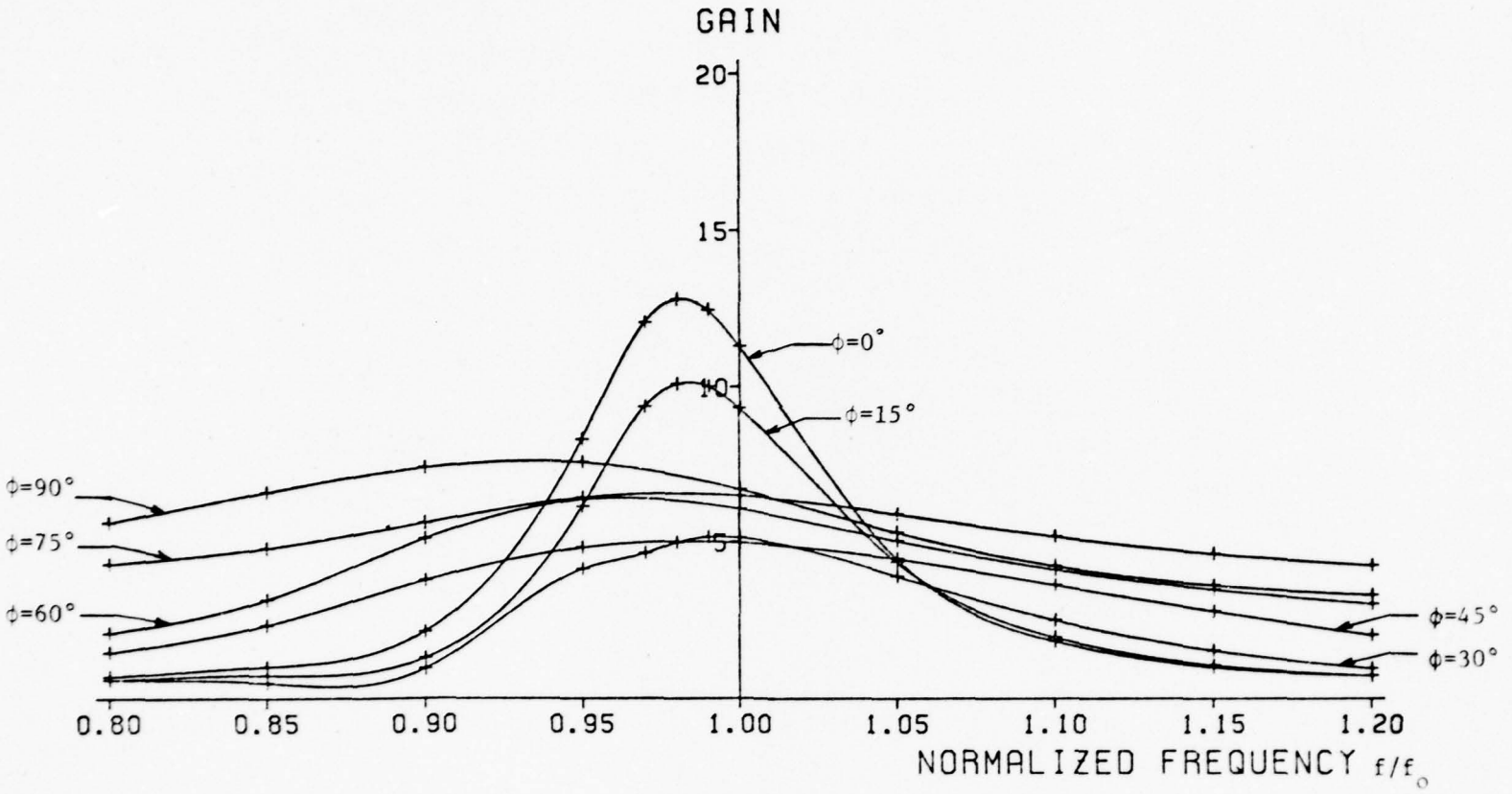

Fig. 3.2. E-plane gain versus frequency for a nine element reactively loaded linear aperture antenna array, where $a/\lambda = a'/\lambda = 0.750$, $b/\lambda = b'/\lambda = 0.375$, $D_y/\lambda = 0$, and $D_t/\lambda = 0.040$.

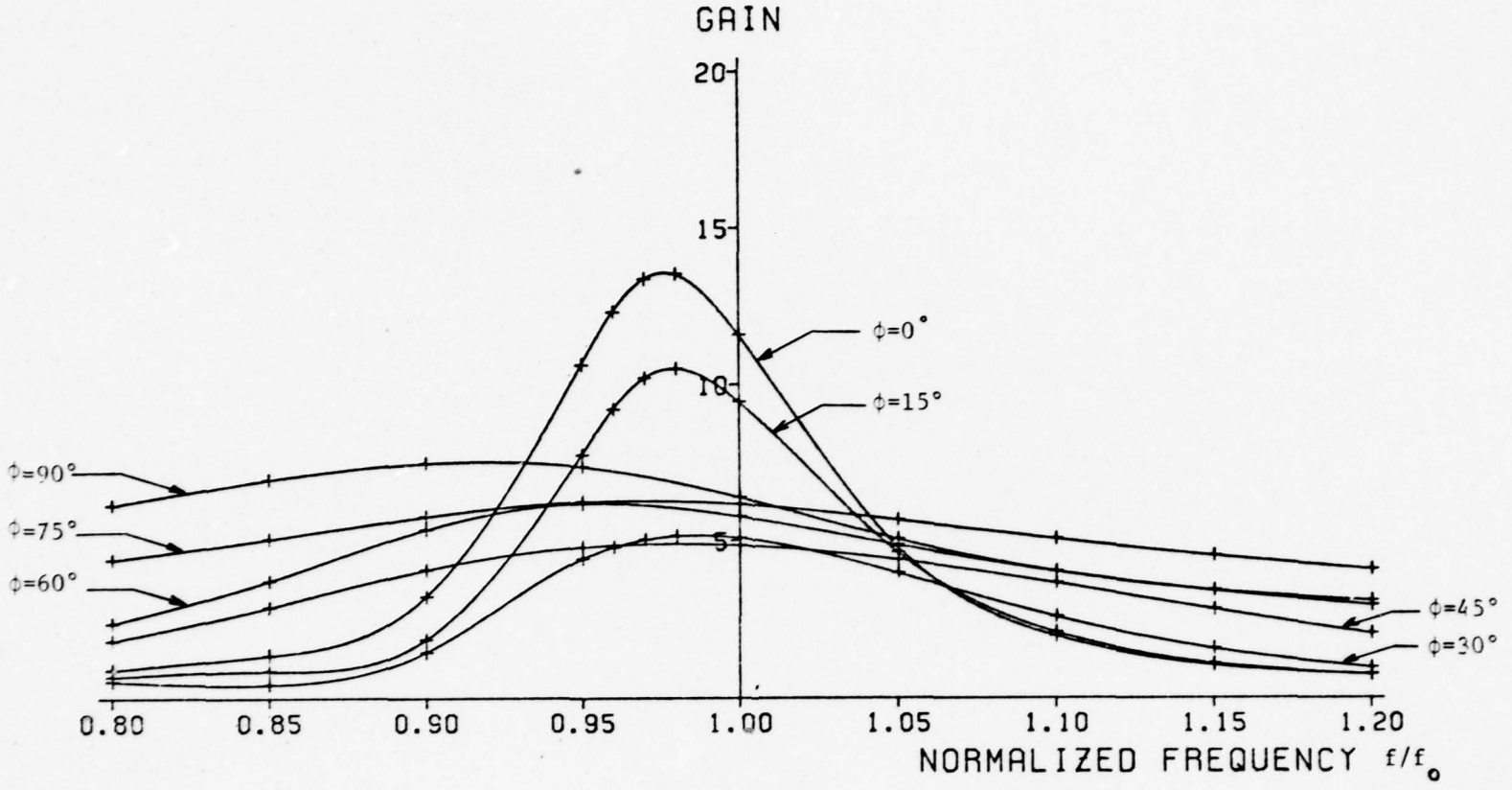

Fig. 3.3. E-plane gain versus frequency for a nine element reactively loaded linear aperture antenna array, where $a/\lambda = 0.750$, $a'/\lambda = 0.650$, $b/\lambda = 0.375$, $b'/\lambda = 0.325$, $D_y/\lambda = 0$, and $D_t/\lambda = 0.040$.

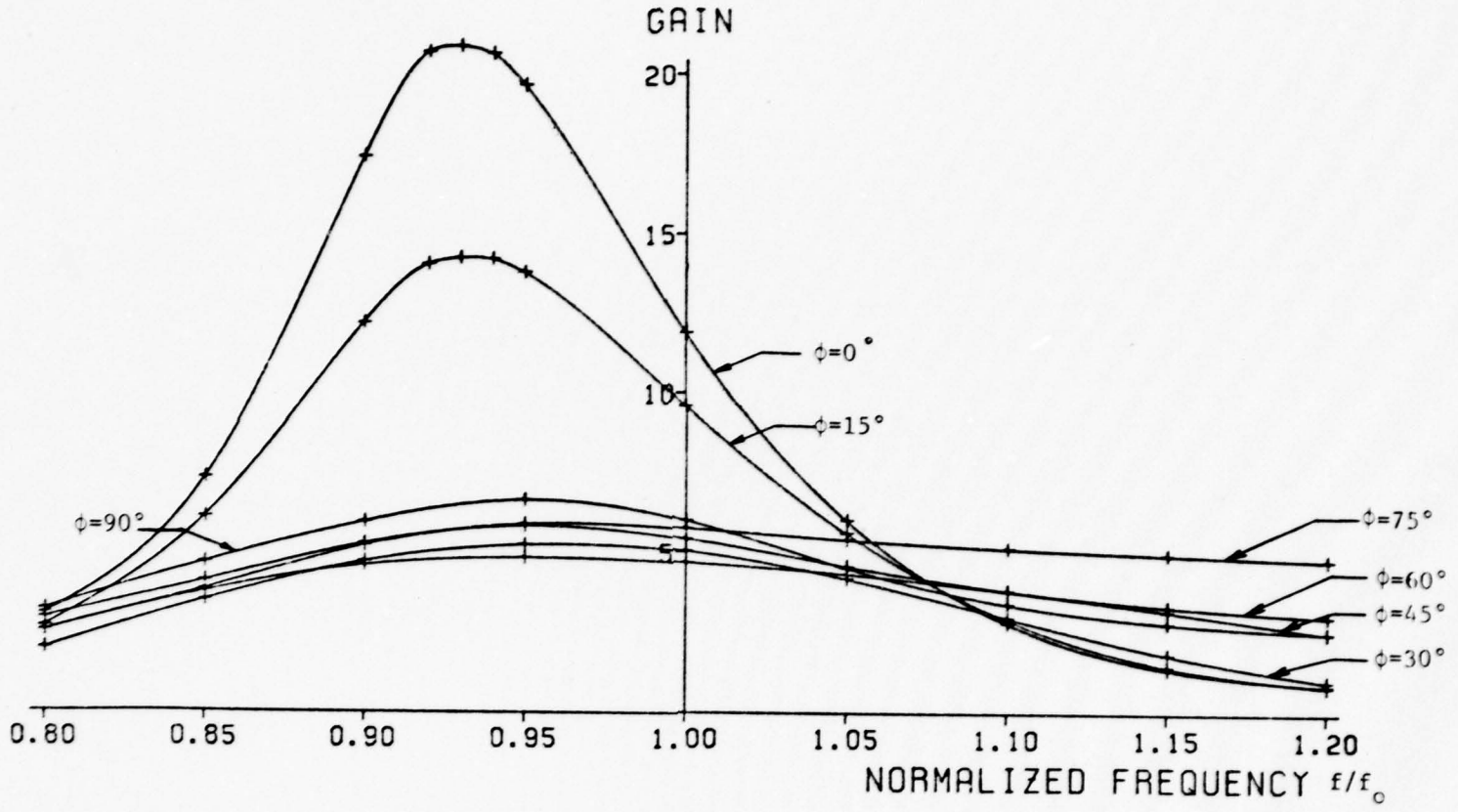

Fig. 3.4. E-plane gain versus frequency for a nine element reactively loaded linear aperture antenna array, where $a/\lambda = 0.750$, $a'/\lambda = 0.500$, $b/\lambda = 0.375$, $b'/\lambda = 0.250$, $D_y/\lambda = 0$, and $D_t/\lambda = 0.040$.

the curves in these three figures is the fact that greater gain is obtained at a frequency lower than $f = f_o$, the optimization frequency. The main reason for this is that for lower frequencies, the apertures are closer together in terms of wavelength which increases the mutual coupling. An increase in mutual coupling, especially at the lower beam steering angles ϕ (the angle ϕ is measured from the aperture plane), increases the gain (see Figure 3.13).

Figures 3.5 summarizes the gain and bandwidth results shown in Figures 3.2 - 3.4 as a function of beam steering angle for a frequency of $f = f_o$. Both the gain and bandwidth curves for all three cases have about the same values except for beam steering angles greater than 60° where the bandwidth curves diverge. However, if we choose a frequency of $f = 0.95\ f_o$, case (c) ($a'/\lambda = 0.500$, $b'/\lambda = 0.250$) would show greater gain and bandwidth at the low beam steering angles than the other two cases.

3-3.2. Match

Mismatch between the incident wave and aperture admittances of the antenna represents a decrease in the effective antenna gain and system efficiency. The relative power transmitted is a measure of the match between the source and antenna. Figures 3.6 - 3.8 show the relative power transmitted for a nine element reactively loaded aperture antenna array as a function of frequency f and beam steering angle ϕ.

A comparison of Figures 3.6 - 3.8 with the corresponding Figures 3.2 - 3.4 for gain shows that the decrease in the relative power transmitted at the low beam steering angles (ϕ = 0, 15°, and 30°) occurs when

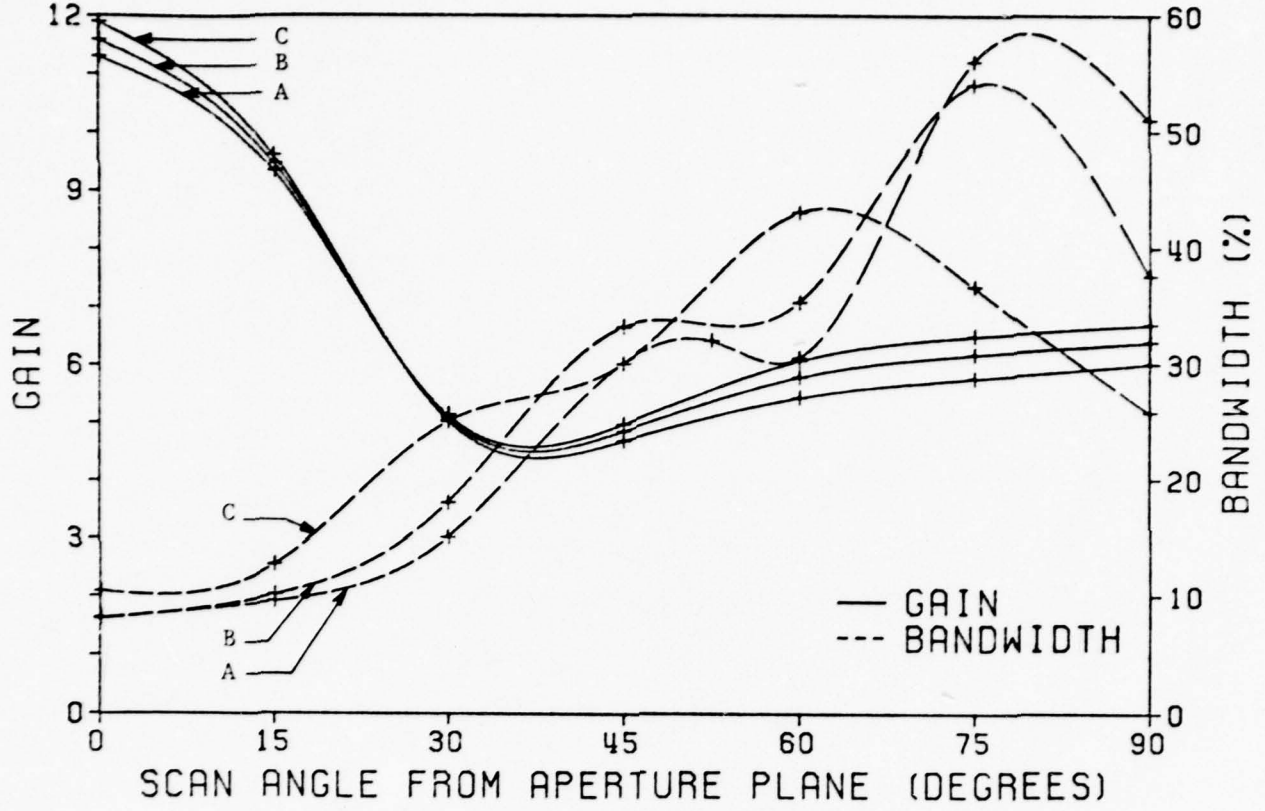

Fig. 3.5. E-plane gain and bandwidth versus beam steering angle ϕ for a nine element reactively loaded aperture antenna array, where $f = f_o$, $a/\lambda = 0.750$, $b/\lambda = 0.375$, $D_y/\lambda = 0$, $D_t/\lambda = 0.040$, case (A) - $a'/\lambda = 0.750$, $b'/\lambda = 0.375$, case (B) - $a'/\lambda = 0.650$, $b'/\lambda = 0.325$, and case (C) - $a'/\lambda = 0.500$, $b'/\lambda = 0.250$.

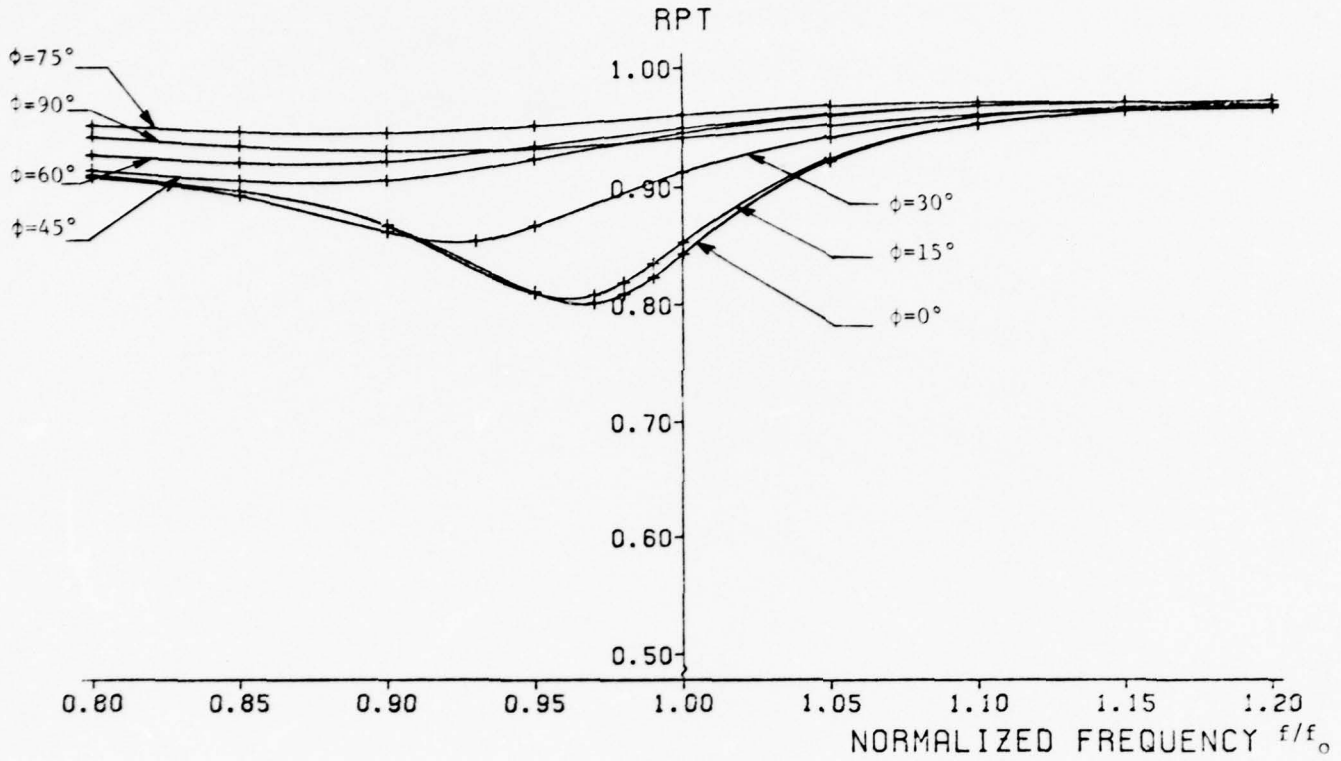

Fig. 3.6. Relative power transmitted versus frequency for a nine element reactively loaded linear aperture antenna array, where $a/\lambda = a'/\lambda = 0.750$, $b/\lambda = b'/\lambda = 0.375$, $D_y/\lambda = 0$, and $D_t/\lambda = 0.040$.

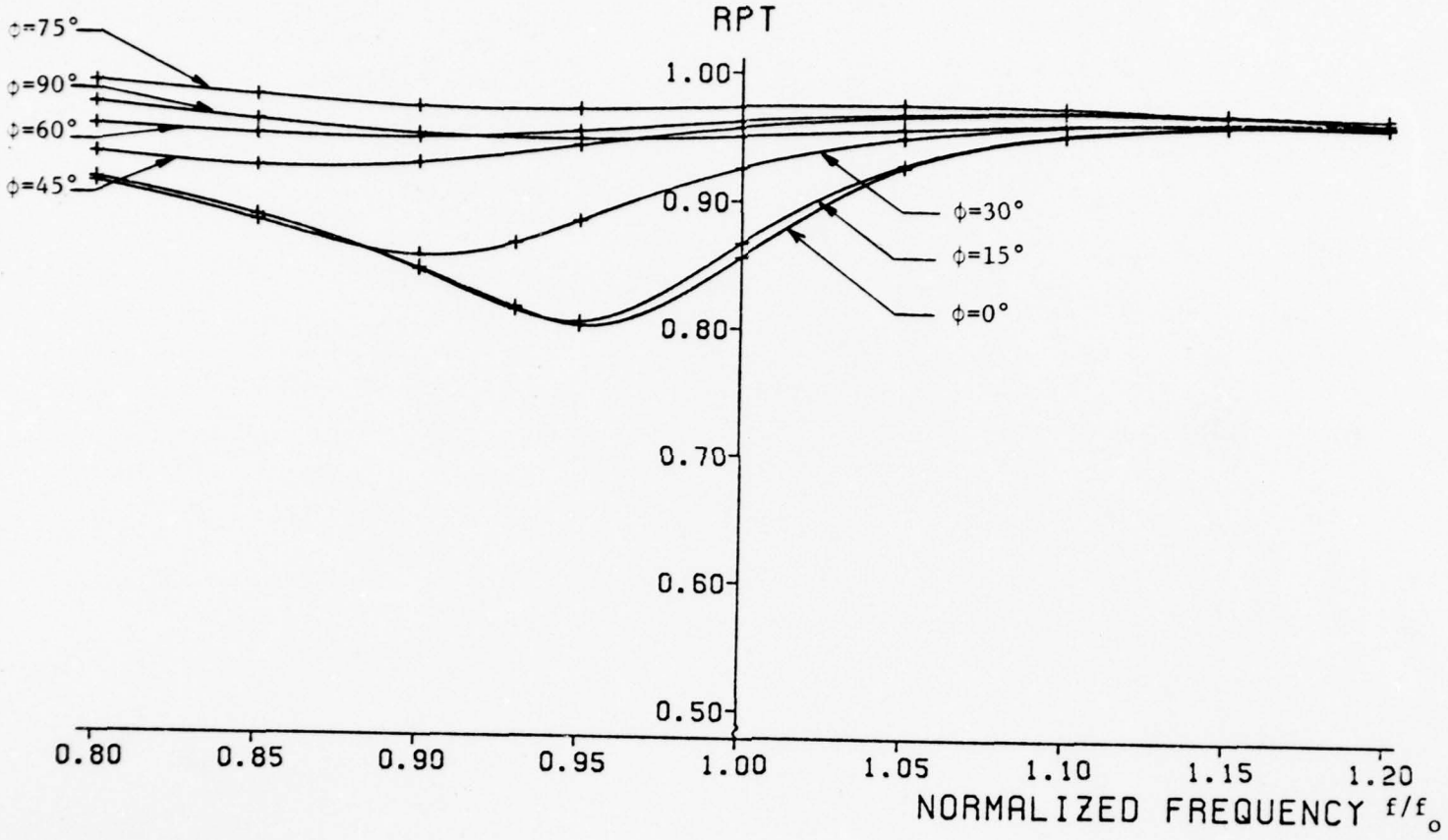

Fig. 3.7. Relative power transmitted versus frequency for a nine element reactively loaded linear aperture antenna array, where $a/\lambda = 0.750$, $a'/\lambda = 0.650$, $b/\lambda = 0.375$, $b'/\lambda = 0.325$, $D_y/\lambda = 0$, and $D_t/\lambda = 0.040$.

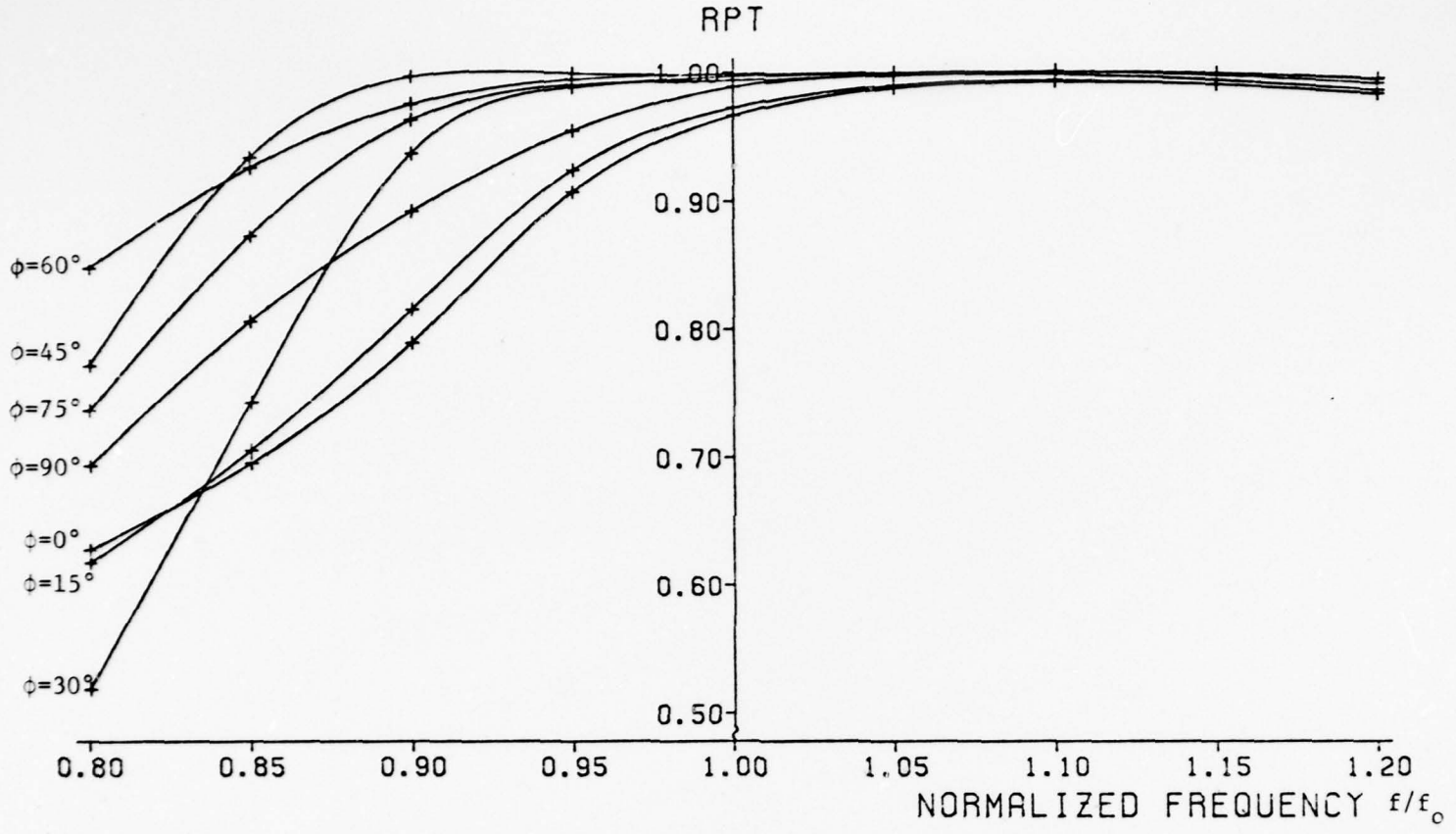

Fig. 3.8. Relative power transmitted versus frequency for a nine element reactively loaded linear aperture antenna array, where $a/\lambda = 0.750$, $a'/\lambda = 0.500$, $b/\lambda = 0.375$, $b'/\lambda = 0.250$, $D_y/\lambda = 0$, and $D_t/\lambda = 0.040$.

there is a corresponding rise in the power gain curves. In effect, the gain increases at the expense of decreasing match.

The curves in Figure 3.8 show a better match at frequencies above f_o, but a poorer match at frequencies below, than do the curves in Figures 3.6 and 3.7. Besides the decrease in match associated with the increase in gain at frequencies below f_o, the relative aperture size is reduced, which results in more energy reflected and a poorer match.

3-3.3. Power Gain

The E-plane polar gain patterns for a nine element reactively loaded aperture array are given in Figures 3.9 - 3.11 for five frequencies and three beam steering angles. Two different aperture size cases (A - $a'/\lambda = 0.750$, $b'/\lambda = 0.375$, and C - $a'/\lambda = 0.500$, $b'/\lambda = 0.250$) are analyzed.

In Figure 3.9 ($\phi = 0$), aperture case C has greater gain at more frequencies than aperture case A. Above frequency f_o, both cases are unusable. In Figure 3.10 ($\phi = 45°$), both cases have similar patterns. In Figure 3.11 ($\phi = 90°$), both cases have similar patterns except that the gain is slightly larger for aperture case A. The corresponding H-plane pattern for the $\phi = 90°$ E-plane case would show the magnitude for case A exceeding the magnitude for case C at all frequencies and the beamwidth for both cases varying between 50° - 70° as the frequency is changed.

The E-plane polar gain patterns at a frequency f_o and four beam steering angles for cases A and C are given in Figure 3.12. The patterns

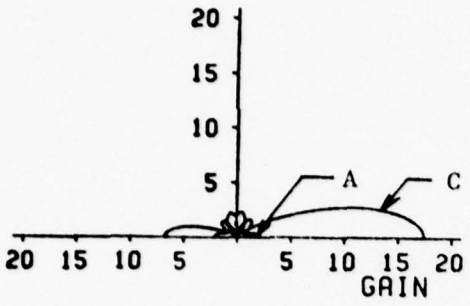

(a) $f = 0.90\ f_o$

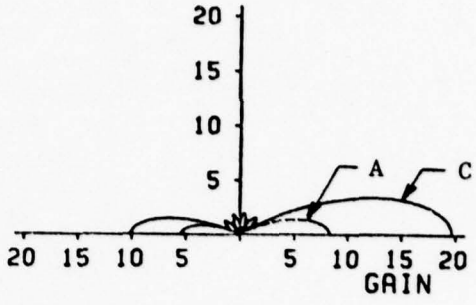

(b) $f = 0.95\ f_o$

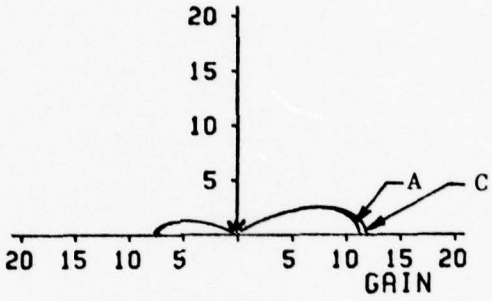

(c) $f = f_o$

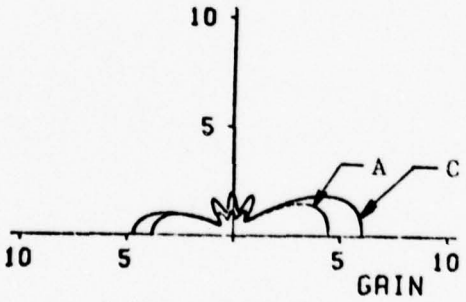

(d) $f = 1.05\ f_o$

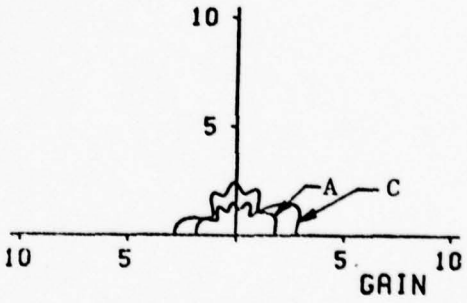

(e) $f = 1.10\ f_o$

Fig. 3.9. E-plane polar gain as a function of frequency f for a nine element reactively loaded linear aperture antenna array, where $\phi = 0$, $a/\lambda = 0.750$, $b/\lambda = 0.375$, $D_y/\lambda = 0$, $D_t/\lambda = 0.040$, case (A) - $a'/\lambda = 0.750$, $b'/\lambda = 0.375$, and case (C) - $a'/\lambda = 0.500$, $b'/\lambda = 0.250$.

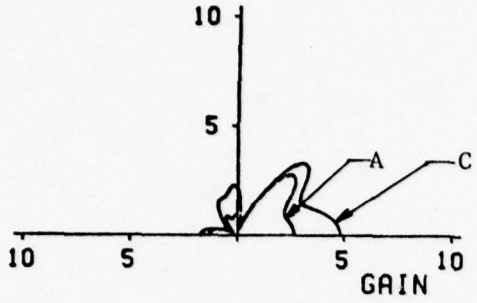

(a) f = 0.90 f_o

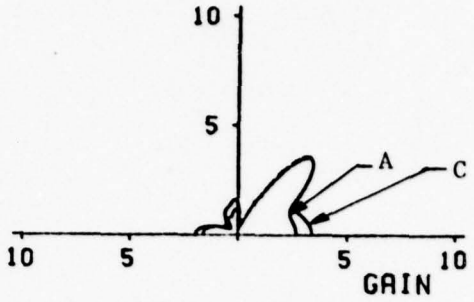

(b) f = 0.95 f_o

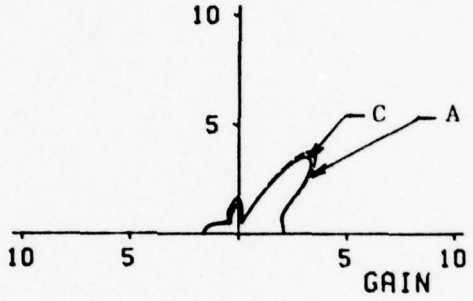

(c) f = f_o

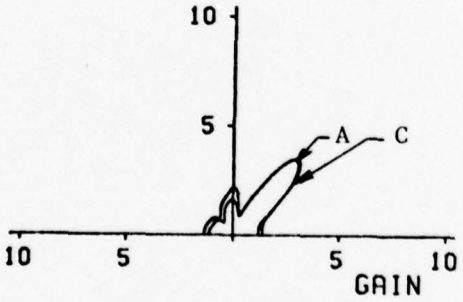

(d) f = 1.05 f_o

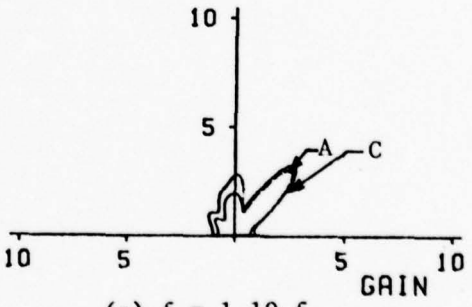

(e) f = 1.10 f_o

Fig. 3.10. E-plane polar gain as a function of frequency f for a nine element reactively loaded linear aperture antenna array, where $\phi = 45°$, $a/\lambda = 0.750$, $b/\lambda = 0.375$, $D_y/\lambda = 0$, $D_t/\lambda = 0.04$, case (A) - $a'/\lambda = 0.750$, $b'/\lambda = 0.375$, and case (C) - $a'/\lambda = 0.500$, $b'/\lambda = 0.250$.

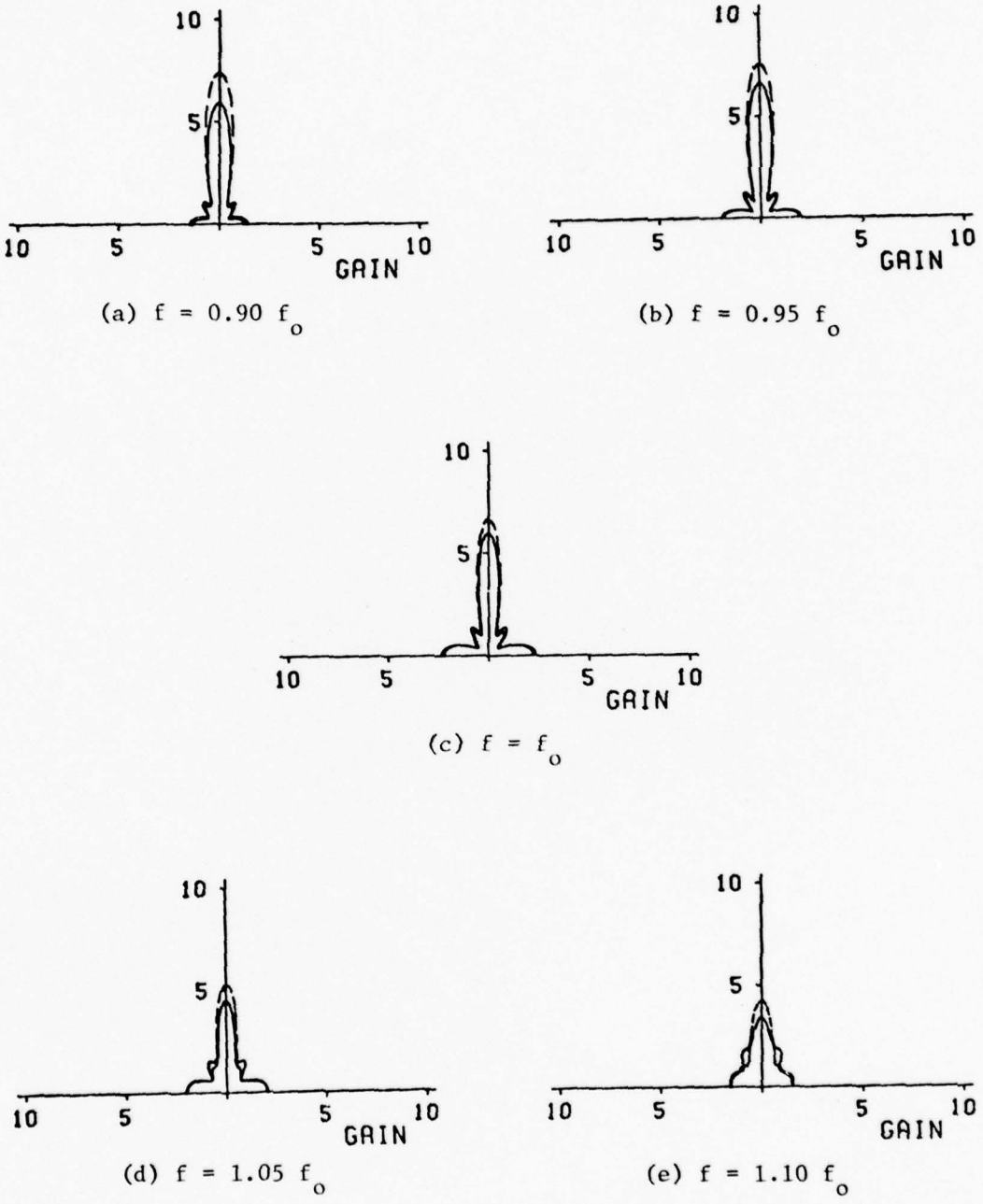

(a) f = 0.90 f_o

(b) f = 0.95 f_o

(c) f = f_o

(d) f = 1.05 f_o

(e) f = 1.10 f_o

Fig. 3.11. E-plane polar gain as a function of frequency f for a nine element reactively loaded linear aperture antenna array, where ϕ = 90°, a/λ = 0.750, b/λ = 0.375, D_y/λ = 0, D_t/λ = 0.040, (---) a'/λ = 0.750, b'/λ = 0.375, and (——) a'/λ = 0.500, b'/λ = 0.250.

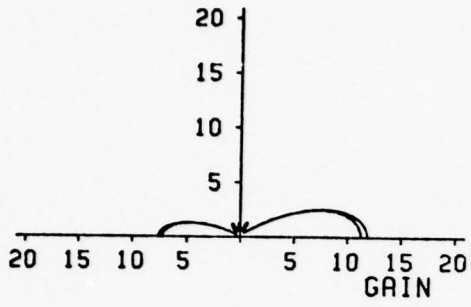

(a) $\phi = 0^{\circ}$

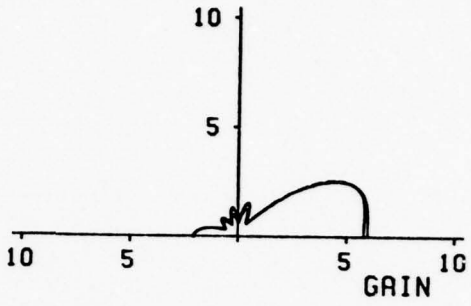

(b) $\phi = 30°$

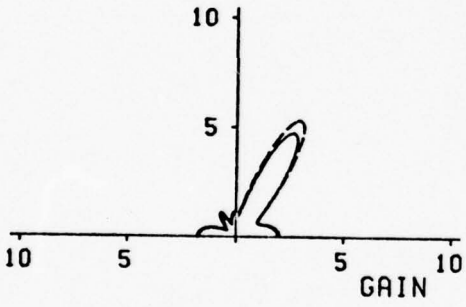

(c) $\phi = 60°$

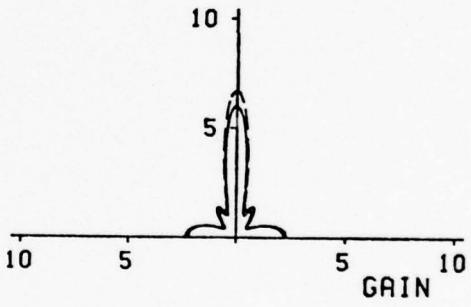

(d) $\phi = 90°$

Fig. 3.12. E-plane polar gain as a function of beam steering angle ϕ for a nine element reactively loaded linear aperture antenna array, where $f = f_o$, $a/\lambda = 0.750$, $b/\lambda = 0.375$, $D_y/\lambda = 0$, $D_t/\lambda = 0.040$, (---) $a'/\lambda = 0.750$, $b'/\lambda = 0.375$, and (——) $a'/\lambda = 0.500$, $b'/\lambda = 0.250$.

for both cases are almost identical at every beam steering angle. The corresponding H-plane patterns for both cases would show almost identical patterns for all beam steering angles and the beamwidths varying between 40° - 70° as the frequency is changed.

Figure 3.13 shows the E-plane power gain that is obtained by optimizing at each of nine discrete frequencies for a nine element reactively loaded aperture antenna array. The gain at a beam steering angle $\phi = 0$ for cases A, B ($a'/\lambda = 0.650$, $b'/\lambda = 0.325$), and C increases quite rapidly for decreasing frequencies from 1.1 f_o to 0.9 f_o, at which time the gain levels off. The gain for case A at beam steering angles of 45° and 90° increases more gradually as the frequency decreases.

Since Figure 3.13 shows that the gain for all three aperture sizes is approximately the same for a fixed frequency and beam steering angle, the increase in gain for decreasing frequencies is probably due to the increase in mutual coupling resulting from a decrease in effective distance between apertures. To demonstrate this point, Figure 3.14 compares the E-plane reactively loaded gain for two waveguide wall thickness, $D_t/\lambda = 0.01$ and $D_t/\lambda = 0.04$, and for four beam steering angles for a nine element linear aperture antenna array at a frequency f_o. (The distance between waveguides is still zero — $D_y/\lambda = 0$.) In every case the gain is greater for the closer spacing without pattern degradation. The waveguide wall thickness $D_t/\lambda = 0.04$ was chosen for the examples in this chapter because it approximates the wall thickness of commercially available waveguide.

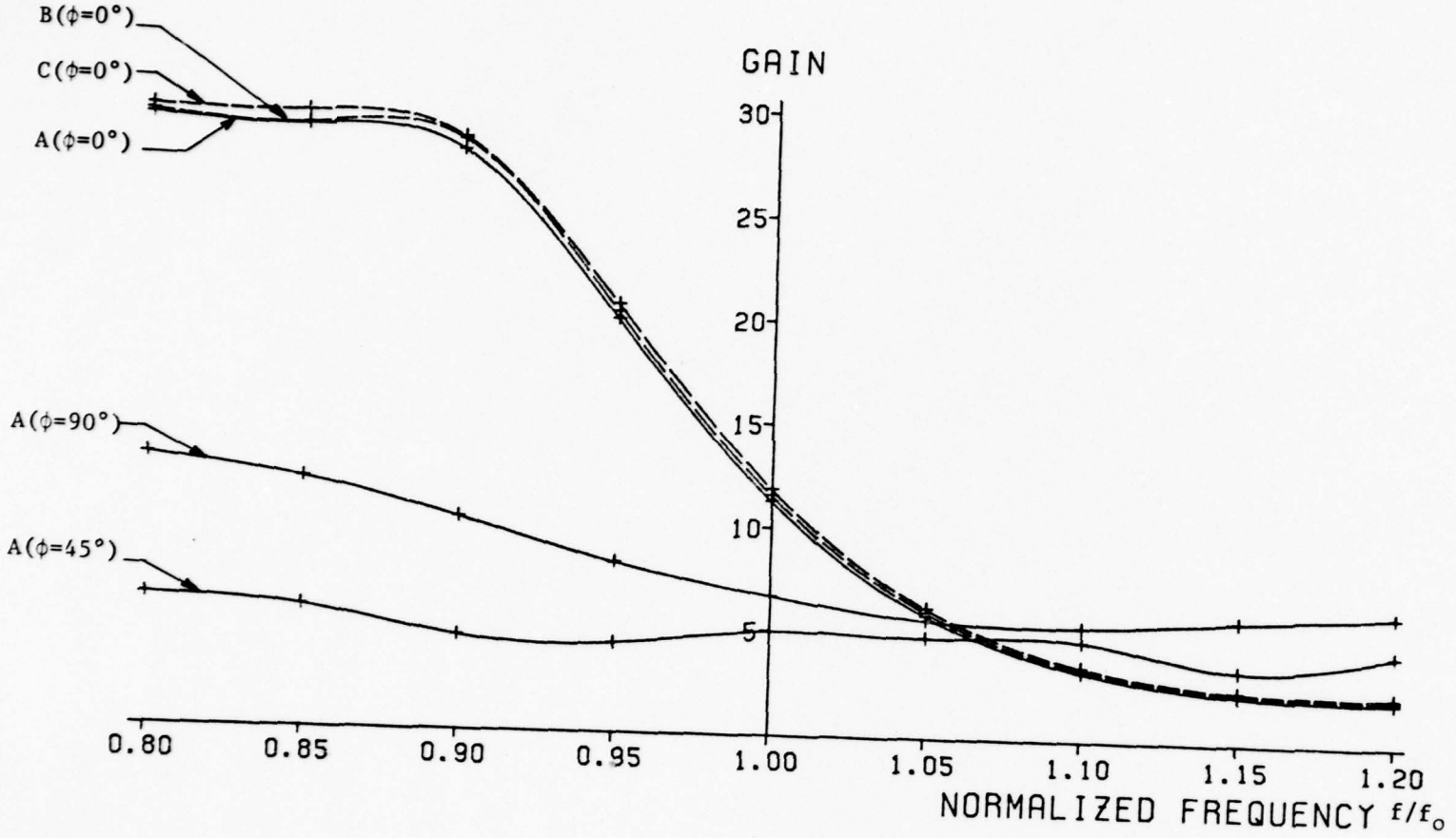

Fig. 3.13. E-plane optimized gain versus frequency for a nine element reactively loaded linear aperture antenna array, where $a/\lambda = 0.750$, $b/\lambda = 0.375$, $D_y/\lambda = 0$, $D_t/\lambda = 0.040$, case (A) - $a'/\lambda = 0.750$, $b'/\lambda = 0.375$, case (B) - $a'/\lambda = 0.650$, $b'/\lambda = 0.325$, and case (C) - $a'/\lambda = 0.500$, $b'/\lambda = 0.250$.

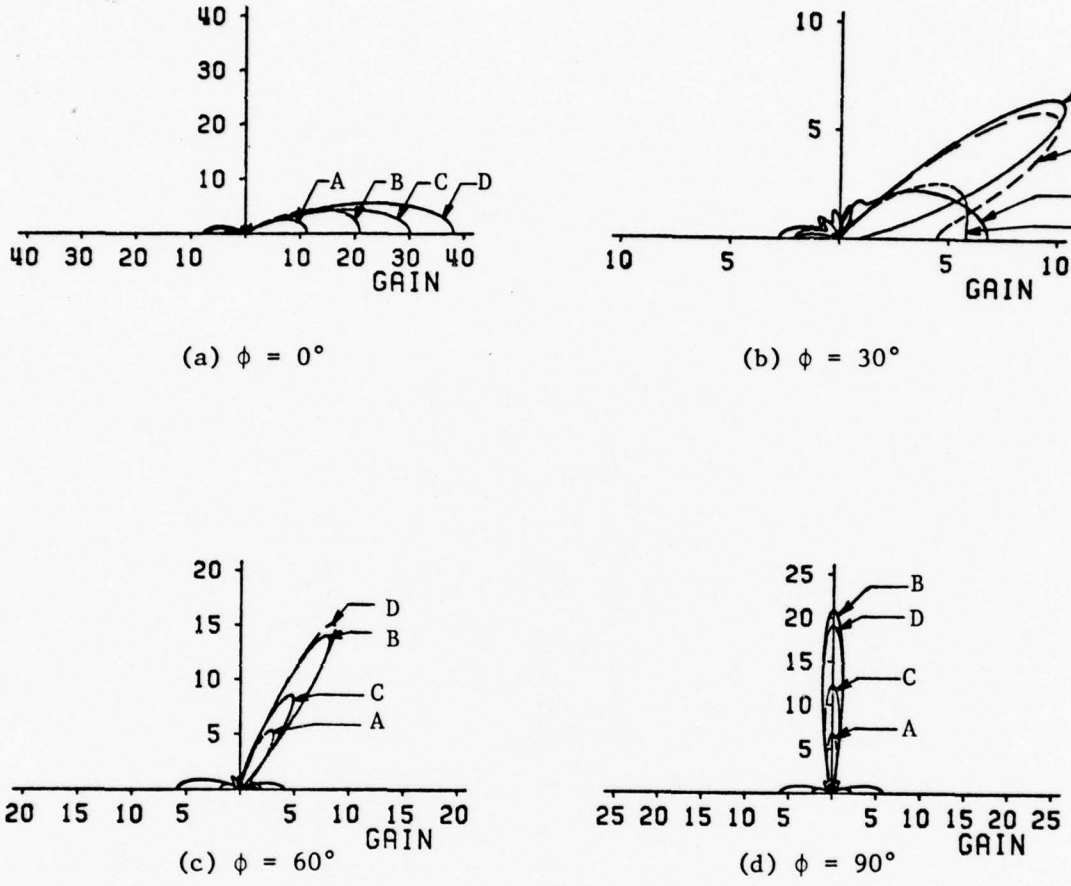

Fig. 3.14. A comparison between E-plane optimum excited (OE) and reactively loaded (RL) gains for two different waveguide spacings for a nine element linear aperture antenna arrays, where $f = f_o$, $a/\lambda = a'/\lambda = 0.750$, $b/\lambda = b'/\lambda = 0.375$, $D_y/\lambda = 0$, case (A) - RL, $D_t/\lambda = 0.040$, case (B) - OE, $D_t/\lambda = 0.040$, case (C) - RL, $D_t/\lambda = 0.010$, and case (D) - OE, $D_t/\lambda = 0.010$.

3-3.4. Reactive Loads

Table 3.1 lists the reactive loads required for some of the results presented in the preceding subsections. No specific trend is obvious from the values presented except that the reactive load values given for a beam steering angle of 0° are close in magnitude for corresponding elements in aperture cases A, B, and C. Also, for a beam steering angle of 90°, the reactive loads are approximately the same for corresponding positions about the driven port (elements - one and nine, two and eight, etc.).

Table 3.2 lists the corresponding waveguide short positions for the reactive loads given in Table 3.1.

Table 3.1. Reactive loads for a nine element reactively loaded linear aperture antenna array, where $f = f_o$, $a/\lambda = 0.750$, $b/\lambda = 0.375$, $D_y/\lambda = 0$, $D_t/\lambda = 0.040$, case (A) - $a'/\lambda = 0.750$, $b'/\lambda = 0.375$, case (B) - $a'/\lambda = 0.650$, $b'/\lambda = 0.325$, case (C) - $a'/\lambda = 0.500$, $b'/\lambda = 0.250$, and ϕ is the beam steering angle.

Case	A	B	C	A	A	A
ϕ	0°	0°	0°	30°	60°	90°
BLOAD (1)	-1.68 m℧	-1.42 m℧	-0.74 m℧	-0.60 m℧	-1.50 m℧	-1.36 m℧
BLOAD (2)	-2.56	-2.21	-1.32	-1.63	-5.22	64.10
BLOAD (3)	-3.00	-2.58	-1.57	-2.25	6.57	-2.00
BLOAD (4)	-3.24	-2.78	-1.70	-2.71	-1.20	11.75
BLOAD (6)	-3.68	-3.17	-1.98	-4.73	-21.53	12.38
BLOAD (7)	-3.73	-3.21	-2.00	-6.26	2.69	-1.99
BLOAD (8)	-3.55	-3.06	-1.91	-10.47	-1.26	132.8
BLOAD (9)	-2.86	-2.42	-1.42	19.42	-2.82	-1.42

Table 3.2. Waveguide short positions (for corresponding reactive loads in Table 3.1) for a nine element reactively loaded linear aperture antenna array, where $f = f_o$, $a/\lambda = 0.750$, $b/\lambda = 0.375$, $D_y/\lambda = 0$, $D_t/\lambda = 0.040$, case (A) - $a'/\lambda = 0.750$, $b'/\lambda = 0.375$ case (B) - $a'/\lambda = 0.650$, $b'/\lambda = 0.325$, case (C) - $a'/\lambda = 0.500$, $b'/\lambda = 0.250$, $\varepsilon_r = 1.0$, and ϕ is the beam steering angle.

Case	A	B	C	A	A	A
ϕ	0°	0°	0°	30°	60°	90°
Short Position (1)	-0.486λ	-0.480λ	-0.405λ	-0.398λ	-0.474λ	-0.464λ
Short Position (2)	-0.530	-0.529	-0.484	-0.483	-0.593	-0.007
Short Position (3)	-0.546	-0.545	-0.509	-0.517	-0.062	-0.504
Short Position (4)	-0.554	-0.552	-0.519	-0.536	-0.452	-0.036
Short Position (6)	-0.566	-0.565	-0.539	-0.586	-0.651	-0.034
Short Position (7)	-0.567	-0.566	-0.540	-0.606	-0.135	-0.504
Short Position (8)	-0.562	-0.562	-0.534	-0.631	-0.457	-0.003
Short Position (9)	-0.542	-0.538	-0.495	-0.022	-0.540	-0.468

3-4. Two Dimensional Aperture Antenna Array

In this section a 27 element two dimensional (three columns of nine elements) reactively loaded aperture antenna array is analyzed. The aperture dimensions are the same as case C ($a'/\lambda = 0.500$, $b'/\lambda = 0.250$) in the previous section. The backing waveguides all have the same dimensions and the separation distance between waveguides is zero.

Figure 3.15 shows the coupling coefficients of the two dimensional array with respect to the driven center port. Note that coupling is greater in the vertical direction than the horizontal direction. Since it was shown in the last section that gain is dependent on mutual coupling, a two dimensional reactively loaded aperture antenna array will

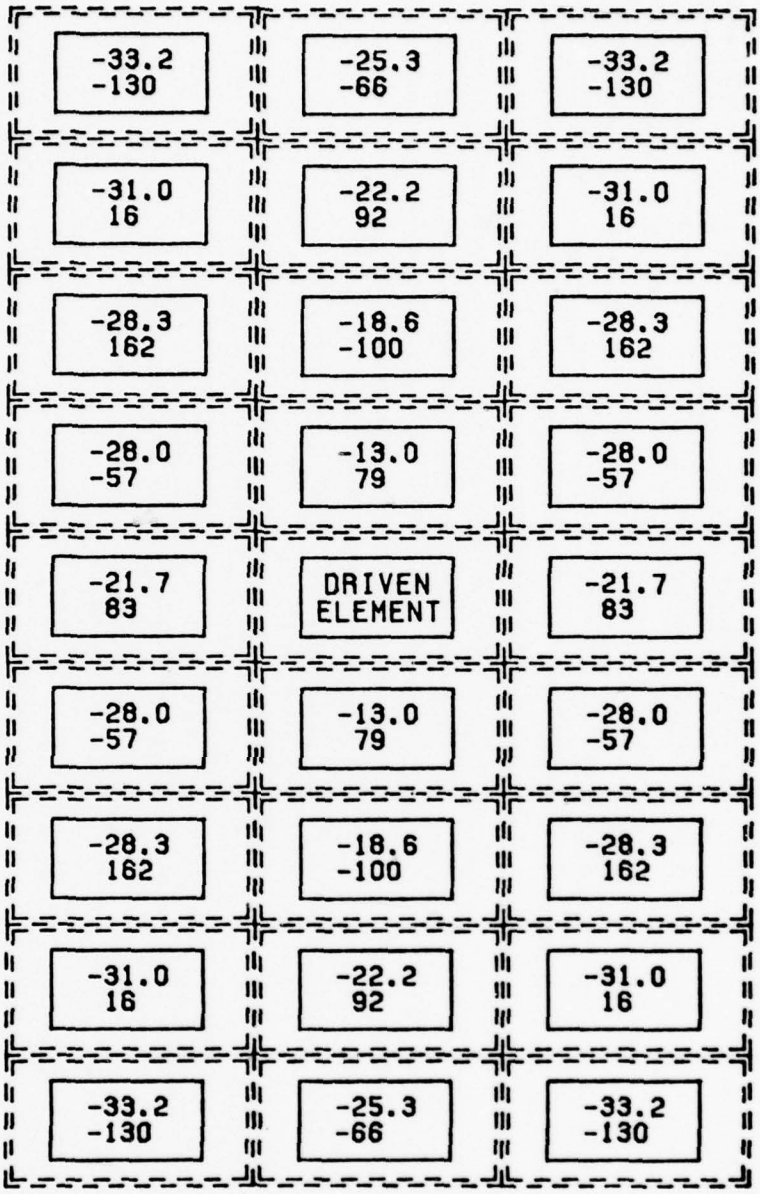

Fig. 3.15. The coupled power 20 log $|S_{i14}|$ and phase of S_{i14} ($i=1,2,\ldots,27 - i \neq 14$) for a 27 element waveguide fed two dimensional aperture antenna array, where $f = f_o$, $a/\lambda = 0.750$, $a'/\lambda = 0.500$, $b/\lambda = 0.375$, $b'/\lambda = 0.250$, $D_x/\lambda = D_y/\lambda = 0$, and $D_t/\lambda = 0.040$. The upper number in each aperture represents coupled power in dB while the lower number represents the phase of S_{i14} in degrees.

usually be of rectangular shape as shown in Figure 3.15. In the following sections the array is analyzed in terms of its characteristics of bandwidth, match, and gain.

3-4.1. Bandwidth

Figure 3.16 shows the E-plane power gain for a 27 element two dimensional reactively loaded aperture antenna array as a function of frequency and beam steering angle ϕ. In the previous section it was observed that the gain always peaked at a frequency lower than the design frequency f_o. An attempt can be made to remedy this situation by optimizing the gain at a frequency higher than $f = f_o$. In Figure 3.16, the dashed lines represent an optimization at frequencies $f = 1.05\ f_o$ and $f = 1.10\ f_o$ for a beam steering angle of 0°. If these results are compared to that obtained for an optimization frequency f_o, one observes that for $f = 1.05\ f_o$ there is a slight shift of the gain curve towards the $f = f_o$ axis at the expense of gain, but for $f = 1.10\ f_o$ the gain curve is degraded. The frequency $f = 1.05\ f_o$ is, therefore, the upper limit for obtaining an acceptable curve. If one optimizes at a frequency higher than a desired center frequency, but equal to or below $f = 1.05\ f_o$, a more centered gain pattern results at the expense of gain. The rest of the curves in Figure 3.16, which are optimized at a frequency $f = f_o$, are very similar in shape to those for a nine element linear aperture antenna array (Figure 3.4), except that all of the curves in Figure 3.16 have a pronounced peak. This peak defines an operating region where increased gain can be obtained.

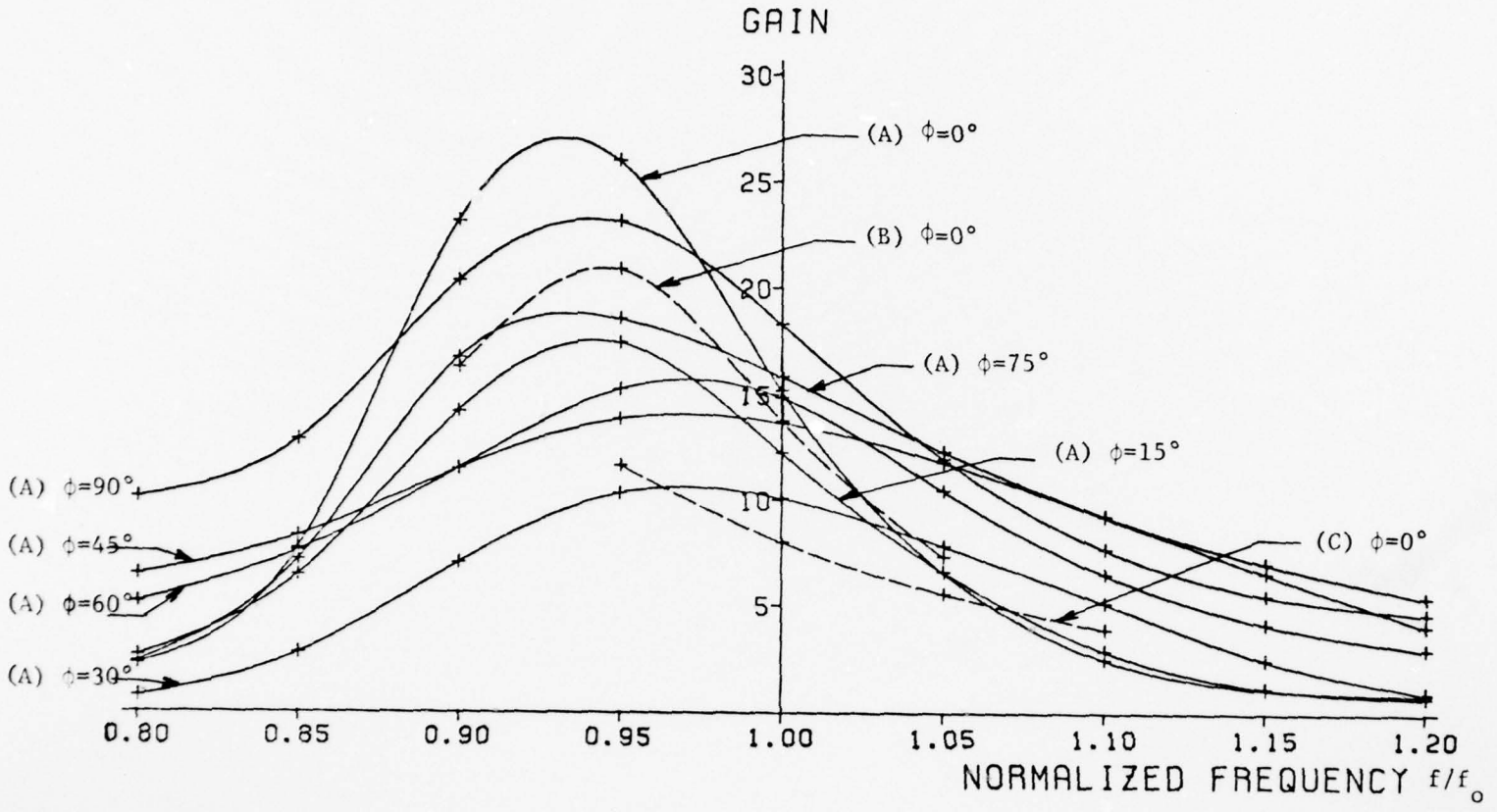

Fig. 3.16. E-plane gain versus frequency for a 27 element reactively loaded two dimensional aperture antenna array where $a/\lambda = 0.750$, $a'/\lambda = 0.500$, $b/\lambda = 0.375$, $b'/\lambda = 0.250$, $D_x/\lambda = D_y/\lambda = 0$, $D_t/\lambda = 0.040$, case (A) - reactive loads for $f = f_o$ optimization, case (B) - reactive loads for $f = 1.05\ f_o$ optimization, and case (C) - reactive loads for $f = 1.10\ f_o$ optimization.

Figure 3.17 summarizes the gain and bandwidth shown in Figure 3.16 for frequencies $f = 0.95\ f_o$ and $f = f_o$. The curves in Figure 3.17 are similar for both frequencies except that the curves at frequency $f = 0.95\ f_o$ exhibit a higher gain-bandwidth product.

3-4.2. Match

Figure 3.18 shows the relative power transmitted for a 27 element two dimensional reactively loaded aperture antenna array as a function of frequency and beam steering angle ϕ. The curves are similar to those for the nine element linear reactively loaded aperture antenna array (Figure 3.8). For both linear and two dimensional cases, the matching characteristics are acceptable above a frequency f_o, but degrade noticeably below that frequency.

3-4.3. Power Gain

E-plane polar gain patterns for a 27 element reactively loaded aperture antenna array are given in Figures 3.19 - 3.21 for five frequencies and three beam steering angles. If one compares Figure 3.19 with Figure 3.9 for the linear array ($\phi = 0$), one observes a small increase in gain but a better mainbeam to backlobe ratio for the two dimensional array. One might expect only a small gain increase since the number of elements in the column containing the driven element is still nine and the adjacent columns couple only a small amount of energy which can be reradiated in the $\phi = 0$ direction. If a comparison is made

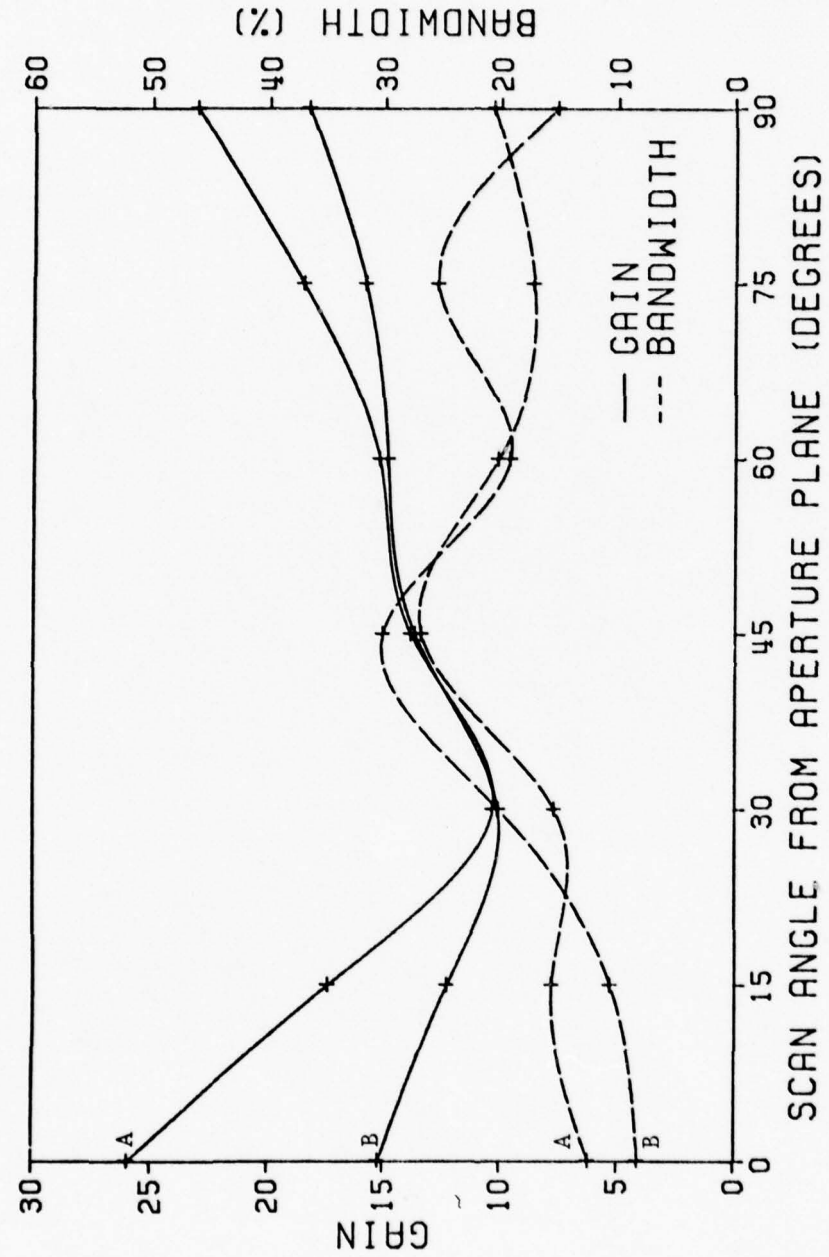

Fig. 3.17. E-plane gain and bandwidth versus beam steering angle ϕ for a 27 element reactively loaded two dimensional aperture antenna array where $a/\lambda = 0.750$, $a'/\lambda = 0.500$, $b/\lambda = 0.375$, $b'/\lambda = 0.250$, $D_x/\lambda = D_y/\lambda = 0$, $D_t/\lambda = 0.040$, case (A) - $f = 0.95\ f_o$, and case (B) - $f = f_o$.

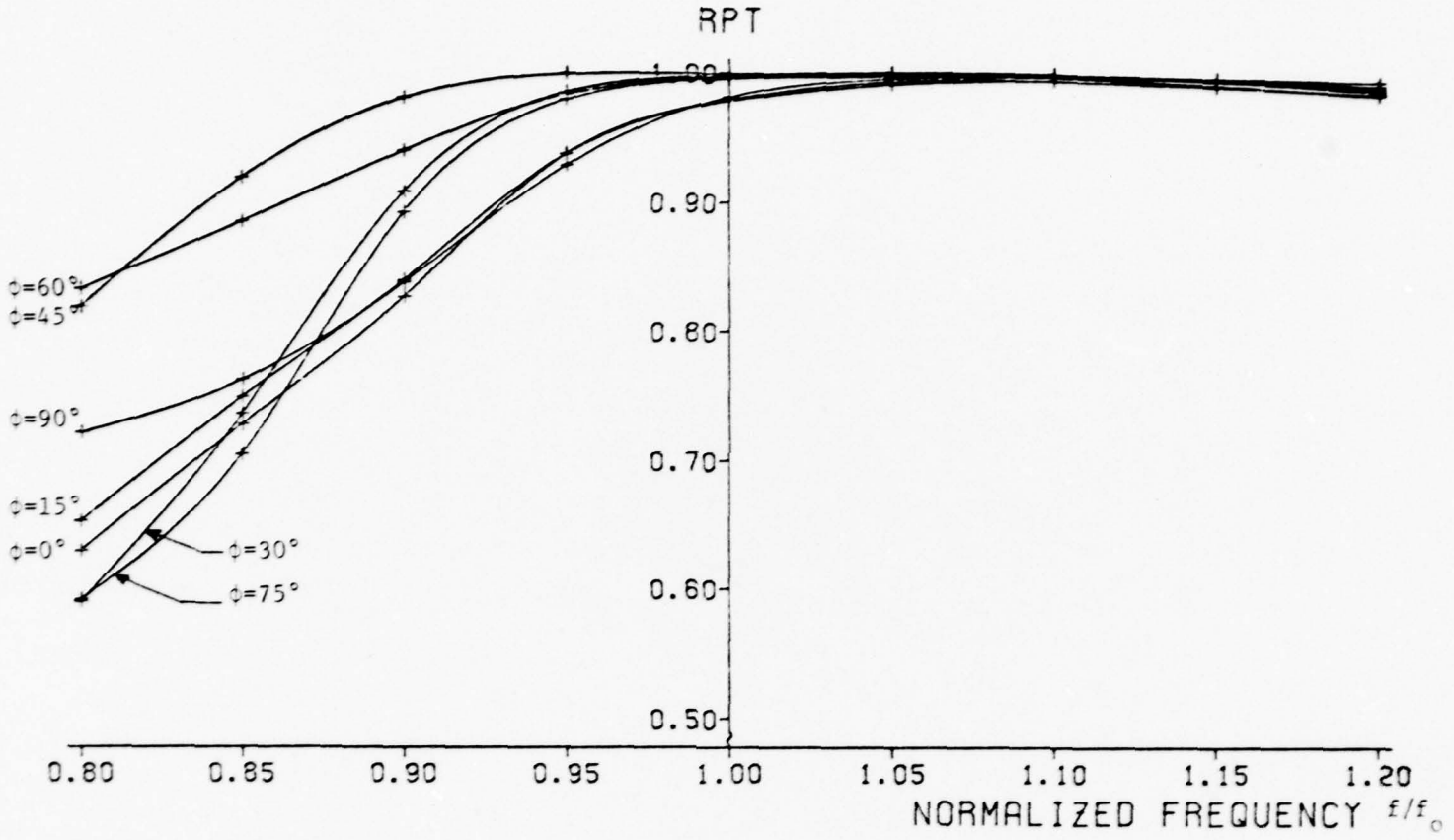

Fig. 3.18. Relative power transmitted versus frequency for a 27 element reactively loaded two dimensional aperture antenna array where $a/\lambda = 0.750$, $a'/\lambda = 0.500$, $b/\lambda = 0.375$, $b'/\lambda = 0.250$, $D_x/\lambda = D_y/\lambda = 0$, and $D_t/\lambda = 0.040$.

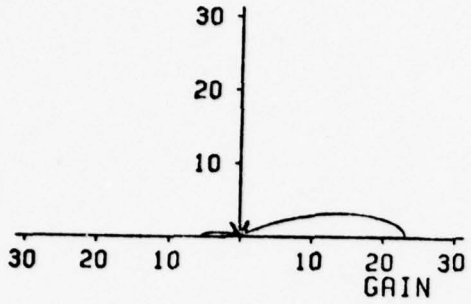

(a) $f = 0.90\ f_o$

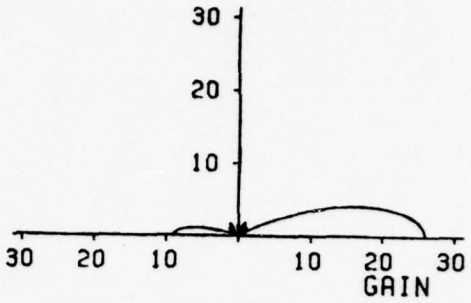

(b) $f = 0.95\ f_o$

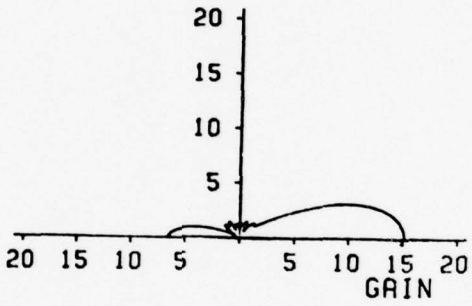

(c) $f = f_o$

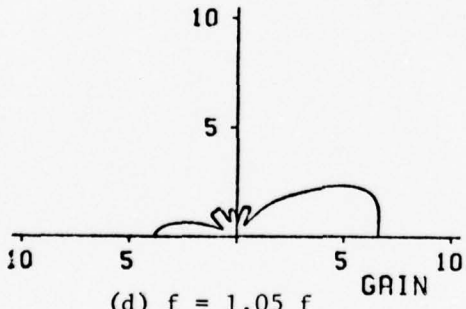

(d) $f = 1.05\ f_o$

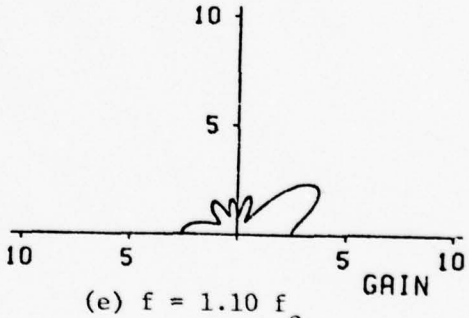

(e) $f = 1.10\ f_o$

Fig. 3.19. E-plane polar gain as a function of frequency f for a 27 element reactively loaded two dimensional aperture antenna array, where $\phi = 0$, $a/\lambda = 0.750$, $a'/\lambda = 0.500$, $b/\lambda = 0.375$, $b'/\lambda = 0.250$, $D_x/\lambda = D_y/\lambda = 0$ and $D_t/\lambda = 0.040$.

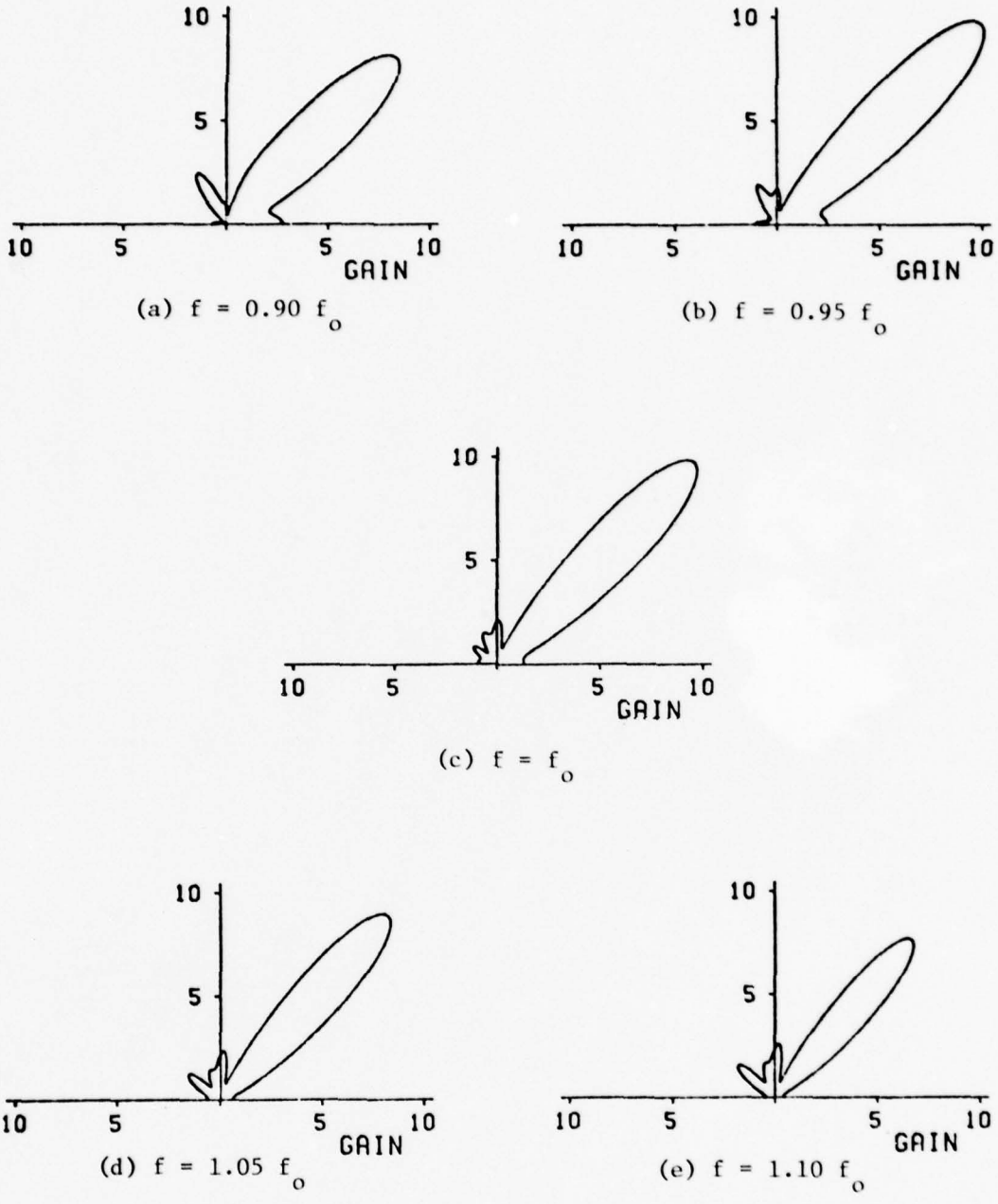

(a) $f = 0.90\ f_o$

(b) $f = 0.95\ f_o$

(c) $f = f_o$

(d) $f = 1.05\ f_o$

(e) $f = 1.10\ f_o$

Fig. 3.20. E-plane polar gain as a function of frequency f for a 27 element reactively loaded two dimensional aperture antenna array, where $\phi = 45°$, $a/\lambda = 0.750$, $a'/\lambda = 0.500$, $b/\lambda = 0.375$, $b'/\lambda = 0.250$, $D_x/\lambda = D_y/\lambda = 0$, and $D_t/\lambda = 0.040$.

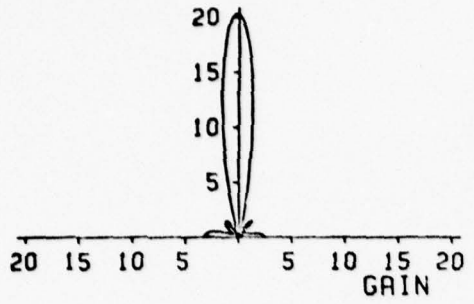

(a) $f = 0.90\ f_o$

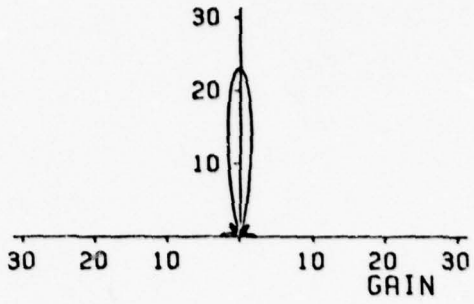

(b) $f = 0.95\ f_o$

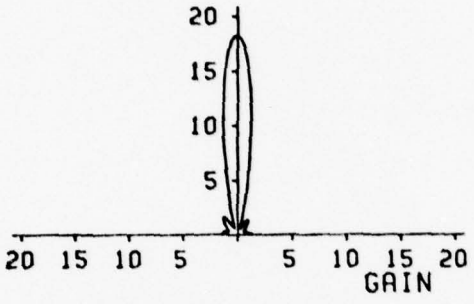

(c) $f = f_o$

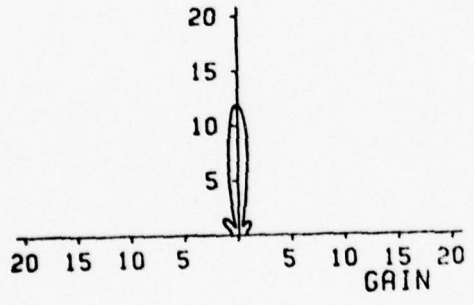

(d) $f = 1.05\ f_o$

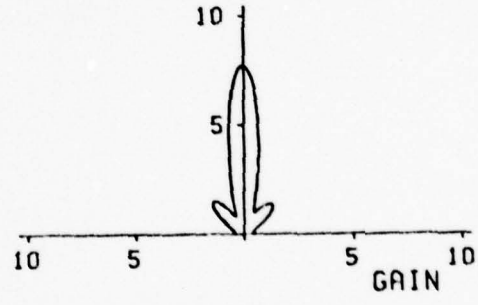

(e) $f = 1.10\ f_o$

Fig. 3.21. E-plane polar gain as a function of frequency f for a 27 element reactively loaded two dimensional aperture antenna array, where $\phi = 90°$, $a/\lambda = 0.750$, $a'/\lambda = 0.500$, $b/\lambda = 0.375$, $b'/\lambda = 0.250$, $D_x/\lambda = D_y/\lambda = 0$, and $D_t/\lambda = 0.040$.

between Figures 3.20 - 3.21 with Figures 3.10 - 3.11 for the linear array (ϕ = 45° and 90°), a large improvement in the gain pattern can be observed. The corresponding H-plane pattern for the ϕ = 90° E-plane case would show the pattern beamwidth varying between 20° and 30° as the frequency is changed. Note that the beamwidth obtained is approximately one-half the value for the nine element reactively loaded linear aperture antenna array discussed in the last section.

The E-plane polar gain patterns at frequencies $f = 0.95\ f_o$ and $f = f_o$ and four beam steering angles are given in Figure 3.22. At three of the four beam steering angles (ϕ = 0, 60°, and 90°), the curves corresponding to a frequency of $f = 0.95\ f_o$ are more acceptable than those curves corresponding to a frequency of $f = f_o$. This fact reinforces the previously mentioned strategy of optimizing at a frequency higher than the desired operating frequency. The corresponding H-plane patterns for both cases would show more acceptable patterns at all four beam steering angles for the curves corresponding to a frequency of $f = 0.95\ f_o$. For both cases, the pattern beamwidth varies between 20° and 30° as the beam is steered from ϕ = 0 to ϕ = 90°.

3-5. Effect of Waveguide Short Position (Reactive Load) Perturbations on Antenna Gain versus Frequency Patterns

In the previous section one observed the effect on the antenna gain versus frequency patterns when all of the waveguide short positions were changed by a fixed amount in the same direction (frequency scaling). These results corresponded to a shifting of the gain versus frequency curves.

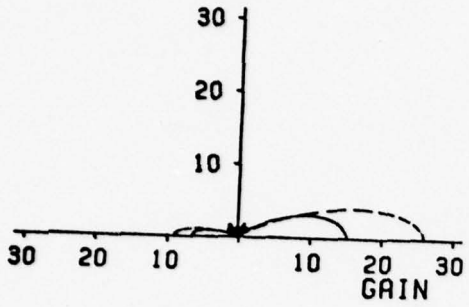

(a) $\phi = 0°$

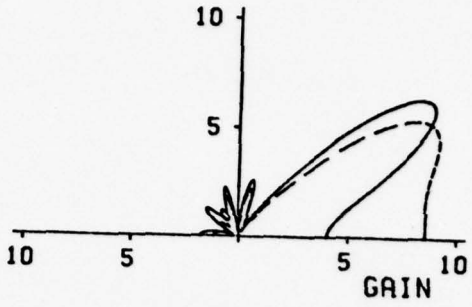

(b) $\phi = 30°$

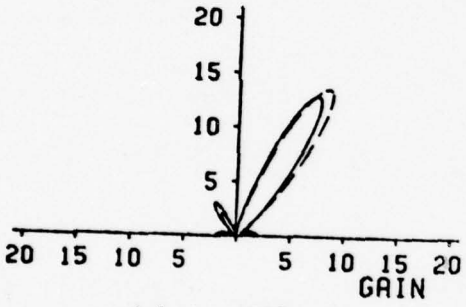

(c) $\phi = 60°$

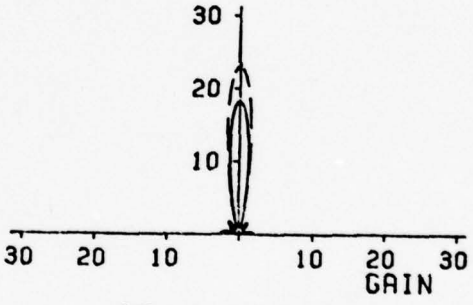

(d) $\phi = 90°$

Fig. 3.22. E-plane polar gain as a function of beam steering angle ϕ for a 27 element relatively loaded two dimensional aperture antenna array, where $a/\lambda = 0.750$, $a'/\lambda = 0.500$, $b/\lambda = 0.375$, $b'/\lambda = 0.250$, $D_x/\lambda = D_y/\lambda = 0$, $D_t/\lambda = 0.040$, (---) $f = 0.95\ f_o$, and (——) $f = f_o$.

In Figures 3.23 - 3.25 a fixed percentage change in waveguide short positions is made for a nine element reactively loaded aperture antenna array. This change alternated from waveguide to waveguide (for the first waveguide, a fixed percentage change in the short position is made toward the aperture while in the second waveguide, the same percentage change is made away from the aperture, etc.). For all three figures the degradation in the polar gain and gain versus frequency patterns at a frequency f_o is relatively small for both 5% and 10% short position changes. The greatest pattern degradation occurs in Figure 3.23 where the gain values are the largest.

3-6. Conclusion

In this chapter both linear and two dimensional reactively loaded aperture antenna arrays were analyzed in terms of their antenna characteristics of bandwidth, match, and power gain. For the linear array examples the array corresponding to aperture dimensions $a'/\lambda = 0.500$, $b'/\lambda = 0.250$ exhibited more acceptable gain pattern characteristics over a larger frequency range than the other cases. The two dimensional array had improved gain pattern characteristics over the linear array examples, especially at beam steering angles other than 0. Finally, it was shown that alternating waveguide short positions by 5% and 10% did not significantly alter the gain versus frequency patterns for a linear array example.

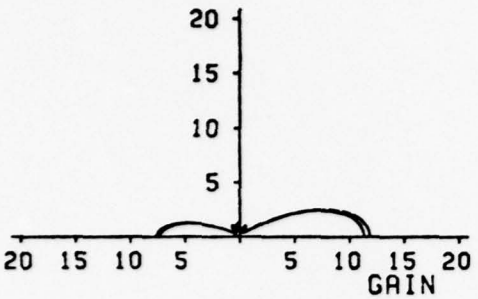

(a) 5% alternating short positions.

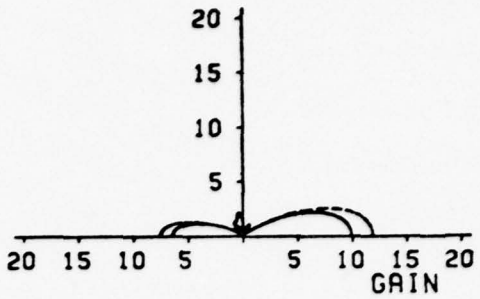

(b) 10% alternating short positions.

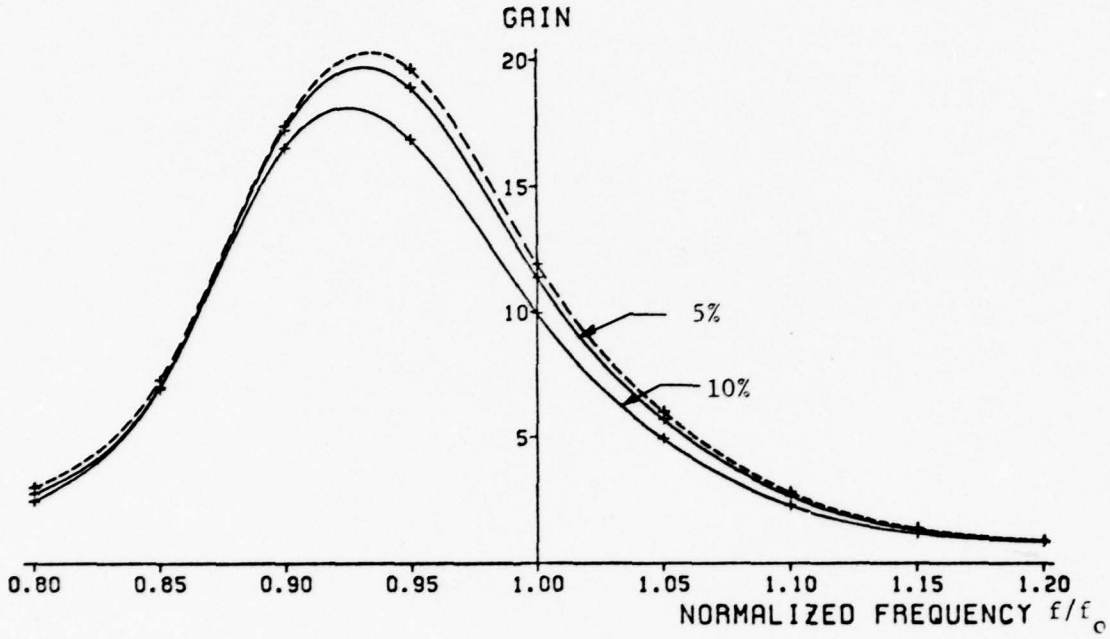

Fig. 3.23. E-plane gain sensitivity for alternating short position perturbations for a nine element reactively loaded linear aperture antenna array, where $\phi = 0$, $a/\lambda = 0.750$, $a'/\lambda = 0.500$, $b/\lambda = 0.375$, $b'/\lambda = 0.250$, $D_y/\lambda = 0$, $D_t/\lambda = 0.040$, and (---) unperturbed response.

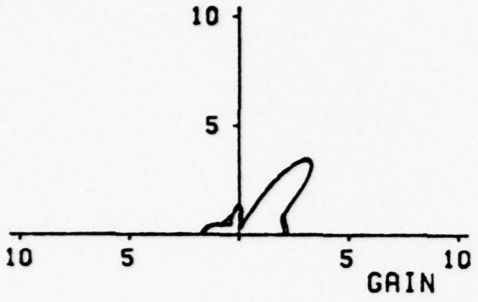

(a) 5% alternating short positions.

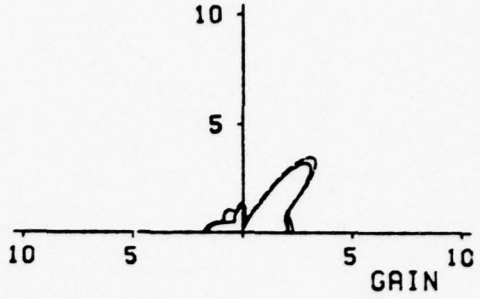

(b) 10% alternating short positions.

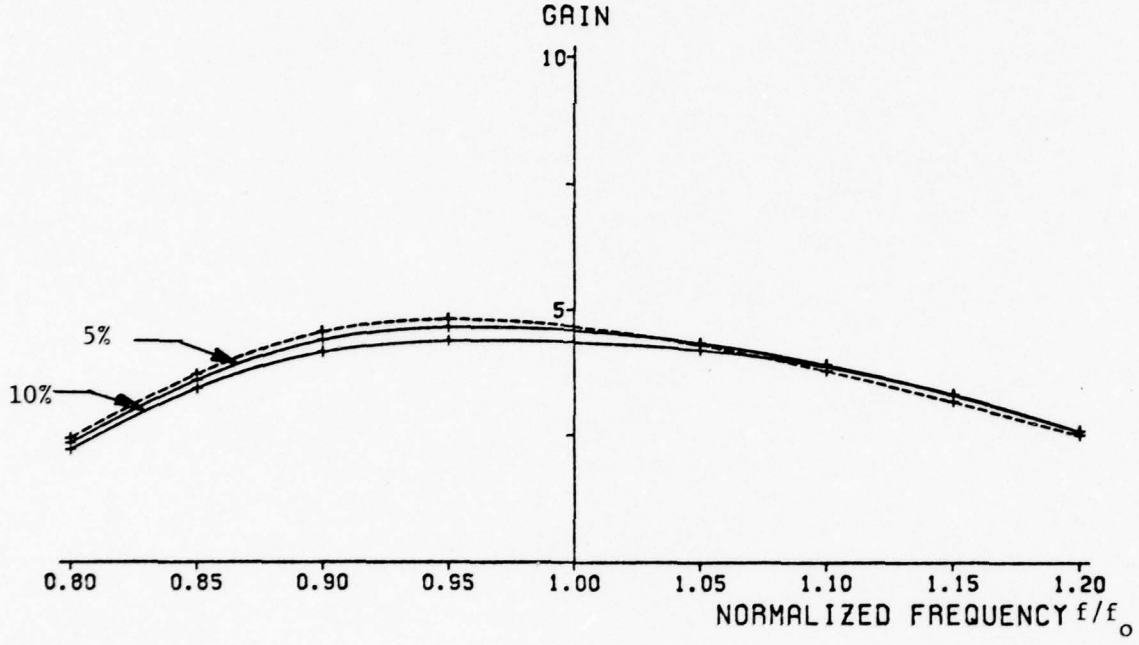

Fig. 3.24. E-plane gain sensitivity for alternating short position perturbations for a nine element reactively loaded linear aperture antenna array, where $\phi = 45°$, $a/\lambda = 0.750$, $a'/\lambda = 0.500$, $b/\lambda = 0.375$, $b'/\lambda = 0.250$, $D_y/\lambda = 0$, $D_t/\lambda = 0.040$, and (---) unperturbed response.

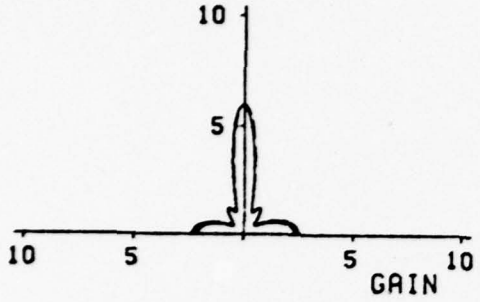

(a) 5% alternating short positions.

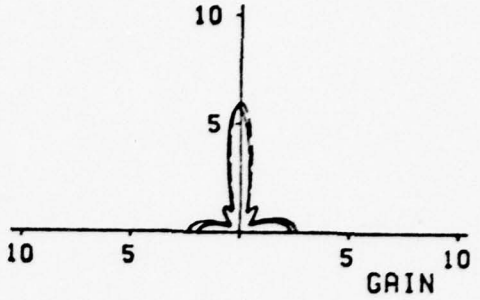

(b) 10% alternating short positions

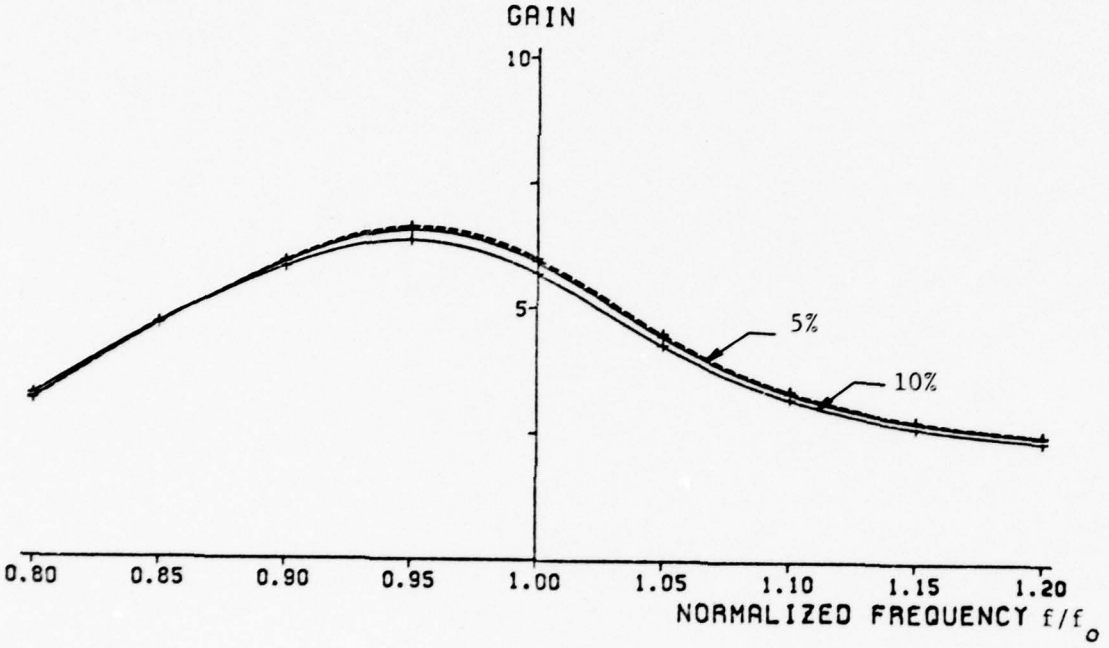

Fig. 3.25. E-plane gain sensitivity for alternating short position perturbations for a nine element reactively loaded linear aperture antenna array, where $\phi = 90°$, $a/\lambda = 0.750$, $a'/\lambda = 0.500$, $b/\lambda = 0.375$, $b'/\lambda = 0.250$, $D_y/\lambda = 0$, $D_t/\lambda = 0.040$, and (---) unperturbed response.

Chapter 4

MAGNITUDE PATTERN SYNTHESIS EXAMPLES

4-1. Introduction

In the previous chapter the antenna characteristics of several reactively loaded aperture antenna array examples were calculated subject to the condition of maximum reactively loaded gain at a specified beam steering angle ϕ and frequency. In this chapter we will investigate through the use of magnitude pattern synthesis the antenna patterns which are most easily realized subject to antenna geometry and excitation constraints.

In many physical cases only the far field power pattern is specified. This, in effect, specifies the far field magnitude and leaves the far field phase arbitrary. Normally, the far field phase does not affect system performance. The synthesis procedure used in this chapter requires a specification of the magnitude of the far field electric field with no restrictions on the phase. Since we are assuming dominant mode excitation for the waveguide-fed aperture antenna array, the far electric field is linearly polarized. Therefore, the square of the magnitude of the far field electric field is proportional to the far field power pattern.

In addition to finding antenna pattern limitations, we will attempt to change the gain versus bandwidth characteristics of the antenna in the $\phi = 0$ direction. If this can be done, we will attain more uniform gain and bandwidth values as the array is scanned from $\phi = 0$ to $\phi = 90°$.

4-2. General Formulation

Consider a source v and the field g it produces on the radiation sphere. Also, let T be a known operator representing the antenna system.

The analysis problem is concerned with determination of the radiation characteristics g for a given voltage distribution v of an antenna T, that is,

$$T\, v = g \tag{4.1}$$

where this is an exact relationship.

The synthesis problem is concerned with determining the voltage distribution v of an antenna T given a specified field pattern g_o, that is,

$$T\, v \simeq g_o \tag{4.2}$$

where this is usually an inexact relationship.

In order to use matrix operations in the synthesis problem (4.2) is discretized as follows. Let

$$v = \sum_{i=1}^{N} v_i\, e_i \tag{4.3}$$

where v_i are constants and e_i are basis elements. Since the source is continuous, the e_i are functions and (4.3) is an approximation to the true source. Define $\vec{v}$ to be the vector having the components v_i, that is,

$$\vec{v} = [v_i]_{N\times 1} \,. \tag{4.4}$$

Next, substitute (4.3) into (4.2) and evaluate (4.2) at P points

(θ_p, ϕ_p), p = 1,2,...,P on the radiation sphere. In matrix notation, we have

$$[T]\vec{v} \simeq \vec{g}_o \tag{4.5}$$

where the pth element of the $\vec{g}_o$ vector is given by

$$g_{op} = g_o(\phi_p) \tag{4.6}$$

and [T] is the matrix

$$[T] = [(T\ e_i)_p]_{P\times N} \quad . \tag{4.7}$$

Here $(T\ e_i)_p$ denotes the pattern of e_i evaluated at the point (θ_p, ϕ_p).

Next we consider an array of N waveguide-fed apertures in the x-y plane (see Figure 2.1). To find the electric field for a single aperture centered at (x_i, y_i), we apply both the equivalence principle and image theory to obtain a strip of magnetic current $-2\underset{\sim}{M}_i$ radiating into half-space producing the original fields in the half-space region. The far electric field in the $\theta = \pi/2$ plane can then be expressed in terms of an electric vector potential as

$$E^i_\phi(\phi) = - jk\ F^i_x(\phi) \tag{4.8}$$

where

$$F^i_x(\phi) = - \frac{1}{2\pi} \iint_{\text{apert.}} \frac{M^i_x\ e^{-jk|\underset{\sim}{r}-\underset{\sim}{r}'|}}{|\underset{\sim}{r}-\underset{\sim}{r}'|}\ ds \tag{4.9}$$

($\underset{\sim}{r}$ and $\underset{\sim}{r}'$ are respectively the vectors to the field and source points and k is the free space propagation constant).

For our problem

$$\underset{\sim}{M}^i = \underset{\sim}{u}_z \times \underset{\sim}{u}_y E_y^i \Big|_{\text{apert.}}$$

$$= - V_i P_i(x,y) \cos \frac{\pi}{a'} (x-x_i) \underset{\sim}{u}_x \tag{4.10}$$

where

$$P_i(x,y) = \begin{cases} \sqrt{\frac{2}{a'b'}} & \begin{cases} x_i - \frac{a'}{2} \le x \le x_i + \frac{a'}{2} \\ y_i - \frac{b'}{2} \le y \le y_i + \frac{b'}{2} \end{cases} \\ 0 & \text{all other } x,y \ . \end{cases} \tag{4.11}$$

Substituting the far-field approximation

$$\frac{e^{-jk|\underset{\sim}{r}-\underset{\sim}{r}'|}}{|\underset{\sim}{r}-\underset{\sim}{r}'|} \simeq \frac{e^{-jkr}}{r} e^{jky' \cos \phi} \tag{4.12}$$

and (4.10) - (4.11) into (4.9), we obtain

$$F_x^i(\phi) = - \frac{1}{2\pi} \sqrt{\frac{2}{a'b'}} \frac{e^{-jkr}}{r} V_i \int_{y_i - \frac{b'}{2}}^{y_i + \frac{b'}{2}} dy' e^{jky' \cos\phi} \int_{x_i - \frac{a'}{2}}^{x_i + \frac{a'}{2}} dx' \cos \frac{\pi}{a'} (x'-x_i)$$

$$= - \frac{1}{\pi^2} \sqrt{2a'b'} \frac{e^{-jkr}}{r} V_i e^{jky_i \cos\phi} \frac{\sin(\frac{kb'}{2} \cos\phi)}{\frac{kb'}{2} \cos\phi} \ . \tag{4.13}$$

Substituting (4.13) into (4.8), we obtain

$$E_x^i(\phi) = - \frac{jk}{\pi^2} \sqrt{2a'b'} \frac{e^{-jkr}}{r} V_i e^{-jky_i \cos\phi} \frac{\sin(\frac{kb'}{2} \cos\phi)}{\frac{kb'}{2} \cos\phi}$$

$$= K \, G^i(\phi) \tag{4.14}$$

where

$$K = - \frac{jk}{\pi^2} \sqrt{2a'b'} \frac{e^{-jkr}}{r} \tag{4.15}$$

$$G^i(\phi) = V_i \, e^{jky_i \cos\phi} \, \frac{\sin(\frac{kb'}{2}\cos\phi)}{\frac{kb'}{2}\cos\phi} \tag{4.16}$$

(when $\phi = \frac{\pi}{2}$, the $\sin(\frac{kb'}{2}\cos\phi)/(\frac{kb'}{2}\cos\phi)$ in (4.16) is to be replaced by its limit 1). Since we are interested only in pattern shape, the far electric field can be represented by $G^i(\phi)$ or for N apertures

$$G(\phi) = \sum_{i=1}^{N} G^i(\phi) \, . \tag{4.17}$$

The pattern magnitude synthesis procedure uses N_f frequencies and P points from the desired pattern $|\vec{g}_o|$ and finds a source $\vec{V}$ such that the pattern error

$$\begin{aligned} \varepsilon &= \sum_{n=1}^{N_f} \sum_{p=1}^{P} w_{np} \, \| G_n(\phi_p) | - |g_o(\phi_p)| \|^2 \\ &= \sum_{n=1}^{N_f} \sum_{p=1}^{P} w_{np} \, \| \sum_{i=1}^{N} V_{ni} T_{npi} | - |g_o(\phi_p)| \|^2 \end{aligned} \tag{4.18}$$

is minimized. Here w_{np} is a weighting function ($w_{np} > 0$), $G_n(\phi_p)$ is equal to $G(\phi_p)$ at the nth frequency, and

$$T_{npi} = \{ e^{jky_i \cos\phi_p} \, \frac{\sin(\frac{kb'}{2}\cos\phi_p)}{\frac{kb'}{2}\cos\phi_p} \}_n \tag{4.19}$$

($\{ \}_n$ means that the quantity in brackets is evaluated at the nth frequency).

4-2.1. Reactively Loaded Array

For the reactively loaded array, the V_{ni} in (4.18) is equal to

$$V_{ni} = \{[Y^{wg} + Y^{hs}]^{-1} \vec{I}^{imp}\}_{ni} \tag{4.20}$$

($\{\ \}_{ni}$ indicates the ith element of the column matrix $[Y^{wg} + Y^{hs}]^{-1} \vec{I}^{imp}$ is evaluated at the nth frequency). Substituting (4.20) into (4.18), we obtain

$$\varepsilon = \sum_{n=1}^{N_f} \sum_{p=1}^{P} w_{np} \left\| \sum_{i=1}^{N} \{[Y^{wg} + Y^{hs}]^{-1} \vec{I}^{imp}\}_{ni} T_{npi} \right| - |g_o(\phi_p)| \Big\|^2 . \tag{4.21}$$

There are N unknowns in (4.21), namely, N-1 unknown short circuit distances d_i which enter through (2.40) and one unknown excitation coefficient I^{imp}_{NFP}. It is assumed that I^{imp}_{NFP} does not depend on n. The error (4.21) is a complicated function of d_i involving a cotangent and an inverse matrix. The only recourse is to an optimization technique.

For the optimization of (4.21),

$$Y^{wg} + Y^{hs} = Y^{hs} + \text{Real}(Y^{wg}) + jB_L \tag{4.22}$$

where $B_L = \text{Imag}\ (Y^{wg})$. With $B_{L_{NFP}}$ held constant, (4.21) is optimized with respect to the d_i appearing in (2.40) for all i except NFP. For the single frequency case, d_i can be restricted so that

$$0 \leq d_i \leq \frac{\pi}{\beta_o} . \tag{4.23}$$

However, for the multiple frequency case, d_i can take on values

$$0 \leq d_i \leq \infty . \tag{4.24}$$

The upper limit of infinity for d_i in Eq. (4.24) can be explained as follows. The argument of the cotangent function in (2.40) can be written as $\beta_o d_i$ or $\beta_o d_i + n\pi$ where n is a positive integer. If we choose the latter argument, we can write

$$\cot(\beta_o d_i + n\pi) = D_o \tag{4.25}$$

or

$$d_i = \frac{\cot^{-1}(D_o) - n\pi}{\beta_o} \tag{4.26}$$

(the constant β_o was determined at a frequency of f_o). At a frequency other than f_o, the argument of the cotangent function becomes

$$\beta_o' d_i + n\pi = \frac{\beta_o'}{\beta_o} (\cot^{-1}(D_o) - n\pi) + n\pi$$

$$= \frac{\beta_o'}{\beta_o} \cot^{-1}(D_o) + (1 - \frac{\beta_o'}{\beta_o}) n\pi \tag{4.27}$$

where β_o' is B_o determined at the new frequency. As n is varied in (4.27), the cotangent of this argument will vary.

The optimization algorithm chosen to minimize (4.21) was that of Rosenbrock [22]. The Rosenbrock algorithm uses a set of N mutually orthogonal directions in each cycle of searches (stage). After each stage a new set of orthogonal directions are obtained by rotating the former direction vectors.

For the calculated results illustrated in the next two sections, (4.3) and (4.4), N variables are used in the Rosenbrock algorithm (N-1 short circuit distances d_i and the excitation coefficient I_{NFP}^{imp}). It should be mentioned that (4.21) does not depend on the phase of I_{NFP}^{imp}

so that I_{NFP}^{imp} can be taken as real and positive. When this is done, (4.21) becomes a simple quadratic function in I_{NFP}^{imp}. From this quadratic the optimum value of I_{NFP}^{imp} can be easily obtained for fixed short circuit distances d_i. If this optimum value of I_{NFP}^{imp} were substituted back into (4.21), only the N-1 short circuit distances d_i would enter into the Rosenbrock search.

4-2.2. Optimum Excitation

In this subsection a solution is given for the same array analyzed in the preceding subsection but with all the elements driven. In the next section (4.3) a comparison of the synthesized patterns will be made between the reactively loaded array and the optimum excited array to indicate the degree of degradation due to the restricted excitation for the reactively loaded array.

The far electric field magnitude at a point p in the $\theta = \pi/2$ plane has the same form as the single frequency ($T_{npi} = T_{pi}$) reactively loaded case, that is,

$$|G(\phi_p)| = \left| \sum_{i=1}^{N} v_i \, T_{pi} \right| . \tag{4.28}$$

Here, v_i can take on any complex value in contrast to the restricted values for the reactively loaded case. A solution for the pattern magnitude synthesis problem using (4.28) can be found in [23], and the following is a summary of the formulation.

The error function to be minimized for the general synthesis problem where both magnitude and phase of the desired pattern $\vec{g}_o$ are specified is

$$\varepsilon = \sum_{p=1}^{P} w_p \left| \sum_{i=1}^{N} v_i T_{pi} - g_o(\phi_p) \right|^2 \quad . \tag{4.29}$$

Note that Eq. (4.29) is evaluated at only one frequency while Eq. (4.18) for the reactively loaded case is evaluated at many frequencies up to N_f. Multi-frequency synthesis is used for the reactively loaded case to both broaden and shift the displaced gain versus frequency curve. For the optimum excited case the gain versus frequency curve was centered at the design frequency. The vector $\vec{v}$ of the coefficients v_i which minimize (4.29) (see section V of [23] with $\alpha = 0$) is

$$\vec{v} = [\tilde{T}^* W T]^{-1} [\tilde{T}^* W] \vec{g}_o \tag{4.30}$$

where * signifies complex conjugate, ~ signifies transpose, and [W] is a weighting matrix.

When the pattern magnitude only is specified, the error function becomes

$$\varepsilon = \sum_{p=1}^{P} w_p \left| \left| \sum_{i=1}^{N} v_i T_{pi} \right| - |g_o(\phi_p)| \right|^2 \quad . \tag{4.31}$$

To circumvent the inner magnitude operation in (4.31), we consider the following more general error function

$$\varepsilon(\vec{\beta}) = \sum_{p=1}^{P} w_p \left| \sum_{i=1}^{N} v_i T_{pi} - |g_o(\phi_p)| e^{j\beta_p} \right|^2 \quad . \tag{4.32}$$

In other words we are specifying a phase for the pattern magnitude in order to obtain a more easily solved expression. For v_i fixed, a minimum is obtained when both terms within the outer magnitude sign of (4.32) are in phase, that is,

$$e^{j\beta_p} = \frac{\sum_{i=1}^{N} v_i T_{pi}}{\left|\sum_{i=1}^{N} v_i T_{pi}\right|} \quad . \tag{4.33}$$

Since substitution of (4.33) into (4.32) gives (4.31), the minimum of (4.32) with respect to $\vec{v}$ and $\vec{\beta}$ is equal to the minimum of (4.31) with respect to $\vec{v}$.

To find the minimum of (4.32), the following iterative procedure is used:

1. Assume starting values for $\beta_1, \beta_2, \ldots, \beta_p$.
2. Keep the β_p fixed and calculate the v_i which minimizes ε using (4.30)[1].
3. Keep the v_i fixed and calculate the β_p which minimizes ε using (4.33).
4. Go to step (2).

This procedure converges to a stationary point because steps (2) and (3) cannot increase ε.

4-2.3. Normalized Synthesis Error and Q-Factor

Two figures of merit will be used in the next section to evaluate the synthesis results. The first figure of merit is the normalized synthesis error which is defined as

---

[1] It should be noted that if $[\tilde{T}^*WT]$ is ill-conditioned, the procedure will fail since small rounding errors that occur in its inversion can cause large errors in its inverse $[\tilde{T}^*WT]^{-1}$. To use this procedure, the ratio of the largest eigenvalue to the smallest of $[\tilde{T}^*WT]$ should be on the order of 10^3 or less.

$$\varepsilon_{syn} = \frac{\sum_{p=1}^{P} w_p \left| |G(\phi_p)| - |g_o(\phi_p)| \right|^2}{\sum_{p=1}^{P} w_p |g_o(\phi_p)|^2} \quad . \tag{4.34}$$

The smaller the value of ε_{syn}, the closer the synthesized pattern is to the desired pattern.

The second figure of merit is the Q or quality factor. The Q-factor is a measure of the magnitude of the element excitation required to produce a given pattern. The larger the value of Q, the more impractical the pattern realization becomes due to the larger element excitation required. Lo, Lee, and Lee [24] defined the Q-factor as

$$Q = \frac{\sum_{i=1}^{N} |V_i|^2}{\int_{4\pi} |P(\theta,\phi)|^2 d\Omega} \tag{4.35}$$

where V_i is the ith element voltage excitation value and $P(\theta, \phi)$ is the pattern due to the set of voltages V_i.

An expression similar to (4.35) is

$$Q = P \frac{\sum_{i=1}^{N} |V_i|^2}{\sum_{p=1}^{P} |G(\phi_p)|^2} \quad . \tag{4.36}$$

The multiplier P is introduced to make Q relatively insensitive to the number of field points chosen. The main difference between the Q expressions of (4.35) and (4.36) is that the denominator of (4.35) is an integral over the whole radiation sphere while the denominator of (4.36) is a summation over P points in the yz plane.

4-3. Single Frequency Synthesis Results

In this section three cosine squared electric field patterns are synthesized using both reactively loaded and optimum excited nine element linear aperture antenna arrays. In each figure a polar pattern comparison is made between the pattern to be synthesized and the synthesized patterns obtained from reactively loaded and optimum excited arrays. Also in each figure, a comparison is made between the gain versus frequency curves obtained by using reactive loads derived from maximum gain and synthesis procedures. This comparison is necessary to determine gain versus frequency degradation which results from satisfying an error criterion at a single frequency.

Figures 4.1-4.4 illustrate the single frequency ($f = f_o$) synthesis results for cosine squared patterns with half-power beamwidths of 15°, 30°, and 45° and beam steering angles of $\phi = 0$, 30°, 60°, and 90°. (The half-power beamwidth of an antenna is defined as the angular separation between two directions on each side of the main beam maximum at which the power density is reduced by half.) In all four figures the pattern with a beamwidth of 45° was synthesized with the lowest error for both reactively loaded and optimum excited arrays.

Using the reactive loads obtained from all three pattern cases in Figure 4.1, the resulting gain versus frequency curves shifted toward a lower frequency with a small change in the general shape of the curves in comparison to the maximum reactively loaded gain curve. In Figures 4.2-4.4 the gain versus frequency curves for case (c) show the greatest degradation

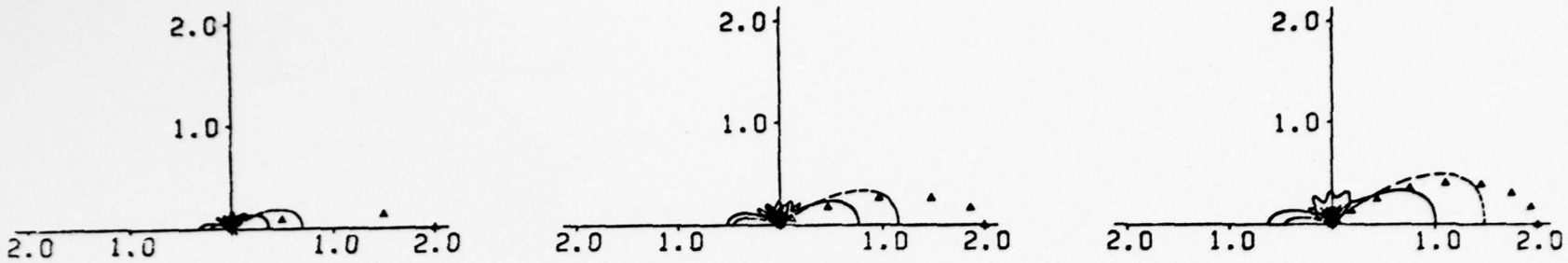

(a) OE: ε_{syn} = 0.58, Q = 0.96
RL: ε_{syn} = 0.78, Q = 1.10

(b) OE: ε_{syn} = 0.29, Q = 0.89
RL: ε_{syn} = 0.53, Q = 0.95

(c) OE: ε_{syn} = 0.12, Q = 0.80
RL: ε_{syn} = 0.40, Q = 0.97

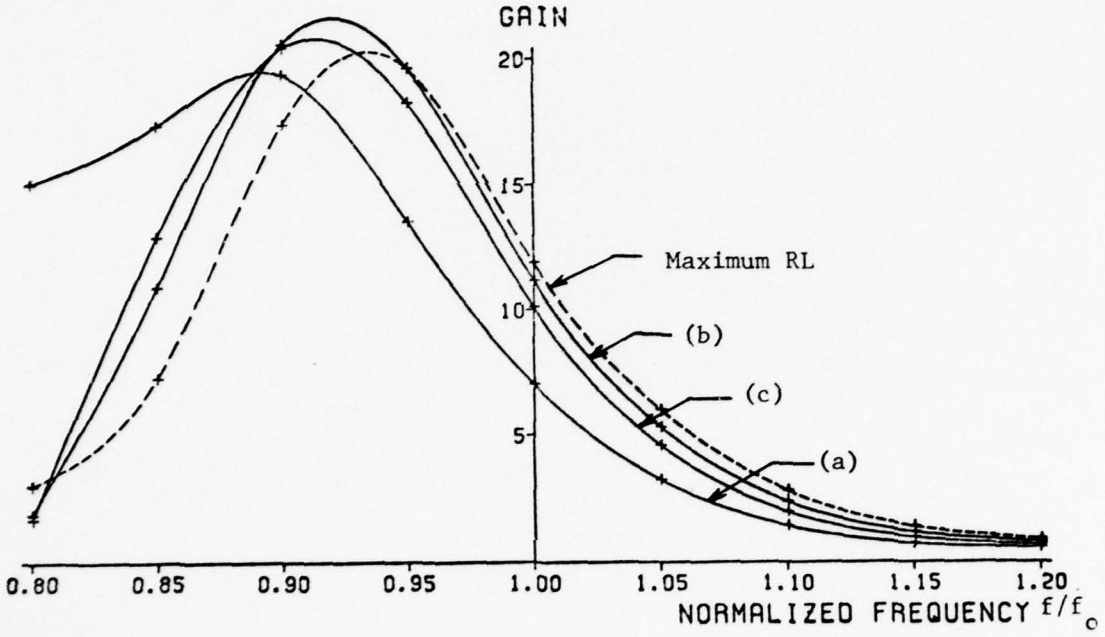

Fig. 4.1. Far electric field synthesized patterns, (a)-(c), for a nine element reactively loaded linear aperture antenna array where ϕ = 0, a/λ = 0.750, a'/λ = 0.500, b/λ = 0.375, b'/λ = 0.250, D_y/λ = 0, D_t/λ = 0.040, and in (a)-(c): Δ-pattern shape to be synthesized, --- OE (optimum excited), —— RL (reactive loading), $f = f_o$, w_{1p} = 1.0, and P = 37.

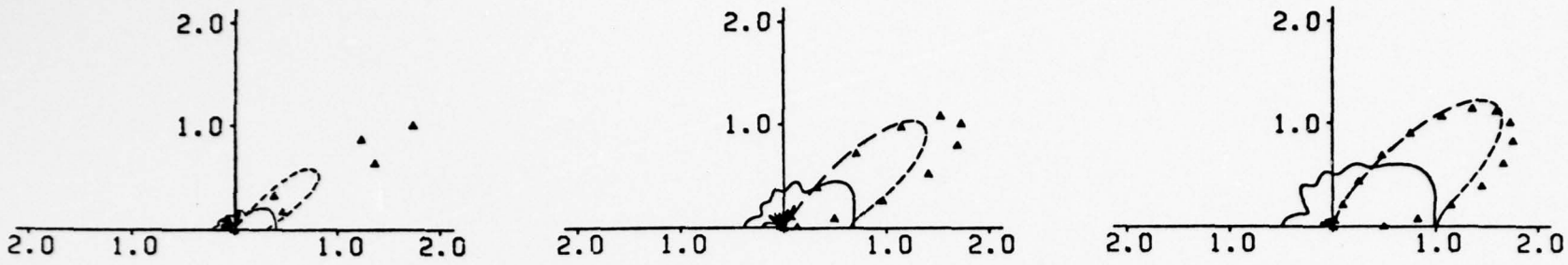

(a) OE: ε_{syn} = 0.40, Q = 0.85
RL: ε_{syn} = 0.74, Q = 0.97

(b) OE: ε_{syn} = 0.11, Q = 0.84
RL: ε_{syn} = 0.53, Q = 1.15

(c) OE: ε_{syn} = 0.02, Q = 0.83
RL: ε_{syn} = 0.37, Q = 1.14

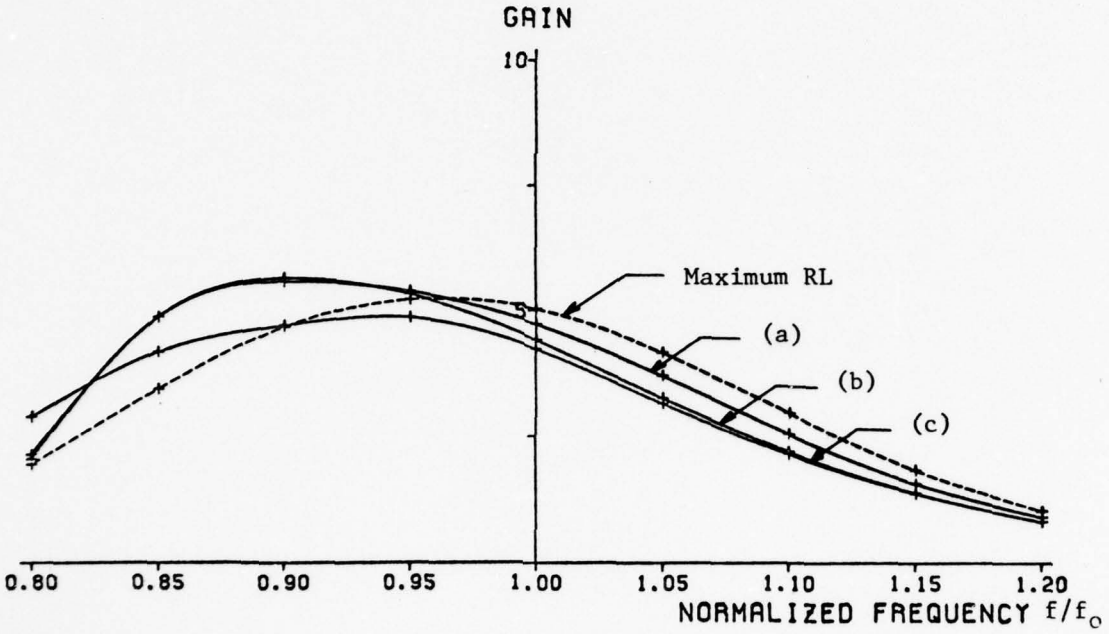

Fig. 4.2. Far electric field synthesized patterns, (a)-(c), for a nine element reactively loaded linear aperture antenna array where ϕ = 30°, a/λ = 0.750, a'/λ = 0.500, b/λ = 0.375, b'/λ = 0.250, D_y/λ = 0, D_t/λ = 0.040, and in (a)-(c): Δ-pattern shape to be synthesized, --- OE (optimum excited), —— RL (reactive loading), f = f_o, w_{1p} = 1.0, and P = 37.

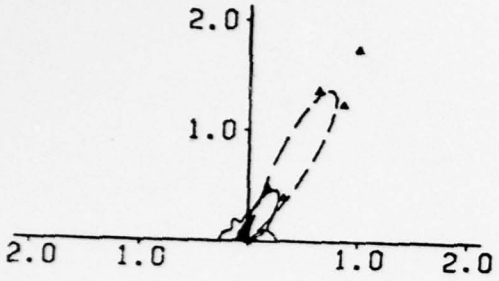

(a) OE: $\varepsilon_{syn} = 0.11$, $Q = 1.30$
RL: $\varepsilon_{syn} = 0.67$, $Q = 1.24$

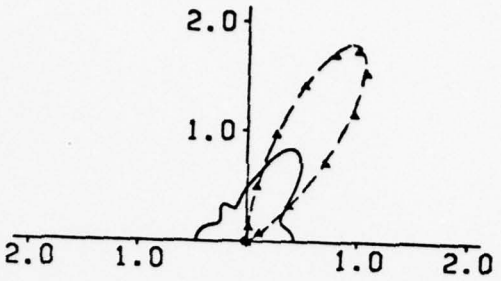

(b) OE: $\varepsilon_{syn} = 0.003$, $Q = 1.29$
RL: $\varepsilon_{syn} = 0.47$, $Q = 1.12$

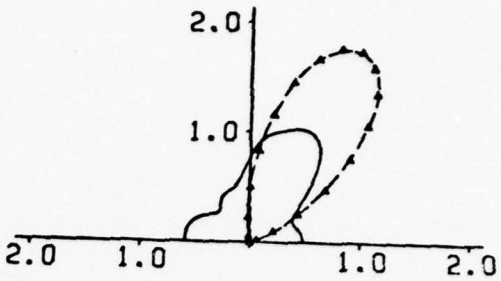

(c) OE: $\varepsilon_{syn} = 0.001$, $Q = 1.27$
RL: $\varepsilon_{syn} = 0.37$ $Q = 1.22$

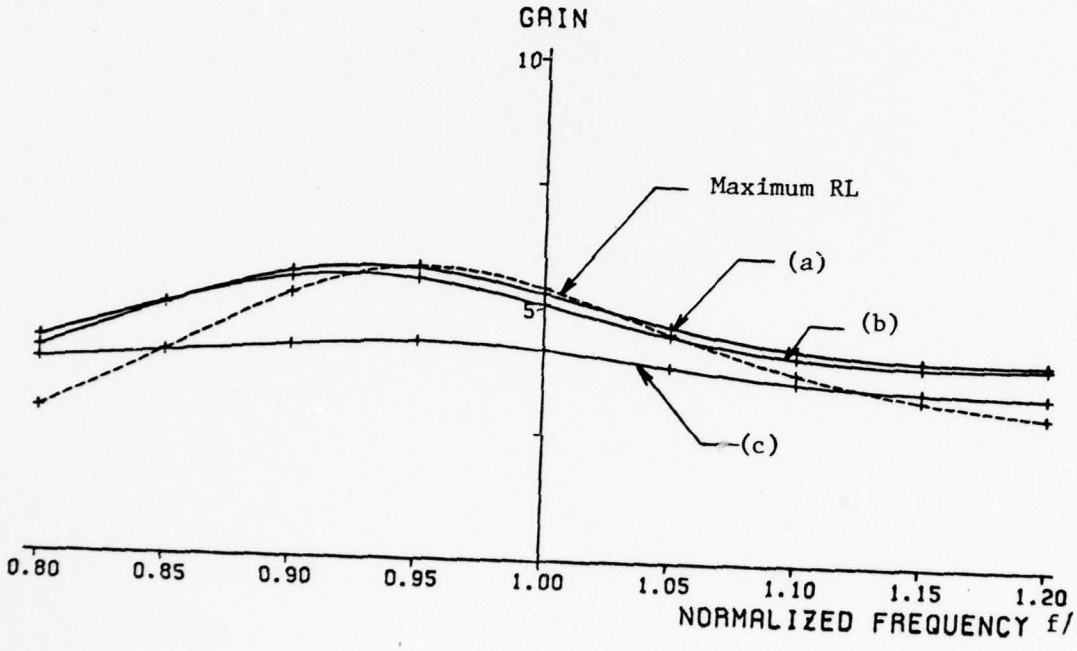

Fig. 4.3. Far electric field synthesized patterns, (a)-(c), for a nine element reactive loaded linear aperture antenna array where $\phi = 60°$, $a/\lambda = 0.750$, $a'/\lambda = 0.500$, $b/\lambda = 0.375$, $b'/\lambda = 0.250$, $D_y/\lambda = 0$, $D_t/\lambda = 0.040$, and in (a)-(c): Δ-pattern shape to be synthesized, --- OE (optimum excited), —— RL (reactive loading), $f = f_o$, $w_{1p} = 1.0$, and $P = 37$.

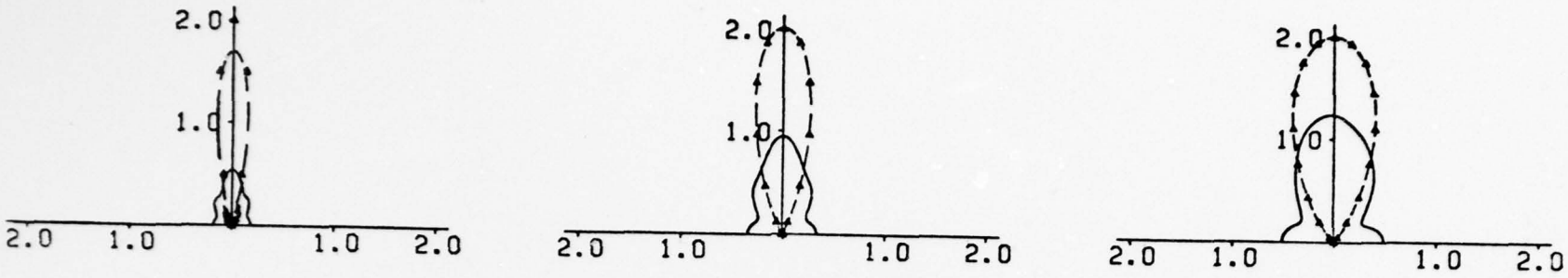

(a) OE: ε_{syn} = 0.06, Q = 1.42
RL: ε_{syn} = 0.66, Q = 1.29

(b) OE: ε_{syn} = 0.001, Q = 1.42
RL: ε_{syn} = 0.45 , Q = 1.30

(c) OE: ε_{syn} = 0.001, Q = 1.41
RL: ε_{syn} = 0.28 , Q = 1.31

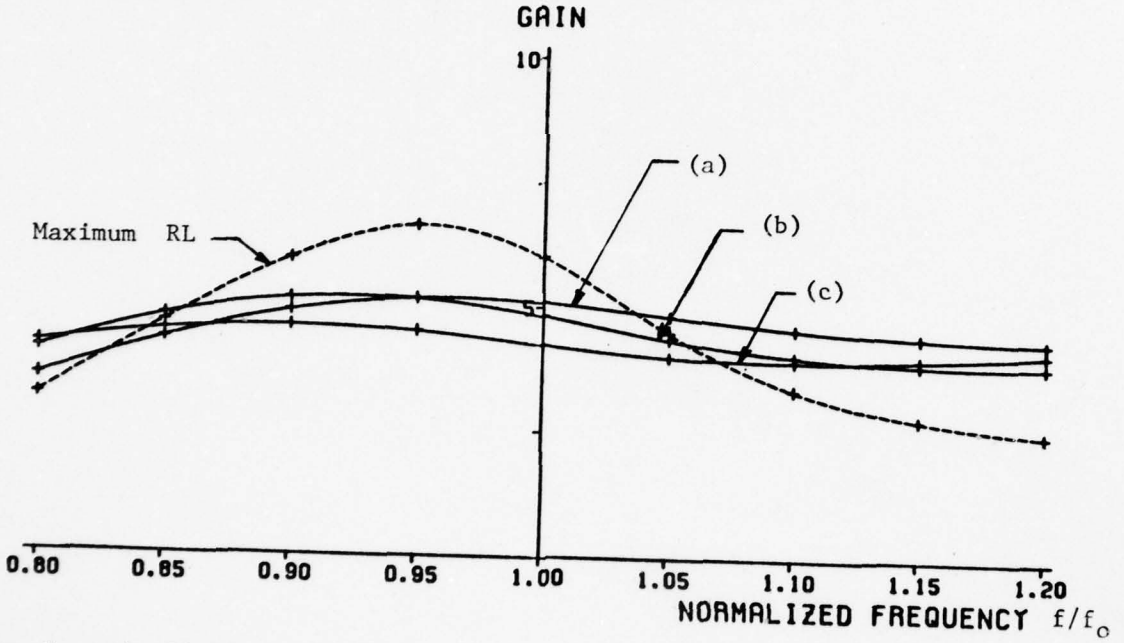

Fig. 4.4. Far electric field synthesized patterns, (a)-(c), for a nine element reactively loaded linear aperture antenna array where ϕ = 90°, a/λ = 0.750, a'/λ = 0.500, b/λ = 0.375, b'/λ = 0.250, D_y/λ = 0, D_t/λ = 0.040, and in (a)-(c): Δ-pattern shape to be synthesized, --- OE (optimum excited), —— RL (reactive loading), f = f_o, w_{1p} = 1.0, and P = 37.

AD-A066 566 SYRACUSE UNIV NY DEPT OF ELECTRICAL AND COMPUTER EN--ETC F/G 9/5
A STUDY OF A REACTIVELY LOADED FINITE PLANAR RECTANGULAR WAVEGU--ETC(U)
FEB 79 J LUZWICK, R F HARRINGTON N00014-76-C-0225
UNCLASSIFIED TR-79-2 NL

2 OF 2
AD A066566

END
DATE FILMED
5-79
DDC

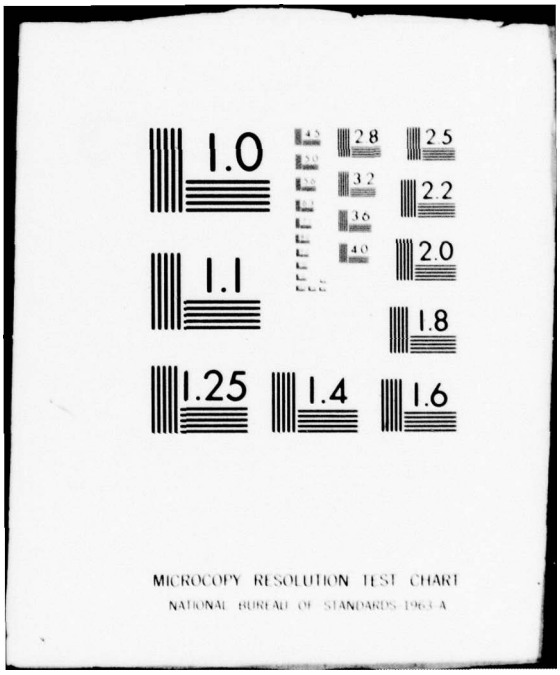
1.0
1.1
1.25
1.4
1.6
2.8
3.2
3.6
4.0
2.5
2.2
2.0
1.8
MICROCOPY RESOLUTION TEST CHART
NATIONAL BUREAU OF STANDARDS 1963-A

from the maximum reactively loaded gain curves. The degradation corresponds to a broadening of the gain versus frequency curve with reduced gain.

The values of Q obtained for all of the synthesis examples were rather low in relation to the values obtained from the indicated bandwidth (gain versus frequency curves) for the reactively loaded array examples. The main reason for this was the fact that equation (4.36) was used to compute Q instead of the more accurate equation (4.35). Therefore, the Q values calculated can be used for comparison purposes in determining which antenna example requires greater excitation but should not be used for bandwidth predictions.

4-4. Double Frequency Synthesis Results

In the previous section we found that by using the reactive loads obtained from the single frequency synthesis procedure at a beam steering angle of $\phi = 0$ (see Figure 4.1), the resulting gain versus frequency curve shifted toward lower frequencies without much change in the shape of the curve in comparison to the maximum reactively loaded gain curve. In this section for a beam steering angle of $\phi = 0$, an attempt is made to both center the gain versus frequency curve at a frequency of $f = f_o$ and to increase the bandwidth while decreasing the gain. If the latter is accomplished, a more uniform gain versus bandwidth characteristic will be obtained as the array is scanned from $\phi = 0$ to $\phi = 90°$.

Figures 4.5 and 4.6 show the results of both single and double frequency synthesis for a 20° beamwidth sector pattern in the $\phi = 0$

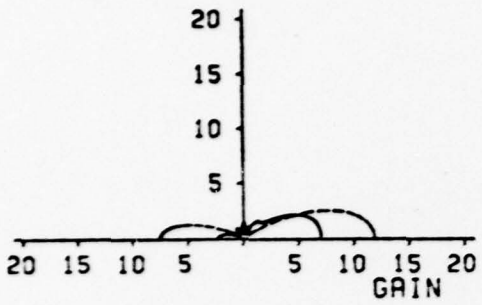

(a) Single frequency synthesis where $f = f_o$, and $w_{1p} = 1.0$.

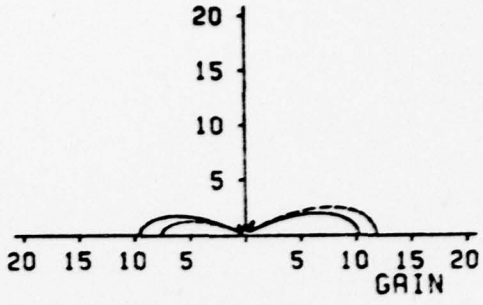

(b) Double frequency synthesis where $f_1 = 0.80\ f_o$, $f_2 = 1.05\ f_o$, $w_{1p} = 1.0$, and $w_{2p} = 5.0$.

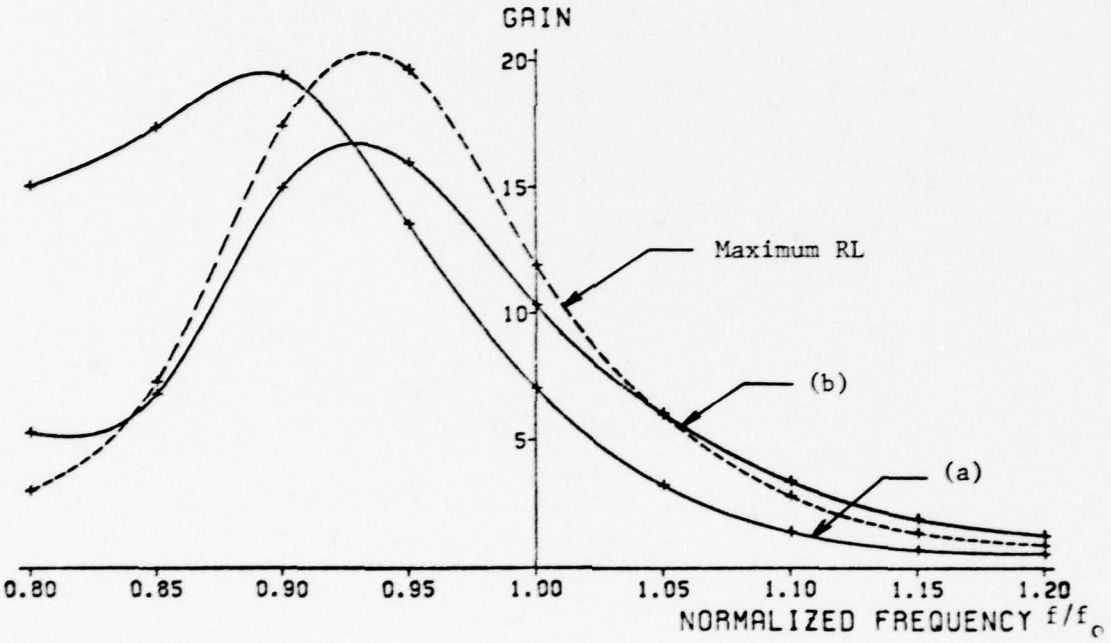

Fig. 4.5. Single and double frequency magnitude pattern synthesis for a nine element reactively loaded (RL) linear aperture antenna array where $a/\lambda = 0.750$, $a'/\lambda = 0.500$, $b/\lambda = 0.375$, $b'/\lambda = 0.250$, $D_x/\lambda = 0$, $D_t/\lambda = 0.040$, $P = 37$ and in (a)~(b): --- maximum reactively loaded, —— synthesis gain. The pattern to be synthesized was a sector pattern of 20° half power beamwidth oriented in the ϕ=0 direction.

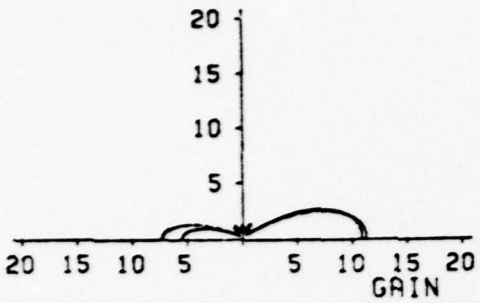

(a) Single frequency synthesis where $f = f_o$, and $w_{1p} = 1.0$

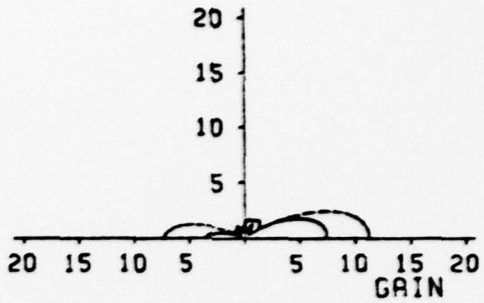

(b) Double frequency synthesis where $f_1 = 0.90\ f_o$, $f_2 = 1.05\ f_o$, $w_{1p} = 1.0$, and $w_{2p} = 3.0$

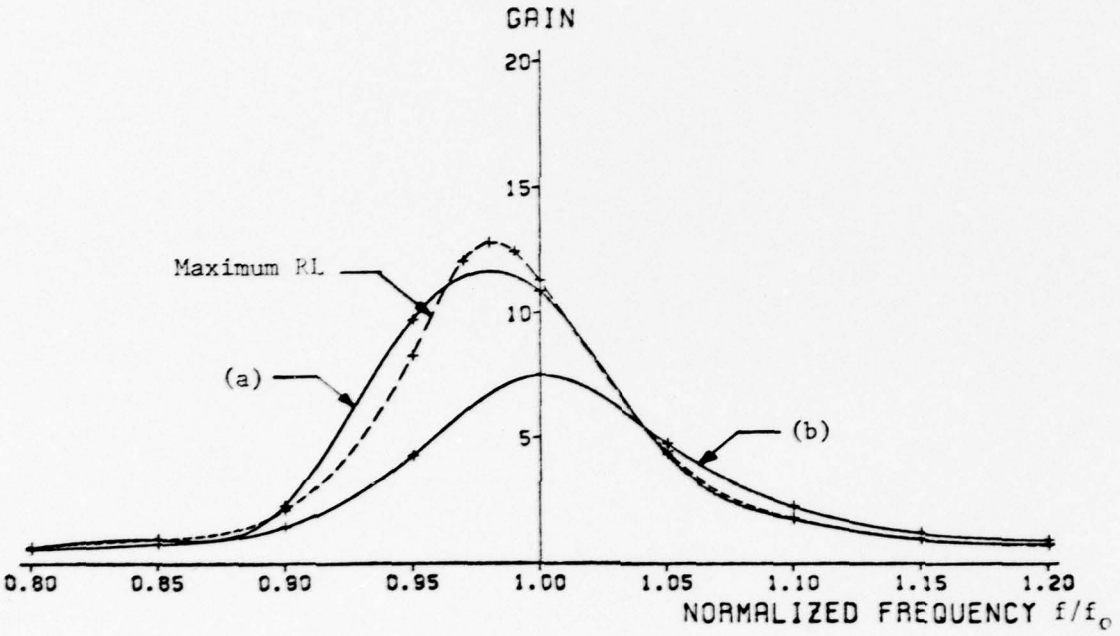

Fig. 4.6. Single and double frequency magnitude pattern synthesis for a nine element reactively loaded (RL) linear aperture antenna array where $a/\lambda = a'/\lambda = 0.750$, $b/\lambda = b'/\lambda = 0.375$, $D_y/\lambda = 0$, $D_t/\lambda = 0.040$, $P = 37$, and in (a)-(b): --- maximum reactively loaded gain, —— *synthesis gain*. The pattern to be synthesized was a sector pattern of 20° half-power beamwidth oriented in the $\phi = 0$ direction.

direction for two different nine element reactively loaded linear aperture antenna arrays. For the double frequency results in these two figures, d_i was restricted to vary between 0 and π/β_o. (Better results might be obtained if d_i can vary between 0 and ∞.) In the following analysis of the two figures, the results described are compared to maximum reactively loaded gain curves.

In Figure 4.5 ($a'/\lambda = 0.500$, $b'/\lambda \approx 0.250$) the single frequency synthesis results show lower gain and a higher mainbeam to backlobe ratio on the polar gain plot and a frequency shift of the gain versus frequency curve (toward lower frequencies) with a minor shape change. The double frequency synthesis results show a lower mainbeam to backlobe ratio on the polar gain plot and a slight broadening of the gain versus frequency curve.

In contrast, the results presented in Figure 4.6 ($a'/\lambda = 0.750$, $b'/\lambda = 0.375$) are much better than that of Figure 4.5 ($a'/\lambda = 0.500$, $b'/\lambda = 0.250$). In Figure 4.6 the single frequency synthesis results show a slight decrease in gain and a higher mainbeam to backlobe ratio on the polar gain plot and a broadened gain versus frequency curve. The double frequency synthesis results show a lower gain and a higher mainbeam to backlobe ratio on the polar gain plot while the gain versus frequency curve is broadened and shifted so that it is centered at a frequency of $f = f_o$.

4-5. Conclusion

Figures 4.1 to 4.4 show that for both reactively loaded and optimum excited nine element linear aperture antenna arrays, a cosine squared pattern with a beamwidth of 45° was synthesized with the lowest error for beam steering angles of ϕ = 0, 30°, 60°, and 90°.

In the ϕ = 0 direction the double frequency synthesis procedure worked satisfactory in realizing lower gain and increased bandwidth while centering the gain versus frequency curve for the case shown in Figure 4.6 but gave unacceptable results for the resonant slot case shown in Figure 4.5.

Chapter 5

CONCLUSIONS AND RECOMMENDATIONS

5-1. Summary with Conclusions

A method of moments formulation has been presented for the analysis of the reactively loaded, parasitically excited, waveguide-backed aperture antenna array. A major part of this formulation is the half-space admittance solution, where the aperture dimensions can be less than the backing waveguide dimensions. Several examples are given to illustrate the effect of antenna geometry (aperture dimensions and array lattice type) on the antenna characteristics of power gain, bandwidth, and match. In addition, pattern magnitude synthesis results are presented to illustrate pattern limitations for a given linear array as a function of beam steering angle and excitation.

The type of antenna array considered in this report has several advantages over the more conventional types of arrays (complete excitation):

a) There is no complex feed system to all of the apertures. The excitation is accomplished by electromagnetic interaction.

b) Only one element is externally fed which simplifies the problem of matching to the transmitter-receiver.

c) Variable reactive loads provide a means for beam steering.

The results presented in Chapter 3 show that even though there is incomplete control of the radiation characteristics for the antenna, the

values obtained are still satisfactory in many applications. One application is that for which the antenna (radiating structure plus feed system) is extremely limited in size. Since mutual coupling is the dominant factor for parasitic excitation, a reactively loaded aperture antenna array design consists of rectangular cells of possibly 3 × 9 elements, with one externally driven element and the other elements reactively loaded.

5-2. Recommendations for Further Research

Several areas of research still exist for further work in reactively loaded antennas. One experimental area is reactive load realization. Two possibilities for reactive loads which should be investigated are a shorted waveguide transmission line in the form of a waveguide-to-microstrip transition [26] followed by p-i-n diodes imbedded in a microstrip transmission line and a ferrite slab with a variable dc magnetic biasing field in a waveguide terminated in a short circuit [27].

Another area for research is pattern and match improvement for the reactively loaded antenna array at the low beam steering angles (ϕ = 0 - 30°). In Chapter 3, it is observed that the antenna pattern beamwidth is large at low beam steering angles. One method of producing a narrower beam at low beam steering angles is to place a dielectric sheet over the apertures. The function of the dielectric sheet is to transform the emanating electromagnetic wave into a surface wave which results in increased directivity. Villeneuve, Behnke, and Kummer of Hughes Aircraft [28] used a surface wave structure, which consisted of 5 layers of 8-mil thick glass

tape for an eight element completely excited aperture antenna array, to obtain an improved antenna beam shape with a higher pattern level at low beam steering angles with almost no pattern change in the broadside direction. Matching over a range of scan angles can also be improved by the addition of a dielectric sheet in front of the array [29]. Further analysis should be made to find out if a compromise dielectric sheet exists for improving both pattern shape and match at these low beam steering angles.

Another area of research would be to reduce the number of phase shifters required for a phased array while improving the array characteristics. This might be accomplished by using phase shifters to feed some of the elements of an array and reactive loads to control the excitation of the other elements. Amitay, Galindo, and Wu [30] considered periodic shorted waveguides (terminal admittances) in an infinite array environment to both eliminate surface wave effects and to improve the overall match.

Finally, further research should include the construction of a reactively loaded aperture antenna array to verify the results predicted by the mathematical formulation used in this report.

APPENDIX A

HALF-SPACE ADMITTANCE Y_{ij}^{hs}

A-1. Evaluation of Y_{ij}^{hs}

Starting with

$$Y_{ij}^{hs} = 2j\omega \iint_{\text{apert.}} (\underset{\sim}{F}_{ij} \cdot \underset{\sim}{W}_i + \phi_{ij}\rho_i)ds \ , \tag{2.48}$$

we define Y_{ij}^{1} by

$$Y_{ij}^{1} = 2j\omega \iint_{\text{apert.}} \underset{\sim}{F}_{ij} \cdot \underset{\sim}{W}_i \, ds \ . \tag{A.1}$$

Substituting (2.17) into (A.1), we obtain

$$Y_{ij}^{1} = \frac{j\omega\epsilon}{\pi a'b'} \int_{y_i - \frac{b'}{2}}^{y_i + \frac{b'}{2}} dy \int_{x_i - \frac{a'}{2}}^{x_i + \frac{a'}{2}} dx \cos\frac{\pi}{a'}(x - x_i)$$

$$\cdot \int_{y_j - \frac{b'}{2}}^{y_j + \frac{b'}{2}} dy' \int_{x_j - \frac{a'}{2}}^{x_j + \frac{a'}{2}} dx' \cos\frac{\pi}{a'}(x' - x_j)\, G(x'-x, y'-y) \tag{A.2}$$

where

$$G(x' - x, y' - y) = \frac{e^{-jk\sqrt{(x'-x)^2 + (y'-y)^2}}}{\sqrt{(x'-x)^2 + (y'-y)^2}} \ . \tag{A.3}$$

Consider

$$I^{y}_{ij}(x' - x) = \int_{y_i - \frac{b'}{2}}^{y_i + \frac{b'}{2}} dy \int_{y_j - \frac{b'}{2}}^{y_j + \frac{b'}{2}} dy' \, G(x' - x, y' - y) \, . \quad (A.4)$$

Substituting the transformation $y' = v + y$ into (A.4), we obtain

$$I^{y}_{ij}(x' - x) = \int_{y_i - \frac{b'}{2}}^{y_i + \frac{b'}{2}} dy \int_{y_j - \frac{b'}{2} - y}^{y_j + \frac{b'}{2} - y} dv \, G(x' - x, v) \, . \quad (A.5)$$

Interchanging the order of integration, we obtain (see Fig. A.1)

$$I^{y}_{ij}(x' - x) = \int_{y_j - y_i - b'}^{y_j - y_i} dv \, G(x' - x, v) \int_{y_j - \frac{b'}{2} - v}^{y_i + \frac{b'}{2}} dy + \int_{y_j - y_i}^{y_j - y_i + b'} dv \, G(x' - x, v) \int_{y_i - \frac{b'}{2}}^{y_j + \frac{b'}{2} - v} dy \, . \quad (A.6)$$

Consider

$$I^{lx}_{ij} = \int_{x_i - \frac{a'}{2}}^{x_i + \frac{a'}{2}} dx \cos \frac{\pi}{a'}(x - x_i) \int_{x_j - \frac{a'}{2}}^{x_j + \frac{a'}{2}} dx' \cos \frac{\pi}{a'}(x' - x_j) I^{y}_{ij}(x' - x) . \quad (A.7)$$

Substituting the transformation $x' = u + x$ into (A.7), we obtain

$$I^{lx}_{ij} = \int_{x_i - \frac{a'}{2}}^{x_i + \frac{a'}{2}} dx \cos \frac{\pi}{a'}(x - x_i) \int_{x_j - \frac{a'}{2} - x}^{x_j + \frac{a'}{2} - x} du \cos \frac{\pi}{a'}(u + x - x_j) I^{y}_{ij}(u) \, . \quad (A.8)$$

Interchanging the order of integration, we obtain

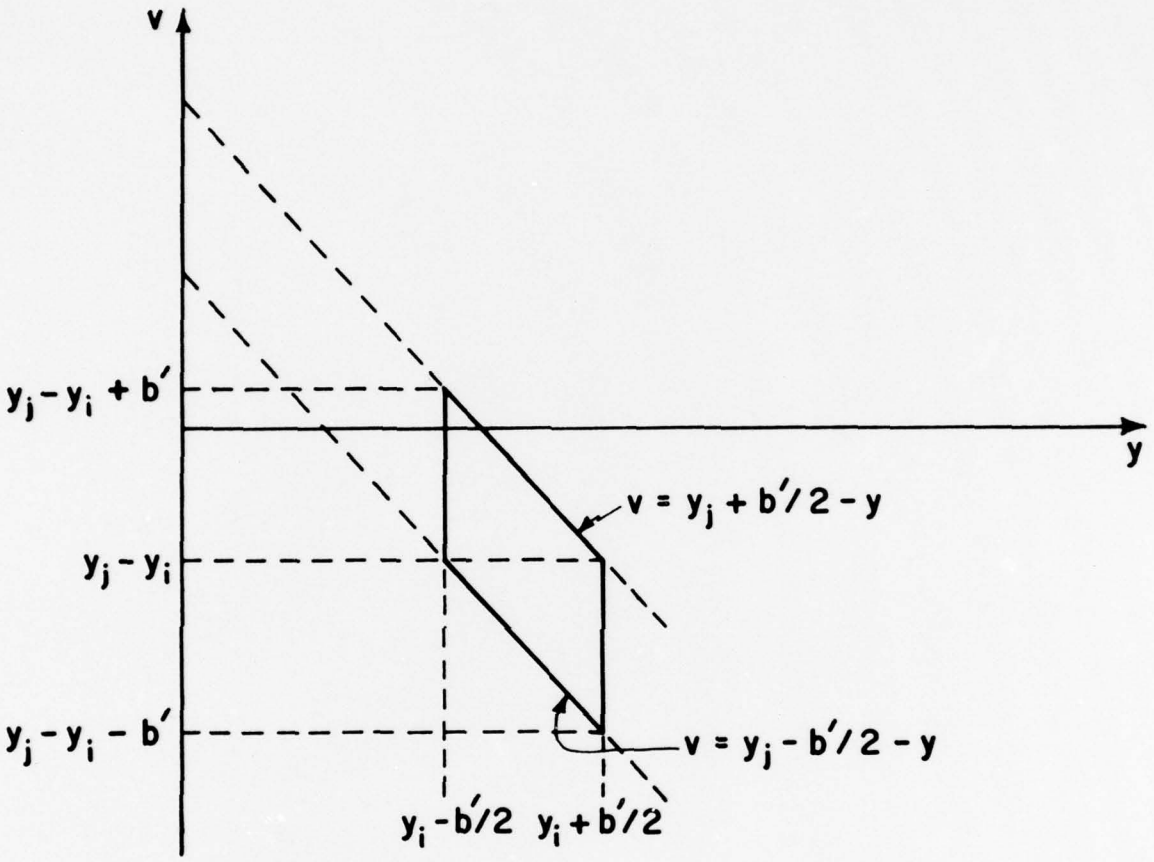

Fig. A.1. Coordinate transformation.

$$I_{ij}^{1x} = \int_{x_j-x_i-a'}^{x_j-x_i} du\, I_{ij}^{y}(u) \int_{x_j-\frac{a'}{2}-u}^{x_i+\frac{a'}{2}} dx \cos\frac{\pi}{a'}(x-x_i)\cos\frac{\pi}{a'}(u+x-x_j)$$

$$+ \int_{x_j-x_i}^{x_j-x_i+a'} du\, I_{ij}^{y}(u) \int_{x_i-\frac{a'}{2}}^{x_j+\frac{a'}{2}-u} dx \cos\frac{\pi}{a'}(x-x_i)\cos\frac{\pi}{a'}(u+x-x_j) \quad . \qquad (A.9)$$

In view of (A.4) and (A.7), (A.2) becomes

$$Y_{ij}^{1} = \frac{j\omega\varepsilon}{\pi a'b'} I_{ij}^{1x} \quad . \qquad (A.10)$$

Next define Y_{ij}^{2} by

$$Y_{ij}^{2} = 2j\omega \iint_{\text{apert.}} \phi_{ij}\rho_i \, ds \quad . \qquad (A.11)$$

Substituting (2.17) into (A.11), we obtain

$$Y_{ij}^{2} = \frac{-j\pi}{\omega\mu a'^{3}b'} \int_{y_i-\frac{b'}{2}}^{y_i+\frac{b'}{2}} dy \int_{x_i-\frac{a'}{2}}^{x_i+\frac{a'}{2}} dx \sin\frac{\pi}{a'}(x-x_i)$$

$$\cdot \int_{y_j-\frac{b'}{2}}^{y_j+\frac{b'}{2}} dy' \int_{x_j-\frac{a'}{2}}^{x_j+\frac{a'}{2}} dx' \sin\frac{\pi}{a'}(x'-x_j)\, G(x'-x,\, y'-y) \quad . \qquad (A.12)$$

Substituting the transformations $x' = u + x$ and $y' = v + y$ into (A.12) and interchanging the order of integration, we obtain

$$Y_{ij}^{2} = \frac{-j\pi}{\omega\mu a'^{3}b'} I_{ij}^{2x} \qquad (A.13)$$

where

$$I_{ij}^{2x} = \int_{x_j-x_i-a'}^{x_j-x_i} du\, I_{ij}^{y}(u) \int_{x_j-\frac{a'}{2}-u}^{x_i+\frac{a'}{2}} dx \sin\frac{\pi}{a'}(x-x_i)\sin\frac{\pi}{a'}(u+x-x_j)$$

$$+ \int_{x_j-x_i}^{x_j-x_i+a'} du\, I_{ij}^{y}(u) \int_{x_i-\frac{a'}{2}}^{x_j+\frac{a'}{2}-u} dx \sin\frac{\pi}{a'}(x-x_i)\sin\frac{\pi}{a'}(u+x-x_j). \qquad (A.14)$$

After a tedious but straightforward evaluation of two integrations for each of the quadruple integrals I_{ij}^{1x} and I_{ij}^{2x}, we obtain

$$Y_{ij}^{hs} = Y_{ij}^{1} + Y_{ij}^{2}$$

$$= \frac{jk}{2\pi\eta a'b'}\Bigg\{\int_{y_j-y_i-b'}^{y_j-y_i} dv(K_1+v)\Bigg[\int_{x_j-x_i-a'}^{x_j-x_i} du\, G(u,v)\left[(K_2+K_3u)\cos\frac{\pi u}{a'} + (K_4+K_5u)\sin\frac{\pi u}{a'}\right]$$

$$+ \int_{x_j-x_i}^{x_j-x_i+a'} du\, G(u,v)\left[(K_7-K_3u)\cos\frac{\pi u}{a'} + (K_8-K_5u)\sin\frac{\pi u}{a'}\right]\Bigg]$$

$$+ \int_{y_j-y_i}^{y_j-y_i+b'} dv(K_6-v)\Bigg[\int_{x_j-x_i-a'}^{x_j-x_i} du\, G(u,v)\left[(K_2+K_3u)\cos\frac{\pi u}{a'} + (K_4+K_5u)\sin\frac{\pi u}{a'}\right]$$

$$+ \int_{x_j-x_i}^{x_j-x_i+a'} du\, G(u,v)\left[(K_7-K_3u)\cos\frac{\pi u}{a'} + (K_8-K_5u)\sin\frac{\pi u}{a'}\right]\Bigg]\Bigg\} \qquad (A.15)$$

where

$$K_1 = y_i - y_j + b' \qquad (A.16)$$

$$K_2 = \left(1 - \frac{\pi^2}{k^2 a'^2}\right)(x_i - x_j + a')\cos\left[\frac{\pi}{a'}(x_j - x_i)\right] + \frac{a'}{\pi}\left(1 + \frac{\pi^2}{k^2 a'^2}\right)\sin\left[\frac{\pi}{a'}(x_j - x_i)\right] \quad (A.17)$$

$$K_3 = \left(1 - \frac{\pi^2}{k^2 a'^2}\right)\cos\left[\frac{\pi}{a'}(x_j - x_i)\right] \quad (A.18)$$

$$K_4 = \left(1 - \frac{\pi^2}{k^2 a'^2}\right)(x_i - x_j + a')\sin\left[\frac{\pi}{a'}(x_j - x_i)\right] - \frac{a'}{\pi}\left(1 + \frac{\pi^2}{k^2 a'^2}\right)\cos\left[\frac{\pi}{a'}(x_j - x_i)\right] \quad (A.19)$$

$$K_5 = \left(1 - \frac{\pi^2}{k^2 a'^2}\right)\sin\left[\frac{\pi}{a'}(x_j - x_i)\right] \quad (A.20)$$

$$K_6 = y_j - y_i + b' \quad (A.21)$$

$$K_7 = \left(1 - \frac{\pi^2}{k^2 a'^2}\right)(x_j - x_i + a')\cos\left[\frac{\pi}{a'}(x_j - x_i)\right] - \frac{a'}{\pi}\left(1 + \frac{\pi^2}{k^2 a'^2}\right)\sin\left[\frac{\pi}{a'}(x_j - x_i)\right] \quad (A.22)$$

$$K_8 = \left(1 - \frac{\pi^2}{k^2 a'^2}\right)(x_j - x_i + a')\sin\left[\frac{\pi}{a'}(x_j - x_i)\right] + \frac{a'}{\pi}\left(1 + \frac{\pi^2}{k^2 a'^2}\right)\cos\left[\frac{\pi}{a'}(x_j - x_i)\right] . \quad (A.23)$$

Substituting the coordinate transformations $u = \rho \cos\theta$ and $v = \rho \sin\theta$ into (A.15) and integrating out the ρ variable, we obtain (see Fig. A.2)

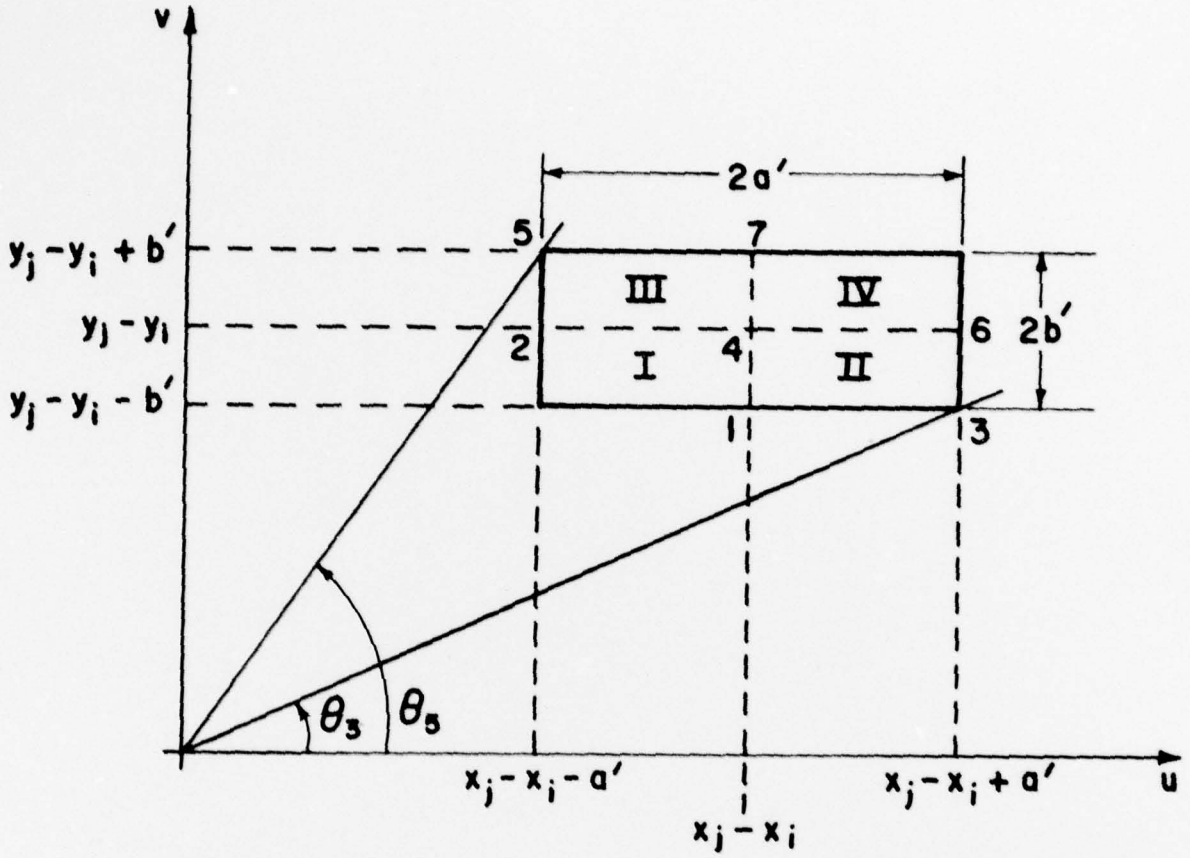

Fig. A.2. Rectangular - polar coordinate integration area.

$$Y_{ij}^{hs} = \frac{jk}{2\pi\eta a'b'}\Bigg\{\int_{\theta_1}^{\theta_2} [K_1[K_2L_1(\theta) + K_3L_3(\theta) + K_4L_2(\theta) + K_5L_4(\theta)]$$

(I)

$$+ [K_2L_5(\theta) + K_3L_7(\theta) + K_4L_6(\theta) + K_5L_8(\theta)]]d\theta$$

$$+ \int_{\theta_3}^{\theta_4} [K_1[K_7L_1(\theta) - K_3L_3(\theta) + K_8L_2(\theta) - K_5L_4(\theta)]$$

(II)

$$+ [K_7L_5(\theta) - K_3L_7(\theta) + K_8L_6(\theta) - K_5L_8(\theta)]]d\theta$$

$$+ \int_{\theta_4}^{\theta_5} [K_6[K_2L_1(\theta) + K_3L_3(\theta) + K_4L_2(\theta) + K_5L_4(\theta)]$$

(III) $$- [K_2L_5(\theta) + K_3L_7(\theta) + K_4L_6(\theta) + K_5L_8(\theta)]]d\theta$$

$$+ \int_{\theta_6}^{\theta_7} [K_6[K_7L_1(\theta) - K_3L_3(\theta) + K_8L_2(\theta) - K_5L_4(\theta)]$$

(IV)

$$- [K_7L_5(\theta) - K_3L_7(\theta) + K_8L_6(\theta) - K_5L_8(\theta)]]d\theta\Bigg\} \qquad \text{(A.24)}$$

where

$$L_1(\theta) = \frac{-j}{2}\left\{\frac{M_1(\theta) - M_2(\theta)}{M_5(\theta)} - \frac{M_3(\theta) - M_4(\theta)}{M_6(\theta)}\right\} \qquad \text{(A.25)}$$

$$L_2(\theta) = -\frac{1}{2}\left\{\frac{M_1(\theta) - M_2(\theta)}{M_5(\theta)} + \frac{M_3(\theta) - M_4(\theta)}{M_6(\theta)}\right\} \qquad \text{(A.26)}$$

$$L_3(\theta) = \cos\theta\left\{\frac{-j}{2}\left[\frac{\rho_2(\theta)M_1(\theta) - \rho_1(\theta)M_2(\theta)}{M_5(\theta)} - \frac{\rho_2(\theta)M_3(\theta) - \rho_1(\theta)M_4(\theta)}{M_6(\theta)}\right]\right.$$

$$\left. + \frac{1}{2}\left[\frac{M_1(\theta) - M_2(\theta)}{(M_5(\theta))^2} + \frac{M_3(\theta) - M_4(\theta)}{(M_6(\theta))^2}\right]\right\} \qquad \text{(A.27)}$$

$$L_4(\theta) = \cos\theta \left\{ -\frac{1}{2}\left[\frac{\rho_2(\theta)M_1(\theta) - \rho_1(\theta)M_2(\theta)}{M_5(\theta)} + \frac{\rho_2(\theta)M_3(\theta) - \rho_1(\theta)M_4(\theta)}{M_6(\theta)}\right]\right.$$

$$\left. - \frac{j}{2}\left[\frac{M_1(\theta) - M_2(\theta)}{(M_5(\theta))^2} - \frac{M_3(\theta) - M_4(\theta)}{(M_6(\theta))^2}\right]\right\} \qquad \text{(A.28)}$$

$$L_5(\theta) = L_3(\theta)\tan\theta \qquad \text{(A.29)}$$

$$L_6(\theta) = L_4(\theta)\tan\theta \qquad \text{(A.30)}$$

$$L_7(\theta) = \sin\theta\cos\theta \left\{ -\frac{j}{2}\left[\frac{\rho_2^2(\theta)M_1(\theta) - \rho_1^2(\theta)M_2(\theta)}{M_5(\theta)} - \frac{\rho_2^2(\theta)M_3(\theta) - \rho_1^2(\theta)M_4(\theta)}{M_6(\theta)}\right]\right.$$

$$+ \frac{\rho_2(\theta)M_1(\theta) - \rho_1(\theta)M_2(\theta)}{(M_5(\theta))^2} + \frac{\rho_2(\theta)M_3(\theta) - \rho_1(\theta)M_4(\theta)}{(M_6(\theta))^2}$$

$$\left. + j\left[\frac{M_1(\theta) - M_2(\theta)}{(M_5(\theta))^3} - \frac{M_3(\theta) - M_4(\theta)}{(M_6(\theta))^3}\right]\right\} \qquad \text{(A.31)}$$

$$L_8(\theta) = \sin\theta\cos\theta \left\{ -\frac{1}{2}\left[\frac{\rho_2^2(\theta)M_1(\theta) - \rho_1^2(\theta)M_2(\theta)}{M_5(\theta)} + \frac{\rho_2^2(\theta)M_3(\theta) - \rho_1^2(\theta)M_4(\theta)}{M_6(\theta)}\right]\right.$$

$$- j\left[\frac{\rho_2(\theta)M_1(\theta) - \rho_1(\theta)M_2(\theta)}{(M_5(\theta))^2} - \frac{\rho_2(\theta)M_3(\theta) - \rho_1(\theta)M_4(\theta)}{(M_6(\theta))^2}\right]$$

$$\left. + \frac{M_1(\theta) - M_2(\theta)}{(M_5(\theta))^3} + \frac{M_3(\theta) - M_4(\theta)}{(M_6(\theta))^3}\right\} \qquad \text{(A.32)}$$

$$M_1(\theta) = e^{j\rho_2(\theta)\,(\frac{\pi}{a'}\cos\theta - k)} \tag{A.33}$$

$$M_2(\theta) = e^{j\rho_1(\theta)\,(\frac{\pi}{a'}\cos\theta - k)} \tag{A.34}$$

$$M_3(\theta) = e^{-j\rho_2(\theta)\,(\frac{\pi}{a'}\cos\theta + k)} \tag{A.35}$$

$$M_4(\theta) = e^{-j\rho_1(\theta)(\frac{\pi}{a'}\cos\theta + k)} \tag{A.36}$$

$$M_5(\theta) = \frac{\pi}{a'}\cos\theta - k \tag{A.37}$$

$$M_6(\theta) = \frac{\pi}{a'}\cos\theta + k \tag{A.38}$$

The variables $\rho_1(\theta)$ and $\rho_2(\theta)$ are respectively the lower and upper limits of integration for the ρ integration in (A.15) after the transformations $u = \rho\cos\theta$ and $v = \rho\sin\theta$ are used. They are dependent on the θ variable and the integration subarea. For instance, when integrating over region IV between θ_4 and θ_7 (see Fig. A.2), $\rho_1(\theta) = (x_j - x_i)/\cos\theta$ and $\rho_2(\theta) = (y_j - y_i + b')/\sin\theta$.

A-2. Limiting Expressions for $L_2(\theta) - L_8(\theta)$

If we apply the procedure used in Section (2.4.2) to $L_2(\theta) - L_8(\theta)$ (A.26-A.32), we obtain

$$L_2(\theta) = -\frac{j}{2}\,(\rho_2(\theta) - \rho_1(\theta)) - \frac{1}{2}\,(\frac{M_3(\theta) - M_4(\theta)}{M_6(\theta)}) \tag{A.39}$$

$$L_3(\theta) = \cos\theta\,\{\frac{1}{4}\,(\rho_2^2(\theta) - \rho_1^2(\theta)) + \frac{j}{2}(\frac{\rho_2(\theta)M_3(\theta) - \rho_1(\theta)M_4(\theta)}{M_6(\theta)}) + \frac{1}{2}\,(\frac{M_3(\theta) - M_4(\theta)}{M_6(\theta))^2})\} \tag{A.40}$$

$$L_4(\theta) = \cos\theta \{-\frac{j}{4}(\rho_2^2(\theta) - \rho_1^2(\theta)) - \frac{1}{2}(\frac{\rho_2(\theta)M_3(\theta) - \rho_1(\theta)M_4(\theta)}{M_6(\theta)}) + \frac{j}{2}(\frac{M_3(\theta) - M_4(\theta)}{(M_6(\theta))^2})\} \quad (A.41)$$

$$L_5(\theta) = L_3(\theta)\tan\theta \quad (A.42)$$

$$L_6(\theta) = L_4(\theta)\tan\theta \quad (A.43)$$

$$L_7(\theta) = \sin\theta\cos\theta \{\frac{1}{6}(\rho_2^3(\theta) - \rho_1^3(\theta)) + \frac{j}{2}(\frac{\rho_2^2(\theta)M_3(\theta) - \rho_1^2(\theta)M_4(\theta)}{M_6(\theta)}) + \frac{\rho_2(\theta)M_3(\theta) - \rho_1(\theta)M_4(\theta)}{(M_6(\theta))^2} - j(\frac{M_3(\theta) - M_4(\theta)}{(M_6(\theta))^3})\} \quad (A.44)$$

$$L_8(\theta) = \sin\theta\cos\theta \{-\frac{j}{6}(\rho_2^3(\theta) - \rho_1^3(\theta)) - \frac{1}{2}(\frac{\rho_2^2(\theta)M_3(\theta) - \rho_1^2(\theta)M_4(\theta)}{M_6(\theta)}) + j(\frac{\rho_2(\theta)M_3(\theta) - \rho_1(\theta)M_4(\theta)}{(M_6(\theta))^2}) + \frac{M_3(\theta) - M_4(\theta)}{(M_6(\theta))^3}\} \quad (A.45)$$

for $|\frac{\pi}{a'}\cos\theta - k| < \varepsilon$, and

$$L_2(\theta) = -\frac{1}{2}(\frac{M_1(\theta) - M_2(\theta)}{M_5(\theta)}) + \frac{j}{2}(\rho_2(\theta) - \rho_1(\theta)) \quad (A.46)$$

$$L_3(\theta) = \cos\theta \{-\frac{j}{2}(\frac{\rho_2(\theta)M_1(\theta) - \rho_1(\theta)M_2(\theta)}{M_5(\theta)}) + \frac{1}{2}(\frac{M_1(\theta) - M_2(\theta)}{(M_5(\theta))^2}) + \frac{1}{4}(\rho_2^2(\theta) - \rho_1^2(\theta))\} \quad (A.47)$$

$$L_4(\theta) = \cos\theta \{-\frac{1}{2}\left(\frac{\rho_2(\theta)M_1(\theta) - \rho_1(\theta)M_2(\theta)}{M_5(\theta)}\right) - \frac{j}{2}\left(\frac{M_1(\theta) - M_2(\theta)}{(M_5(\theta))^2}\right)$$

$$+ \frac{j}{4}(\rho_2^2(\theta) - \rho_1^2(\theta))\} \tag{A.48}$$

$$L_5(\theta) = L_3(\theta)\tan\theta \tag{A.49}$$

$$L_6(\theta) = L_4(\theta)\tan\theta \tag{A.50}$$

$$L_7(\theta) = \sin\theta\cos\theta \{-\frac{j}{2}\left(\frac{\rho_2^2(\theta)M_1(\theta) - \rho_1^2(\theta)M_2(\theta)}{M_5(\theta)}\right)$$

$$+ \frac{\rho_2(\theta)M_1(\theta) - \rho_1(\theta)M_2(\theta)}{(M_5(\theta))^2} + j\left(\frac{M_1(\theta) - M_2(\theta)}{(M_5(\theta))^3}\right)$$

$$+ \frac{1}{6}(\rho_2^3(\theta) - \rho_1^3(\theta))\} \tag{A.51}$$

$$L_8(\theta) = \sin\theta\cos\theta \{-\frac{1}{2}\left(\frac{\rho_2^2(\theta)M_1(\theta) - \rho_1^2(\theta)M_2(\theta)}{M_5(\theta)}\right)$$

$$- j\left(\frac{\rho_2(\theta)M_1(\theta) - \rho_1(\theta)M_2(\theta)}{(M_5(\theta))^2}\right) + \frac{M_1(\theta) - M_2(\theta)}{(M_5(\theta))^3}$$

$$+ \frac{j}{6}(\rho_2^3(\theta) - \rho_1^3(\theta))\} \tag{A.52}$$

for $\left|\frac{\pi}{a'}\cos\theta + k\right| < \varepsilon$.

Appendix B

COMPUTER PROGRAM SUMMARY

The following is a summary of the major computer program subroutines used to compute the results in this report. All of these subroutines can be found in a referenced report or can be programmed directly from referenced equations.

B-1. Waveguide Admittance - Y^{wg}

The computer program subroutine AY which calculates the waveguide admittance for the driven waveguide

$$Y_{ij}^{wg}\ (\text{driven}) = \delta_{ij} \left\{ \sum_{k=0}^{\infty} (A_{ik}^{TE})^2 Y_k^{TE} + \sum_{k=1}^{\infty} (A_{ik}^{TM})^2 Y_k^{TM} \right\} \qquad (B.1)$$

can be found in report [19]. To calculate Y^{wg} (driven), we have to choose the total number of m (LM) and n (LN) modes required to compute the modal amplitudes A_{ik}^{TE} (2.28) and A_{ik}^{TM} (2.29) in (B.1) (only odd m starting with m = 1 and even n starting with n = 0 (TE) or n = 2 (TM) are considered due to the $\sin \frac{m\pi}{2} \cos \frac{n\pi}{2}$ factor appearing in Eq. (2.31)). LM which represents the contribution of the mth waveguide mode in (B.1) should be chosen so that the contribution of the $(1/(m^2a^2 - 1/a'^2))$ $\cos (m\pi\ a'/2a)$ factor in (2.31) results in very small A_{ik}^{TE} and A_{ik}^{TM} values. LN which represents the contribution of the nth mode in (B.1) should be chosen so that the argument $n\pi\ b'/2b$ of the sin ( )/( ) factor in Eq. (2.31) is greater than π.

We can find the short circuit distances d_i (given B_{L_i}) by solving

$$Y_{ij}^{wg}\ (\text{parasitic}) = j\ B_{L_i}\ \delta_{ij}$$

$$= \delta_{ij}\{\sum_{k=1}^{\infty}[(A_{ik}^{TE})^2 Y_k^{TE} + (A_{ik}^{TM})^2 Y_k^{TM}] - j\ A_{io}^2\ Y_o\ \cot\beta_o d_i\} \qquad (B.2)$$

where the first term is calculated in (B.1) minus $(A_{io}^{TE})^2\ Y_o^{TE}$.

B-2. Half-Space Admittance - Y^{hs}

The computer program subroutine YHSP which calculates one column of the half-space admittance matrix $[Y^{hs}]$ can be found in report [19].

To calculate the self-admittance term, an eight point Gaussian quadrature numerical integration is used on the single integrals Eq. (2.53). The same method of solution is used for calculating the half-space mutual admittance for apertures which are close together (centers of any two given apertures are separated by less than 4a'). For greater aperture separations a six point double numerical integration (six points in each variable for a total of 36 points) is performed on the double integrals in Eq. (2.52).

B-3. Measurement Vector - $\vec{P}^m$

The measurement vector $\vec{P}^m$ can be programmed directly from derived equations in Chapter 2.

$(P^m_{\text{E-plane}})_i = (P_i^m)_{xx}$ -- Eq. (2.65). For $\phi = \frac{\pi}{2}$, the sin ( )/( ) term in Eq. (2.65) is to be replaced by its limit one.

$(P^m_{H\text{-plane}})_i = (P^m_i)_{\theta\phi}$ -- Eq. (2.66). For $\theta = 0$ or π or $\phi = \frac{\pi}{2}$, the sin ( )/( ) term in Eq. (2.66) is to be replaced by its limit one. For $\theta = \cos^{-1}(\frac{\pm\pi}{ka'})$, the $\cos(\frac{ka'}{2}\cos\theta)/(\pi^2 - k^2a'^2\cos^2\theta)$ in Eq. (2.66) is to be replaced by its limit $1/4\pi$.

B-4. Univariate Optimization Algorithm

The Univariate procedure is a nongradient algorithm that uses a fixed step size and repetively divides the step size by two when the neighborhood of the local maximum (minimum) has been found. The search technique can be described as follows. First, one variable is adjusted using a one dimensional search until no further improvement is gained. Then another parameter is adjusted until no additional improvement results, and so on. After each parameter has been adjusted once, the process is repeated returning to the first parameter and proceeding as before. If the parameters are non-interacting, which is not very likely, once through the above cycle is enough. If strong interactions and ridges or ravines exist, many cycles may be required.

The Univariate optimization subroutine can be found in report [8]. It was used to maximize power gain in a specified direction. The univariate algorithm is very efficient in reactively loaded problems (see report [7]) since an inverse operation was necessary only once for a complete search in one variable. In other words, for a given set of reactive loads and a search in the variable B_{L_i}, the solution to Eq. (2.16) can be written as

$$\vec{V} = \{[I] - \frac{[Y^i]^{-1}[U^i]}{-j/B_{L_i} + [Y^i]^{-1}_{ii}}\}[Y^i]^{-1}\,\vec{I}^{imp} \qquad (B.3)$$

where

$$[Y^i] = [Y^{hs} + Y^{wg}] - j\,B_{L_i}\,[U^i]$$

$[I]$ ≡ identity matrix

$[U^i]$ = 1 for the iith element

= 0 for all other elements

$i \neq$ NFP (a search is made in N-1 variables).

For our problem the function f = 1/GAIN is minimized by first varying B_{L_1} until f was minimized, then B_{L_2}, and so on. After all of the loads were varied once, the sequence is repeated. There is no assurance that the minimum achieved is the absolute minimum.

B-5. Rosenbrock Optimization Algorithm

The Rosenbrock search technique [22] uses N mutually orthogonal directions during each search cycle to find a relative minimum. This strategy differs from a steepest descent technique which uses successive orthogonal directions, but these successive directions do not necessarily form a mutually orthogonal set. A new set of orthogonal directions for the Rosenbrock algorithm for each search cycle are obtained from Eqs. (8) and (9) of Rosenbrock's paper [22].

The Rosenbrock optimization subroutine can be found in report [9]. It was used in the synthesis procedure for minimizing the synthesis

error function. The Rosenbrock algorithm which changes all of the loads and the excitation for each step in a search cycle was used instead of the univariate procedure in order to minimize the number of multiplicative operations required to evaluate the synthesis error function at P points.

The Rosenbrock subroutine ROSIEM given in [9] was originally used in conjunction with an impedance matrix formulation. Since the synthesis problem in this report was formulated in terms of admittances, a modification should be made to the four IF statements in DO loop 20. These four IF statements should be changed so that when a load susceptance decreases below an arbitrary specified magnitude, a new predetermined susceptance value is substituted with a sign opposite to that of the original susceptance.

B-6. Magnitude Pattern Synthesis (Optimum)

The computer program subroutine for the optimum magnitude pattern synthesis algorithm described in Chapter 4 can be found in report [25].

REFERENCES

[1] T. L. Simpson and J. D. Tillman, "Parasitic Excitation of Circular Antenna Arrays," IRE Trans. on Antennas and Propagation, vol. AP-9, No. 3, pp. 263-267, May 1961.

[2] D. G. Berry, R. G. Malech, and W. A. Kennedy, "The Reflectarray Antenna," IEEE Trans. on Antennas and Propagation, vol. AP-11, No. 6, pp. 645-651, November 1963.

[3] R. J. Coe and G. Held, "A Parasitic Slot Array," IEEE Trans. on Antennas and Propagation, vol. AP-14, No. 1, pp. 10-16, January 1964.

[4] D.P.S. Seth and Y. L. Chow, "On Linear Parasitic Array of Dipoles with Reactive Loading," IEEE Trans. on Antennas and Propagation, vol. AP-21, No. 3, pp. 286-292, May 1973.

[5] S. P. Mathur, "Analysis of a Parallel Array of Waveguide or Cavity-Backed Rectangular Slot Antennas," Ph.D. Dissertation, Michigan State University, 1974.

[6] R. F. Harrington and J. R. Mautz, "Reactively Loaded Directive Antennas," Technical Report No. 1, Contract No. N00014-67-A-0378-0006, Office of Naval Research, September 1974.

[7] J. Luzwick and R. F. Harrington, "A Comparison of Optimization Techniques as Applied to Gain Optimization of a Reactively Loaded Linear Array, "Technical Report No. 1, Contract No. N00014-76-C-0225, Office of Naval Research, February 1976.

[8] R. F. Harrington, R. F. Wallenberg, and A. R. Harvey, "Design of Reactively Controlled Antenna Arrays," Technical Report No. 4, Contract No. N00014-67-A-0378-0006, Office of Naval Research, September 1975.

[9] J. Luzwick and R. F. Harrington, "Pattern Magnitude Synthesis for a Reactively Loaded Circular Antenna Array," Technical Report No. 6, Contract No. N00014-76-C-0225, Office of Naval Research, August 1977.

[10] J. Luzwick and R. F. Harrington, "A Reactively Loaded Aperture Antenna Array," Technical Report No. 3, Contract No. N00014-76-C-0225, Office of Naval Research, September 1976.

[11] J. Luzwick and R. F. Harrington, "A Reactively Loaded Aperture Antenna Array," IEEE Trans. on Antennas and Propagation, vol. AP-26, No. 4, pp. 543-547, July 1978. See also: J. Luzwick and R. F. Harrington, "A Solution for a Wide Aperture Reactively Loaded Antenna Array," Technical Report No. 5, Contract No. N00014-76-C-0225, Office of Naval Research, January 1977.

[12] G. V. Borgiotti, "A Novel Expression for the Mutual Admittance of Planar Radiating Elements," IEEE Trans. on Antennas and Propagation, vol. AP-16, No. 3, pp. 329-333, May 1968.

[13] R. J. Mailloux, "Radiation and Near-Field Coupling Between Two Collinear Open-Ended Waveguides," IEEE Trans. on Antennas and Propagation, vol. AP-17, No. 1, pp. 49-55, January 1969.

[14] R. J. Mailloux, "First-Order Solutions for Mutual Coupling Between Waveguides which Propagate Two Orthogonal Modes," IEEE Trans. on Antennas and Propagation, vol. AP-17, No. 6, pp. 740-746, November 1969.

[15] R. F. Harrington, "Matrix Methods for Field Problems," Proc. of the IEEE, vol. 55, No. 2, pp. 136-149, February 1967.

[16] A. G. Cha and J. K. Hsiao, "A Matrix Formulation for Large Scale Numerical Computation of the Finite Planar Waveguide Array Problem," IEEE Trans. on Antennas and Propagation, vol. AP-22, No. 1, pp. 106-108, January 1974.

[17] M. A. Hidayet, "Finite Phased Array Analysis," Ph.D. Dissertation, University of Michigan, 1974.

[18] J. Luzwick and R. F. Harrington, "Mutual Coupling Analysis in a Finite Planar Rectangular Waveguide Antenna Array," Technical Report No. 7, Contract No. N00014-76-C-0225, Office of Naval Research, June 1978.

[19] J. Luzwick and R. F. Harrington, "Computer Programs for Mutual Coupling in a Finite Planar Rectangular Waveguide Antenna Array," Technical Report No. 8, Contract No. N00014-76-C-0225, Office of Naval Research, July 1978.

[20] R. F. Harrington, Time-Harmonic Electromagnetic Fields, McGraw-Hill Book Company, New York, 1961.

[21] C. H. Papas, Theory of Electromagnetic Wave Propagation, McGraw-Hill Book Company, New York, p. 23, 1965.

[22] H. H. Rosenbrock, "An Automatic Method for Finding the Greatest or Least Value of a Function," The Computer Journal, 3, pp. 175-184, October 1960.

[23] J. R. Mautz and R. F. Harrington, "Computational Methods for Antenna Pattern Synthesis," Technical Report No. 9, Contract No. 19628-73-C-0047, Air Force Cambridge Research Laboratories, August 1973.

[24] Y. T. Lo, S. W. Lee, and Q. H. Lee, "Optimization of Directivity and Signal-to-Noise Ratio of an Arbitrary Antenna Array," Proc. of the IEEE, vol. 54, pp. 1033-1045, August 1966.

[25] J. R. Mautz and R. F. Harrington, "Computer Programs Antenna Pattern Synthesis," Technical Report No. 11, Contract No. 19628-73-C-0047, Air Force Cambridge Research Laboratories, October 1973.

[26] M. E. Davis, "Integrated Diode Phase-Shifted Elements for an X-Band Phased Array Antenna," IEEE Trans. on Microwave Theory and Techniques, pp. 1080-1084, December 1975.

[27] L. R. Whicker and C. W. Young, Jr., "The Evolution of Ferrite Control Components," Microwave Journal, vol. 21, No. 11, pp. 33-37, November 1978.

[28] A. T. Villeneuve, M. C. Behnke, and W. H. Kummer, "Hemispherically Scanned Arrays, "Hughes Aircraft Company, Scientific Report No. 2, Contract No. F19628-72-C-0145, Air Force Cambridge Research Laboratories, Report No. AFCRL-TR-74-0084, December 1973.

[29] E. G. Magill and H. A. Wheeler, "Wide-Angle Impedance Matching of a Planar Array Antenna by a Dielectric Sheet," IEEE Trans. on Antennas and Propagation, vol. AP-14, No. 1, pp. 49-53, January 1966.

[30] N. Amitay, V. Galindo, and C. P. Wu, "Theory and Analysis of Phased Array Antennas," Wiley-Interscience, New York, Chapter 8, 1972.

BIOGRAPHICAL DATA

Name: JOHN LUZWICK

Date and Place of Birth: March 15, 1944, Evanston, Illinois

Elementary School: Chicago and Niles, Illinois School Systems, Graduated 1958.

High School: Maine East High School
Park Ridge, Illinois
Graduated 1962.

College: Illinois Institute of Technology, Chicago, Illinois
BSEE 1966.

Industrial Experience: MIT Lincoln Laboratory, Bedford, Massachusetts, from 1968 to 1970 and 1971-1974.

The MITRE Corporation, Bedford, Massachusstts, from 1974-1975.

Graduate Work: Purdue University, West Lafayette, Indiana
MSEE 1968.

University of Illinois, Champaign-Urbana, Illinois, from 1970-1971.

Syracuse University, Syracuse, New York
Graduate Research/Teaching Assistant
from 1975-1979.